LBL-11895
UC-70

THE MEASUREMENT OF IN-SITU STRESS IN SALT AND ROCK USING NQR TECHNIQUES

E. Schempp, T. Hirschfeld, and S. Klainer

December 1980

Prepared for the U.S. Department of Energy
under Contract W-7405-ENG-48

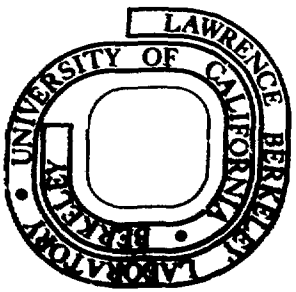

SUMMARY

This Annual Report presents a summary of the first four months' results from investigating the potential for measuring stress/ train in salt using NQR techniques.

This investigation is based on the premise that there exists a need for an improved method of measuring underground stress -- a method which would be reliable, simple to use, relatively fast, non-destructive, and inexpensive. A detailed discussion of how stress and strain affect the quantities which can be measured in an NQR experiment is then given. This shows that, for stresses of the magnitude to be expected at depths up to about 10,000 feet, quadrupole coupling constants will fall in the range of 1-10 kHz for both the sodium and chloride ions in NaCl. The report continues with an examination of various resonance techniques which might be utilized to carry out the measurements. The most promising system involves pulsed nuclear double resonance detection; an alterative is to observe the quadrupolar splitting of the NMR signal. (For studies of aluminum in hard rock, a later phase of this program, the Al^{27} NQR lines would most likely be detected by pure quadrupole resonance.)

An extensive discussion is presented on the choices to be made in the measurement and mapping techniques. The well-known perturbation of the homogenous stress field in the neighborhood of a borehole is shown to be advantageous from the point of view of obtaining directional information on

the stress. Detailed considerations are then given for the construction and operation of a borehole stress sensor.

The important conclusions reached to date are: (1) The NQR technique seems feasible for measuring the magnitude and direction of underground stress with a resolution of about 25 psi, or 2.5% at 1000 psi. (2) Downhole instrumentation suitable for in-situ determinations of stress appears within the state of the art.

Based on the work to date, the authors have identified additional tasks required on the project. These include detailed laboratory measurements on salt as a function of pressure and direction, continued theoretical calculation on the exact line shapes to be expected, and the contribution of lattice defects and impurities to the NQR signals. Finalizing the design of a laboratory NQR instrument and constructing it will also be part of the program for the present fiscal year. It will later be adapted it to a field configuration for in-situ measurements in salt. Preliminary investigation of the NQR signals from Al-containing mineral constituents of hard rock will be carried out in parallel with the above work program.

THE MEASUREMENT OF IN-SITU STRESS IN SALT AND ROCK USING NQR TECHNIQUES

Table of Contents

I. Introduction 1

A. Overview 1
B. Boreholes 3
1. The Leeman Rosette Gauge ("doorstopper") 5
2. Enclosed Probes 5
3. Hydraulic Fracturing 5
C. Program Plan 7
D. Prognosis 7

II. Technical Discussion 9

A. An Introduction to NQR 9
B. NQR and Strain Measurements 12
C. Resonance Techniques 24
1. Direct Detection 24
2. Quadrupolar Perturbed NMR 26
3. Double Resonance 29
D. Choice of Measurement Technique 35
1. Choice of Measurement Technique 35
2. Choice of Mapping Method 37
3. Mapping of the Surrounding Strata by NQR 37
4. Mapping the Borehole Perturbation by NQR 44
E. Description of an NQR Stress Sensor for Borehole Operation 48
1. Magnetic Field Generator 48
a. Field solenoid 48
b. Power supply 53
c. Cooling system 55
2. NMR/NQR Double Resonance Transmitter-Receiver 55
a. NQR irradiator 55
b. A rotating transmit/receive coil 56
c. A matched switching network and preamplifier 58
d. NMR transmitter/receiver system 64
e. Data system 65
F. Predicted Sensitivities on Stress/Strain Determinations . . . 66

III. Conclusions and Recommendations 77

A. Conclusions 77
B. Recommendations 77

IV. References 79

V. Appendices

A. Practical Applications of FT-NQR Spectroscopy. A-1
B. Axial Field of a Coil of Finite Height and Width B-1
C. Effect of Finite Winding Height on Axial Field of Toroidal Coil. C-1
D. Effect of Finite Annular Width on Axial Field of Toroidal Coil. D-1
E. Optimum NQR Coil for Constant Maximum Field. E-1
G. Power Requirements in NQR Coil G-1
H. NQR Signal Loss for Finite Length Excitation Pulses. H-1

THE MEASUREMENT OF IN-SITU STRESS IN SALT AND ROCK USING NQR TECHNIQUES

I. INTRODUCTION

A. Overview

The measurement of the in situ state of stress underground is one of the most challenging and important problems presented to geoscience and engineering. Upon accurate knowledge of the stress and the strength of rock materials rests all designs for both surface structure and underground excavations. A special case of this need is the measurement of stress in rock and/or salt to assure the integrity of an underground nuclear waste repository. Knowledge of present, and if possible past, stresses are important in developing a deeper understanding of the forces which have shaped and are continuing to shape the earth's landforms. In a time of ever greater human demands on the earth's crustal resources, such a broader understanding is increasingly vital. Moreover, growing population densities place more and more people in areas subject to risk from earthquakes, volcanoes, and other geological forces which can dramatically affect lives and economies. If improved techniques for making more numerous and more accurate stress measurements can be discovered, our knowledge and ability to predict the structural soundness of excavations in rock and salt will be greatly aided.

In spite of the fundamental role played by stress, techniques and instrumentation for its measurement have developed slowly. In some of the most frequently used techniques it is necessary to interrupt the drilling operation to carry out the measurements, a procedure which is obviously costly. Other methods are both costly and destructive. The technology for making rapid, non-destructive stress determinations does not exist. No existing methods are available for carrying out measurements at a particular depth in a borehole over a period of time, and hence observations of changes in stress over time are almost unobtainable. Clearly, in areas where knowledge of sudden build-ups or release of stress would be important, such as in earthquake and fault zones and near waste repositories and volcanoes, an improved more versatile technique for determining stress would be very valuable.

It is the purpose of this research work to examine the feasibility of using NQR (Nuclear Quadrupole Resonance) techniques, a new procedure for measuring stress, and to develop the instrumentation necessary to permit field evaluation.

Although several concepts are under evaluation which are all based on the microscopic response of crystalline materials to stress and utilize sophisticated notions drawn from experience in solid state physics, the present total emphasis is on NQR. The approaches being considered include changes in the nuclear spin-lattice relaxation times of NMR signals, changes in the electron-spin resonance (ESR) signals from iron-bearing minerals in rock, and the pressure-dependence of nuclear quadrupole resonance (NQR) signals. The focus of this report is on salt, NaCl, which while normally cubic, under stress changes its symmetry and thus develops a NQR spectrum which depends on the stress-induced strains. In the following pages the theoretical and

experimental details are described in full. Once the salt studies have demonstrated the feasibility of the technique, then the use of NQR to determine stress in aluminum-containing rocks will be addressed.

B. Boreholes

Knowledge of the *in situ* state of stress is important in the design of underground openings. The stability, safety, and long-term behavior of underground structures depends largely on the properties of the rock found at the site of the proposed works, and good design requires accurate knowledge of the relevant parameters. The overall mechanical properties of rock depend upon all of the structural features and the state of stress in the rocks throughout the site. Whenever the stresses exceed the relevant materials strengths, the design of the layout must be modified to obviate this situation or the rock must be reinforced to ensure stability.

Boreholes drilled to penetrate the rock mass provide the most reliable way, short of full-scale excavation, of obtaining information on the rocks at depth and it is, therefore, from boreholes that one would like to be able to measure the stress.

Rocks underground are subject to a variety of forces. The most obvious is the lithostatic pressure from the weight of the overburden. Other forces include those from tectonic movements, i.e., horizontal or sideways thrusts of the type responsible for uplift, folding, and faulting. In principle, the separate vector forces can be added to give a resultant force, and then from this a net pressure (force per unit area) acting in a known direction can be derived. This simple approach, however, does not take into account the deformability of materials. Owing to strains, dimensional changes arising

from stress, a simple vertical pressure will be converted into horizontal forces. Hence one prefers to analyze the situation in terms of the stress tensor. In general, therefore, rocks are subjected to a 3-dimensional stress made up of both diagonal (normal) elements, which are usually compressive, and off-diagonal shear elements. A complete specification of the tensor requires knowing all six elements, or the three diagonal elements in the principal axes system and the three angles which specify the orientation of the principal axes. For a full description of the philosophical origins of the concept of stress and its detailed mathematical treatment, the reader is referred to standard works on the theory of elasticity, e.g., the one by Love.[1]

One probelm presented by the concept of underground stress is that the quantity of interest is not directly accessible to measurement. The reason for this is that in order to get to the point where a measurement is desired, a hole has to be made, and the hole itself perturbs the stress field. There can, of course, be no normal stress on a surface facing the opening. In most cases, where the stress is reasonably homogeneous and the rock can be considered a continuous medium, the stress in the region of the borehole can be calculated using the Laplace equation. Thus from measurements of the radial and tangential components of the stress near the borehole, the Cartesian components present before the hole was drilled can be calculated.

A large number of techniques have been devised to measure stress. Three of these, widely used in borehole situations, will be briefly described. A number of other methods are discussed by Jaeger and Cook.[2]

1) The Leeman Rosette Gauge ("doorstopper")[3]

In this technique, a hole is drilled to the depth of interest. The main drilling bit is then pulled out, and a small pilot hole about 1 or 2 inches in diameter is drilled an additional 10-20 inches. The bottom of this hole is carefully faced to be smooth and flat. Then three rosettes of three strain gauges each is inserted and cemented directly to the surface of the rock at the bottom of the borehole. After the cement has dried, electrical measurements are made, the connecting cables are disconnected, the main coring bit is re-lowered, and the pilot hole with the implanted strain gauge is overcored, thus releasing the stress from the surrounding rock. When the core is brought to the surface, a new set of measurements from the strain gauges is taken. This scheme represents a significant improvement over previous methods in that one set of measurements from a single borehole provides sufficient data to enable the complete state of stress to be determined at the measurement point.

2) Enclosed Probes

Rocha and Silverio[4] and Blackwood[5] developed a second technique in which the strain gauges are imbedded in a solid epoxy probe. This is bonded into the pilot hole and overcored as above. Later Pender and Duncan-Fama[6] developed and analyzed an improved technique utilizing a thin-walled epoxy cylinder in which the strain gauges were placed.

3) Hydraulic Fracturing

In this meth d a section of the borehole is sealed off by two packers and the region between them pumped full of water at high pressure. The pressure is increased until the rock walls fracture, and then by measuring the subsequent "shut-in pressure" and "secondary breakdown pressures" parameters are obtained from which the stress may be inferred, if the pore pressure and

hydrofracture tensile strength of the rock is known from laboratory measurements a priori. The directions of the stress are obtained by observing the directions of the cracks produced in the borehole wall, either by lowering a camera or some device for making impressions of the wall surfaces down the hole.

It is apparent that all these methods are relatively cumbersome and time-consuming. The first two using triaxial strain gauges require that the drilling operation be interrupted, the pilot hole drilled, the probe inserted, and the overcoring drilling step. It is obviously difficult to repeat this at frequent intervals. Moreover, they cannot be applied to pre-existing holes. Other problems are present: (a) the Leeman "doorstopper" technique is not very satisfactory under wet conditions. (b) The epoxy probes may give wrong readings if the bond between the rock and the probe is broken by tensile stresses introduced by overcoring and (c) the hydrofracture method is, to say the least, an indirect way of obtaining the stress; it involves considerable skill in setting up the experiment; it requires laboratory studies on the rocks from the region of the borehole; and, of course, it also inflicts permanent damage on the walls of the borehole. None of these methods is suitable for measuring the time evolution of the stress because the measurements cannot be repeated at a later time.

In contrast, the NQR method offers the possibility of lowering an instrument down a borehole in salt and making as many measurements as desired at arbitrary increments in depth, and these can be repeated as often as necessary. Each measurement should be completed in a half hour or less.

Underground stresses vary over a wide range with values as large as 10,000 psi (680 atm) having been reported.[2] The majority of measurements, however, fall under 2500 psi (140 atm), particularly for lighter rock types

such as salt.[7] At depth, all rock is subjected to a vertical lithostatic stress, and it is frequently assumed that at great depth (> 1000 m) it is only this stress which matters. This idea has been called Heim's rule.[2] This situation gives rise to horizontal stresses of the same order as the vertical, although many situations are known where the horizontal stresses σ_1 and σ_2 are higher than the vertical. Often, the two horizontal components of the stress tensor obey $\sigma_1/\sigma_2 \simeq 0.5$.

C. Program Plan

The overall program objectives are to demonstrate that in-situ stress can be measured in salt and aluminum-containing rocks using NQR techniques. The investigation has been initiated using salt because this represents a simple, i.e., essentially one species, natural system. Once feasibility in salt has been demonstrated with optimized laboratory measurements, the study plan calls for two parallel programs: (a) in-situ stress measurements of salt and (b) development of techniques for determining stress in rocks. The details of the anticipated plan are shown in Table 1.

D. Prognosis

It was recognized, when this program was initiated, that there were many unanswered questions regarding the ability of NQR spectroscopy to provide stress information which was relevant to the rock mechanics experts. In particular there was the question of converting spectral data to useable mechanical information. Furthermore, there were questions as to what stress

Table 1. Anticipated Program Plan for NQR Measurements of Stress/Strain in Rocks

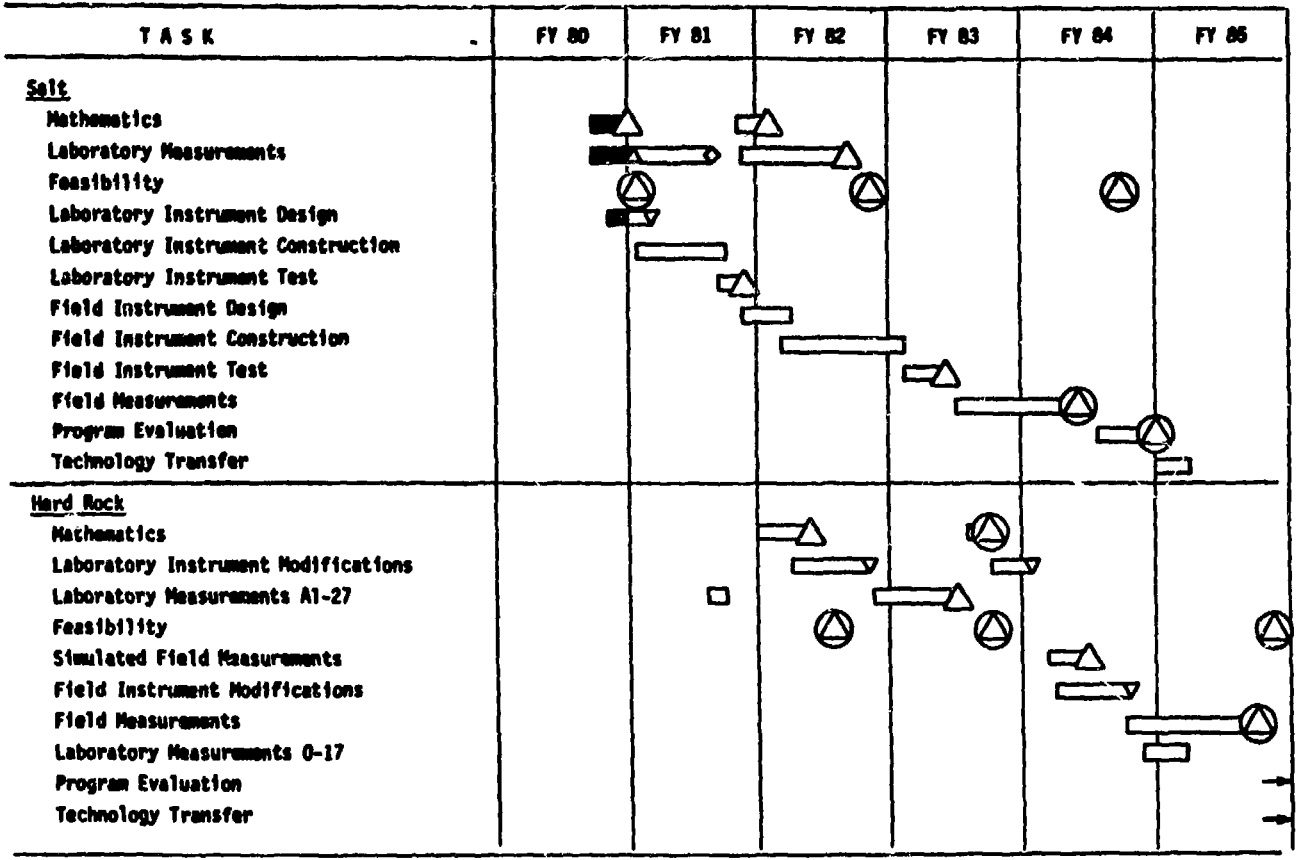

differences were resolvable and if instrumentation existed, or could be conceptually designed, which would have the capability of making the prescribed measurements.

LBL has not underestimated the difficulty of accomplishing the proposed objectives. To reach our goals requires fundamental research in both physics and instrumentation engineering. It also involves the synthesis of skills from several technical disciplines. It has not been possible to answer all questions or solve all problems in the first four months. However, considering the slow progress with which other stress measuring techniques have developed, outstanding progress has been made. The results are favorable and success of the program now appears within reach. Examination of the physics, spectroscopy, rock mechanics and (instrumental) engineering indicate there were no flaws in the original postulations. Calculations using spectral signal-to-noise indicates that three-dimentional pressures of 1.5 to 10 psi can be resolved.

II. TECHNICAL DISCUSSION

A. An Introduction to NQR

Nuclear quadrupole resonance (NQR) is a radio-frequency spectroscopic technique which, like nuclear magnetic resonance (NMR) uses the nucleus as a small, highly specific, probe of its environment. In NQR, one employs certain nuclei which possess electric quadrupole moments (those with spin $I \geq 1$) to study the electric fields with which they interact, or more specifically the electric field gradient (EFG) tensor. The EFG, in turn, varies in relation to

all the chemistry and physics in the crystal including the bonding configuration and distribution of valence electrons, the crystallographic site symmetry, crystal defects such as dislocations and impurities, and strains arising from both internal and external stress. Because the EFG is so very sensitive to the state of the lattice and because NQR is a resonance spectroscopic technique, it is often possible to see variations of one part in 10^5 or better. An overview of modern NQR spectrocopy appears in Appendix A.

Most details of the crystal lattice and chemistry express themselves primarily in terms of electrostatics, which NQR senses directly (the local magnetic fields studied in NMR are usually only a secondary consequence of changes experienced first in the EFG). Two other features serve to make NQR attractive to studies in geochemistry: (1) NQR is applied to solids--single crystals, polycrystalline materials, or amorphous materials (it does not work in liquids), and (2) NQR is suitable for field studies since it does not require a large heavy magnet as does NMR because the field parameter, the EFG, is intrinsic to the material.

In the studies undertaken as part of this project the focus has been on determining strain in rock salt, NaCl. In unstrained salt, both the sodium and chloride ions occupy sites of cubic symmetry, which by very general principles cannot possess an EFG. Thus the quadrupole coupling is zero. However, when subjected to non-isostatic stress, the crystal will deform producing non-cubic site symmetries at the Cl atom positions, thus producing a small EFG. For example, a compressive stress along [100] will make the crystal tetragonal, a stress applied along [110] makes the crystal orthorhombic, a stress along [111] changes the crystal to the trigonal class, etc. The field

gradient must reflect the site symmetry of the lattice. Experiments by Marsh and Casabella[8] indicate that the NQR frequency shift for Cl^{35} in NaCl is on the order of 30 Hz/atm.

The field gradient is not observed directly, but in the product e^2qQ where eQ is the nuclear quadrupole moment and is known a priori and eq is the maximum component of the EFG in the coordinate system in which the tensor is diagonal; e^2qQ is known as the quadrupole coupling constant and is usually expressed in units of frequency by dividing by Planck's constant, h. The existence of a non-zero e^2qQ means that the nuclei in the crystal will have a preferred orientation in space, and each orientation will be associated with a definite energy.[9] Owing to the quantum mechanical spin properties of nuclei, only certain orientations are allowed, giving rise to discrete energy levels. The nuclei in a solid can be made to absorb quanta of rf radiation as they "flip" between these energy levels. This is the phenomenon of resonance. In the case of Na^{23} and Cl^{35}, both of which possess nuclear spin 3/2, the resonance frequency ν is related to the quadrupole coupling constant via

$$\nu = \frac{1}{2} e^2qQ\left(1 + \frac{\eta^2}{3}\right)^{1/2} \qquad (1)$$

η is a quantity which depends on the departure of the EFG from axial symmetry. In the case of stressed salt, a measurement of ν determines q which in turn depends on the stress.

When e^2qQ is small, less than about 0.5 MHz, the pure quadrupole resonance is usually not observed directly because the sensitivity of detection becomes small. In this case, the quadrupolar coupling can be detected as

a perturbation on the NQR signal or by use of so-called double resonance techniques. The mathmematical and experimental details are described in the following sections.

B. NQR and Strain Measurements

From the theory of elasticity in linear media stressed below the elastic limit, the strain ϵ is related to the stress σ by the compliances s, giving Hooke's law in three-dimensions as

$$\epsilon_{ij} = s_{ijkl}\,\sigma_{kl} \tag{2}$$

(where the summation convention is used, meaning that a Σ over all repeated indices in an expression is to be understood). Although the s_{ijkl} form the components of a 4th rank tensor and thus consist of 81 separate elements, energy conservation considerations reduce the number to 36 independent elements in the general case, and in the cubic system, which concerns us here, to only three independent components s_{1111}, s_{1122}, and s_{2323} (Nye).[10] In the nearly universally used matrix notation in which the indices are condensed and summed from 1 to 6, we have

$$\epsilon_i = s_{ij}\,\sigma_j \tag{3}$$

with non-vanishing components in the NaCl class m3m

$$s_{11} = s_{22} = s_{33},$$
$$s_{12} = s_{13} = s_{23},$$
and
$$s_{44} = s_{55} = s_{66}. \qquad (4)$$

Measured values of the elastic compliances for NaCl exist in the literature (Nye)[10]

$$s_{11} = 2.21 \times 10^{-12} \text{ cm}^2/\text{dyne} \simeq 2.24 \times 10^{-6}/\text{atm}$$
$$s_{12} = -0.45 \times 10^{-12} \text{ cm}^2/\text{dyne} \simeq -0.45 \times 10^{-6}/\text{atm}$$
$$s_{44} = 7.83 \times 10^{-12} \text{ cm}^2/\text{dyne} \simeq 7.93 \times 10^{-6}/\text{atm}$$

In this work there are two other tensor properties of crystalline material of considerable importance. One is the electric field gradient (EFG) tensor ϕ_{ij} which determines the quadrupole interaction, and hence the resonance frequencies. The 2nd rank EFG tensor is traceless and symmetric (Schempp)[9], and thus contains five independent components, three of which can be thought of as determining the orientation of the principal axes, leaving two independent diagonal elements. In the following we shall adopt the usage that ϕ_{ij} represents the general EFG tensor with elements $\partial^2/\partial x_i \, \partial x_j \, (1/r^2)$ having dimensions of cm^{-3}. The parameters of importance to NQR, q and η are related to the components of the tensor V_{ii} in the coordinate system in which ϕ_{ij} is diagonal, where

$V_{ii} = e\phi'_{ii}$, e is the electron charge

$eq \equiv V_{zz}$ when the axes are chosen so that $|V_{zz}| \geq |V_{yy}| \geq |V_{xx}|$

and $\eta \equiv \dfrac{V_{xx} - V_{yy}}{V_{zz}}$ (5)

eq therefore has dimensions of volts/cm^3, and can be expressed in terms of frequency by multiplying by eQ/h; η is dimensionless satisfying $0 \leq \eta \leq 1$.

The other tensor property of interest is the "gradient elastic tensor," g_{ijkl} which relates the strain to the EFG via

$$\phi_{ij} - \phi^{o}_{ij} = g_{ijkl}\,\epsilon_{kl} \tag{6}$$

where ϕ^{o}_{ij} is the value of the EFG in the absence of strain. For cubic site symmetry, $\phi^{o}_{ij} = 0$, giving in matric notation

$$\phi_{ij} = g_{ij}\,\epsilon_{j} \tag{7}$$

Since the g_{ij}'s are a crystal property, they must obey the same invariance under symmetry operations as the elastic coefficients, resulting in a reduction of the 36 elements again to just three in the cubic case, g_{11}, g_{12}, and g_{44}. However, owing to the tracelessness of the ϕ_i tensor/matrix, one can only observe $(g_{11} - g_{12})$ and g_{44} as can easily be seen by writing out the components

$\Sigma\phi_i = 0$ requires $g_{11}(\epsilon_1 + \epsilon_2 + \epsilon_3) + 2g_{12}(\epsilon_1 + \epsilon_2 + \epsilon_3) = 0$

or $g_{12} = -1/2\,g_{11}$ (8)

The EFG can be written in terms of the stress by combining equations (2) and (6) or (3) and (7) to give

$$\phi_{ij} = g_{ijkl} s_{klmn} \sigma_{mn} = C_{ijmn} \sigma_{mn} \tag{9}$$

where

$$C_{ijmn} = g_{ijkl} s_{klmn}. \tag{10}$$

The C's may be called the "gradient-stress" tensor (Shulman).[11] In matrix notation, which will be used uniformly throughout the following, we have

$$\phi_i = g_{ij} s_{jk} \sigma_k = C_{ij} \sigma_j, \qquad i = 1 \text{ to } 6 \tag{11}$$

Making use of (4) and (8) for the cubic case, one obtains

$$\begin{aligned}
&\phi_1 = g_{11} [(s_{11} - s_{12})(\sigma_1 - 1/2 (\sigma_2 + \sigma_3)] = C_{11} [\sigma_1 - 1/2 (\sigma_2 + \sigma_3] \\
&\phi_2 \text{ and } \phi_3 \text{ obtained by cylic permutation of the indices} \\
&\phi_4 = g_{44} s_{44} \sigma_4 = C_{44} \sigma_4 \\
&\phi_5 = C_{44} \sigma_5 \\
&\phi_6 = C_{44} \sigma_6
\end{aligned} \tag{12}$$

Values of the g's and C's have been measured experimentally by several methods and although there is some scatter in the data, approximate values can be used to determine the magnitudes to be expected in NaCl (Table 2) (Kanert and Mehring).[12]

Table 2

Values of the Gradient Elastic and Gradient Stress Tensors in NaCl

	g_{11}	g_{44}	C_{11}	C_{44}
	10^{15} dyne$^{\frac{1}{2}}$ cm^{-2}		10^{3} dyne$^{-\frac{1}{2}}$	
Na^{23}	2.7	0.95	7.5	7.4
Cl^{35}	2.9	3.9	8.0	30.8

All these results have been obtained for compressive stresses and apparently no measurements have been made to date for tensile stresses.

It is possible to calculate the field gradients and NQR frequencies in a few special cases to see the general effects. For this we consider a cubic crystal oriented such that the [100] direction is along X_1, [010] along X_2, etc.

1. The simplest case involves a homogeneous uniaxial stress σ_0 applied along [100]

$$\sigma = \sigma_0 \begin{pmatrix} 1 & 0 & 0 \\ 0 & 0 & 0 \\ 0 & 0 & 0 \end{pmatrix} \tag{13}$$

Then

$$\phi_1 = C_{11}\sigma_0, \phi_2 = \phi_3 = -1/2\, C_{11}\sigma_0 = -1/2\,\phi_1, \text{ and } \phi_4 = \phi_5 = \phi_6 = 0 \tag{13}$$

or

$$|\phi| = -1/2 C_{11}\sigma_0 \begin{pmatrix} 2 & 0 & 0 \\ 0 & -1 & 0 \\ 0 & 0 & -1 \end{pmatrix} \tag{14}$$

The maximum component of the EFG is thus parallel to the stress direction, [100], giving $q = e\phi_1$ or e^2qQ_{Cl} = 46 Hz/atm, η = o

e^2qQ_{Na} = 55 Hz/atm, η = o

Since the NQR frequencies are given for the I = 3/2 case by

$$\nu = \frac{1}{2} e^2qQ\,(1 + \frac{\eta^2}{3})^{1/2} \tag{15}$$

we obtain in a uniform stress field of 100 atm

$$\nu_{Cl} = 2.3 \text{ kHz}$$

$$\nu_{Na} = 2.8 \text{ kHz} \tag{16}$$

These results can only be considered accurate to within a factor of 2. Marsh and Casabella,[8] for example, report equal frequency shifts for the Na and Cl for [100] stress. Accurate determination of the constants during the detailed laboratory phase of the work is a prerequisite for field work.

2. For a stress applied along [110], the stress tensor becomes, after carrying out a rotation of the coordinates,

$$\sigma = \sigma_0 \begin{pmatrix} 1/2 & -1/2 & 0 \\ -1/2 & 1/2 & 0 \\ 0 & 0 & 0 \end{pmatrix} \tag{17}$$

Thus

$$|\phi| = 1/4\,\sigma_0 C_{11} \begin{pmatrix} 1/4C_{11} & -1/2C_{44} & 0 \\ -1/2C_{44} & 1/4C_{11} & 0 \\ 0 & 0 & -1/2C_{11} \end{pmatrix} \tag{18}$$

Introducing the quantities $c = s_{44}/(s_{11} - s_{12})$ and $\gamma = g_{44}/g_{11}$, ϕ can be rewritten as

$$|\phi| = 1/4\sigma_0 c_{11} \begin{pmatrix} 1 & -2\gamma c & 0 \\ -2\gamma c & 1 & 0 \\ 0 & 0 & 0 \end{pmatrix} \tag{19}$$

This must be diagonalized in order to find the NQR parameters, resulting in

$$|\phi| = 1/4C_{11}\sigma_0 \begin{pmatrix} 1 + 2\gamma c & & 0 \\ & 1 - 2\gamma c & \\ 0 & & -2 \end{pmatrix} \tag{20}$$

In NaCl, using the data in Table 2, we find c = 2.94, $\gamma_{Cl} \simeq 1.34$, and $\gamma_{Na} \simeq 0.35$. The component of ϕ which determines the z-axis and q depends on whether $1+2\gamma c<2$, which means that $q = \phi_{zz}$, or whether $1+2\gamma c>2$ which means that $q = \phi_{xx}$. For Cl, $2\gamma c \simeq 7.88$, giving

$$|V|_{Cl} = 116 \text{ kHz} \begin{pmatrix} -2 & & 0 \\ & -6.88 & \\ 0 & & 8.88 \end{pmatrix}$$

$$e^2qQ_{Cl} = 10.3 \text{ Hz/atm}, \eta = 0.55$$

$$\nu_{Cl} = 5.2 \text{ kHz at 100 atm} \tag{21}$$

For Na, $2\gamma c \simeq 2.06$

$$|V|_{Na} = 1.37 \text{ kHz} \begin{pmatrix} -1.07 & & 0 \\ & -2 & \\ 0 & & 3.07 \end{pmatrix}$$

$$e^2qQ_{Na} = 42.2 \text{ Hz/atm}, \eta = 0.02$$

$$\nu_{Na} = 2.1 \text{ kHz at 100 atm} \tag{22}$$

For stress applied along [110], the principal axes directions are along [001], [110], and $[\bar{1}10]$.

3. If the stress is applied along the [111] direction, we first carry out a rotation of 45° around the z-axis, and then about y'-axis by 35.26°

$$\sigma'' = BA\sigma A^{-1}B^{-1}$$

$$\sigma_{111} = 1/3\sigma_0 \begin{pmatrix} 1 & 1 & 1 \\ 1 & 1 & 1 \\ 1 & 1 & 1 \end{pmatrix} \tag{23}$$

$$|e| = 1/3C_{44}\sigma_0 \begin{pmatrix} 0 & 1 & 1 \\ 1 & 0 & 1 \\ 1 & 1 & 0 \end{pmatrix} \tag{24}$$

which after diagonalizing, yields

$$|V| = 1/3C_{44}\sigma_0\begin{pmatrix} 1 & & 0 \\ & 1 & \\ 0 & & -2 \end{pmatrix}$$

$$e^2qQ_{Cl} = 119 \text{ Hz/atm}, \eta = 0$$

$$\nu_{Cl} = 6.0 \text{ kHz at } 100 \text{ atm}$$

$$e^2qQ_{Na} = 36 \text{ Hz/atm}, \eta = 0$$

$$\nu_{Na} = 1.8 \text{ kHz at } 100 \text{ atm} \qquad (25)$$

where the z-axis is along [111].

The intensity of the NQR lines depends upon the orientation of the linearly-polarized rf exciting field to the axis of the cylindrically symmetric EFG (the $\eta \neq 0$ case is more complicated). The intensity of the lines is a maximum when the field lies in a plane perpendicular to the symmetry axis (the Z-direction) and is zero when the field is parallel to the symmetry axis (Lucken).[13] This fact must be taken into account when working out the line-shapes to be expected for the general homogeneous stress. For example, in the [110] case, if the rf field is parallel to the stress direction, the line will not be observed.

No more than an estimate of the situation in a randomly-oriented polycrystalline sample can be given at this time. To do the calculation properly, one must determine the probability that a crystallite will have a given orientation with respect to the applied stress and weight the ensemble of field gradients by this orientation factor and the transition probabilities. However, it can be seen that the three special cases considered above represent extreme cases, and every other orientation must give rise to frequencies lying in the regions shown in Table 3.

Table 3

NQR Frequencies (in kHz) in NaCl as a Function of Orientation at σ = 100 atm

	[100]	[110]	[111]
Na^{23}	1.8	2.1	2.8
Cl^{35}	2.3	5.2	6.0
Cl^{37}	1.8	4.1	4.7

A completely random distribution, then, will result in lines approximately 3.5 kHz wide for Cl and 1 kHz wide for Na. A computer program is being generated to work out the line shapes in detail.

The petrofabric in the region of a salt-dome borehole may not present a wholly random orientation of the crystallites. In certain beds, very large "single" crystals with dimensions on the order of a foot or more have been found (Muehlberger).[14] It is generally accepted that a preferred orientation of crystallites in the final fabric is strongly related to the stress system applied (Kern).[15] There is some evidence that the [001] axes in halite are preferentially oriented parallel to the principal stress direction, i.e. [001] perpendicular to the axial planes of isoclinal folds in salt domes, which is in agreement with thermodynamic theory for stable crystal orientations under nonhydrostatic stress (Carter and Heard[16] and Kamb[17]). Therefore, although a polycrystalline mass may be expected, the crystallites may display a large degree of local order, i.e., a narrow distribution of orientation angles may exist. This will result in the NQR spectra also having narrower widths.

In the general case of stresses underground, the stress tensor is not uniaxial, but triaxial, i.e.,

$$\sigma = \begin{pmatrix} \sigma_1 & & 0 \\ & \sigma_2 & \\ 0 & & \sigma_3 \end{pmatrix} \tag{26}$$

The effect of additional non-zero elements in the stress tensor is generally additive, taking appropriate care of the signs. For a crystal having [001] // σ_3 and [010] // σ_2

$$|\phi| = C_{11} \begin{pmatrix} \sigma_1 - 1/2(\sigma_2 + \sigma_3) & & 0 \\ & \sigma_2 - 1/2(\sigma_1 + \sigma_3) & \\ 0 & & \sigma_3 - 1/2(\sigma_1 + \sigma_2) \end{pmatrix} \tag{27}$$

It can be seen that in the case of hydrostatic pressure, $\sigma_1 = \sigma_2 = \sigma_3$, this result assures that $|\phi| = 0$ as must be true in a cubic crystal. If σ_3 = 100 atm, and $\sigma_1 = \sigma_2$ = 50 atm, a situation which might be encountered at depth, we find

$$\begin{aligned} e^2qQ_{C\ell} &= 2.3 \text{ kHz}, \ \eta = 0 \\ \nu_{C\ell} &= 1.15 \text{ kHz}. \end{aligned} \tag{28}$$

Another factor to be considered is that the stress distribution around a borehole in a previously uniform stress field is no longer uniform, but the

radial component of the stress σ_r is a function of the distance from the borehole wall. At $\theta = 0$, for example,

$$\sigma_r = \sigma_x \left(1 - \frac{5}{2}\frac{R^2}{r^2} + \frac{3}{2}\frac{R^4}{r^4}\right) + \sigma_y \left(\frac{3}{2}\frac{R^2}{r^2} - \frac{3}{2}\frac{R^4}{r^4}\right) \tag{29}$$

which means that crystallites will experience differing stresses depending on their distance from the borehole wall (Cook).[2] The effect of such an inhomogeneous stress will be to further broaden the NQR lines. This can be taken into account by spectral line narrowing techniques such as deconvoluting the NQR lineshapes with the appropriate broadening function.

One final factor enters the picture. The frequencies of NQR lines sometimes show a temperature dependence which is related to the thermal motion of the atoms in the crystal lattice. In the case of salt, this effect will make the gradient elastic tensor, g_{ij}, temperature dependent. The elastic compliances, s_{ij}, will also be expected to show some temperature dependence, but for T<200°C this is expected to be small. Two different values for the geothermal gradient in Gulf Coast salt domes have been measured: 36°C/km and 22°C/km (Nichols[18] and Moses[19]). Therefore, temperatures 20° to 60°C above ambient may be expected in typical boreholes of interest. No information on the sensitivity of the values for NaCl in Table 2 to changes in temperatures is available at this time. From other NQR information, however, these variances are not expected to be critical. These would be measured in laboratory studies over the anticipated temperature ranges prior to field trials.

C. Resonance Techniques

Based on the results of Section B, the problem is to detect either the sodium or the chlorine quadrupole coupling in sufficient detail to extract the strain/stress information. The quadrupolar coupling will lie in the 1-15 kHz region for stresses up to 300 atm and the lines will be, perhaps, 1-10 kHz wide, depending on the degree of crystallite misalignment; the nature of the impurities, dislocations, and other crystal imperfections; and the inhomogeneity of the stress field resulting from the borehole deformation. There are three basic approaches: (1) direct detection (pure NQR), (2) quadrupolar perturbed NMR, and (3) double resonance methods. Each of these techniques has numerous variations. These are discussed below.

1) Direct Detection

Direct detection of the proton NMR signals in the earth's magnetic field (~0.5G) is routinely carried out in magnetometers; the resonant frequency here is ca. 2.1 kHz. NQR in chlorine will be more difficult because (a) the sensitivity of Cl NMR relative to protons is 4.7×10^{-3}, (b) the magnetometers employ a liquid which has a sharp line in contrast to the broad line from solid NaCl, (c) the proton instrument can be optimized for a single frequency, and (d) line shape information is not required. Overall it is likely that the instrinsic Cl S/N ratio will be at least 10^{-5} times smaller.

The idea, nonetheless, would be to apply a strong pulse to the sample in such a way that it's Fourier spectrum covers the bandwidth of interest, nominally a DC delta function. This would excite NQR transitions. A tuned receiver would then receive free induction decay signals, and the total spectrum mapped out by changing the receiver center frequency. Standard pulse techniques utilizing 90° and 180° pulses probably will not work here

because at 5 kHz "rf frequency" a single cycle is 0.2 msec long, which will not be short compared to $1/T_2^*$ as required (T_2^* is the dipolar linewidth).

Such an experiment has not been previously performed to the authors' knowledge, and would involve a considerable theoretical and engineering effort to determine its practicality. On the positive side, it eliminates the need for a large magnetic field and many complications from attempting remote detection of a double resonance signal, but it would not eliminate the intrinsic overlap between the Cl^{35}, Cl^{37}, and Na^{23} spectra.

This overlap arises from the fact that the quadrupole coupling constants of the three nuclear species present fall in the same range. Although the exact line shapes are not yet known, on the basis of preliminary considerations each nuclear species may produce a line something like the sketch below in a randomly-oriented polycrystalline sample.

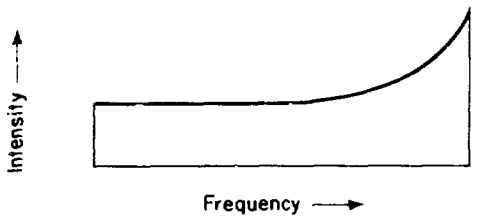

XBL 8012-2481

Since the two chlorine isotopes have quadrupole frequencies simply related by the ratio of their quadrupole moments, $Q^{Cl-37}/Q^{Cl-35} = 0.7883$, and intensities related by their isotopic abundance (Cl^{35} = .5%, Cl^{37} = 25%), there will be a superposition which can be determined. The position of the sodium line does not bear a deterministic relationship to the chlorines because the values of the Cl and Na gradient-elastic tensors differ, presumably owing to Sternheimer[13] anti-shielding effects. The composite line

will thus have roughly the form shown (for a random polycrystalline sample at 100 atm) in Figure 1.

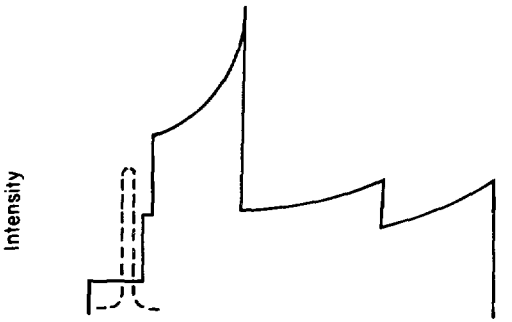

XBL 8012-2488

Figure 1. Shape of a polycrystalline NQR line in stressed NaCl (estimated).

The dotted line at 2.1 kHz will arise from the hydrogen in water resonant in the earth's magnetic field. This asymmetric line shape may prove to be an aid in identifying and measuring the spectral parameters related to stress.

Estimates of the water content in interstices and inclusions range from 0.1 to 1%. Although this percentage is low, the proton signals are relatively strong, and thus it is likely that the proton liquid NMR signal will appear. It will, however, be a constant independant of orientation and depth and, therefore, probably can be subtracted out. (The Na NMR frequency in the earth's field is 550 Hz, and that for the chlorines is even lower.)

2) Quadrupolar Perturbed NMR

In an NMR experiment a large, reasonably homogeneous magnetic field would have to be provided. For this discussion we will assume that a 1 kG field can

be obtained. In this case the chlorines will have a Larmor frequency of 0.4 MHz, and the sodiums will have a frequency of 1.12 MHz. This effects almost complete separation of the spectra, eliminating overlap. The sodium quadrupolar interaction is in the range of 2 ± 1 kHz. This method has been used to measure the quadrupole frequencies of neighboring shells around Br impurities in doped NaCl (Andersson[20]). It is well known that, when the quadrupole interaction is small compared to the Zeeman interaction, the transition energies are shifted, giving rise to a "powder pattern" in a random polycrystalline sample.[21]

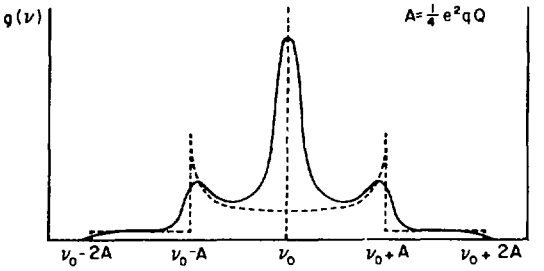

Figure 2. First-order quadrupole perturbation. Line shape for I = 3/2 in powdered samples of axially symmetric crystals (broken line). With dipolar broadening superimposed the full curve results. Frequently the satellites are spread out over such a large frequency range that the wings become unobservable.

In the event that there is a range of quadrupole interactions in the solid, a superposition of powder patterns is observed, which tends to produce a broad line. In this case, the details of the quadrupole interactions will have to be extracted in a different way, by using computer fitting, instead of visual inspection.

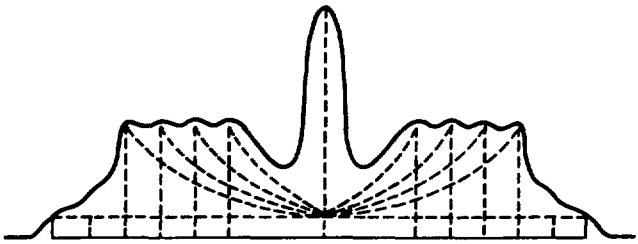

XBL 8012-6545

Figure 3. The overlap of many spectral components results in a broad line spectrum.

Since the interaction remains small enough that first-order perturbation theory is applicable, an unshifted "central" transition remains from the $+\frac{1}{2} \rightarrow -\frac{1}{2}$ spin states (Cohen and Reif).[21] This central transition contains no direct information about the quadrupole interactions present, but its amplitude grows smaller as more and more intensity is shifted to the wings. This feature has been used to measure quadrupole effects, including those due to stresses in cubic materials (Kanert and Mehring)[12] when a single value of e^2qQ is present throughout the sample. This approach will be complex to use in the presence of an inhomogeneous EFG such as expected in natural systems.

If a sufficient number of resolution elements can be obtained, the NMR method offers experimental simplicity. A magnetic field can be generated by a solenoid coaxial with the borehole, a simple 90° rf pulse applied, and the free induction decay (FID) recorded. The FID contains all the line-shape information (Lowe and Norberg).[22] Corrections for magnetic field and rf field inhomogeneities would be required.

3) Double Resonance

Double resonance techniques have been developed in recent years which offer enormous increases in sensitivity in the detection of weak NMR and NQR signals. The idea behind double resonance techniques in magnetic resonance is to use the strong signal presented by one nuclear species (A) to detect a weak signal offered by another species (R), where the weakness may arise from low isotopic abundance, low frequency, or long relaxation time. In the case of quadrupole effects in stressed NaCl, the problem is the low frequencies of the stress-induced quadrupole coupling constant (QCC). A number of different schemes have been developed to obtain a gain in sensitivity.

These techniques consist essentially of "NQR calorimetry" performed between two spin systems which can be prepared at different spin temperatures. The A spins are abundant and this magnetization is easy to measure. The second species R are rare or otherwise difficult to detect directly. The experimental cycle consists of a basic four-step process:

i. The A spins are prepared in a polarized state;

ii. The R spins are polarized by making thermal contact between the two spin systems;

iii. An oscillating magnetic field of frequency ω_R is applied to the sample at the R-spin transition frequency;

iv. Steps ii and iii are repeated several times, or maintained for a long time, and the state of the A spin system is re-determined. A heating of the A spins is evidence for power having been absorbed by the R spins, and thus the R resonance is detected indirectly.

Of several double resonance methods, a few can be dismissed as not suitable for the experiments on salt. These include spin echo double resonance (SEDOR) because large static magnetic fields are required giving no advantage

over conventional resonance methods; double resonance in the rotating frame (DRRF) suffers from the same defect; double resonance in the laboratory frame (DRLF) is not generally suitable for detection of quadrupole interactions below 200 kHz, and in any case often renders details of the line shapes unobservable.

This leaves two methods with a high probablity of success--spin-mixing by level crossing (DRLC) and continuous coupling. Both methods are closely related (Koo[23], Hahn[24], Edmonds[25]). Continuous coupling requires magnetic field cycling and a three-step experimental cycle: polarization, irradiation, and detection. The sample is intially placed in a large magnetic field H_0 for a time sufficient for both sets of spins (the A and the R) to reach equilibrium with the lattic temperature T_L. This time will be at most on the order of several times the longest T_1 in the sample; since T_1 (Na) $\simeq$ 12 secs, the equilibrium time might be as much as 30 secs. The magnetic field should be as large as practicable, about 1 kG for a field instrument or 10 kG for a laboratory set-up. A 1 kG field is practical in the presently conceived in-situ measuring configuration.

The sample is now removed bodily from the magnetic field, or the field is switched rigorously off in a time as short as possible, < 1 sec. During this time, the Zeeman splitting of the A spins (Na^{23}) collapses, and in doing so crosses over the quadrupole energy levels of the R spins (Cl^{35} and Cl^{37}). The R spins thus become partially polarized by energy exchange, and now reside in a zero applied field.

Immediately after the H_0 field is zero, a continuous rf field at frequency ω_R (the chlorine transition frequencies) is applied for a time

necessary to saturate the R spins (3-5) secs). At the completion of this irradiation, the magnetic field H_o is switched back on again, and the A spin magnetization measured, by applying a single $\pi/2$ pulse and observing the free induction decay signal (FID). This cycle is repeated for different values of ω_R until the region of interest is covered--in the case of Cl in salt, 2-10 kHz. Before the start of each new cycle, a saturation comb of $\pi/2$ pulses for the A spins initializes the polarization in that system.

The sensitivity of the method depends on the number of R system "spin flips" which occur during the R-irradiation phase. This will depend upon the number of Cl transitions excited within the bandwidth of the ω_R pulse when it is desired to detect a broad line, as in the case of salt. The sensitivity can be very high, particularly for the spin 3/2 case (Edmonds).[25] It is not clear how much resolution may be obtained. Double resonance by continuous coupling has had considerable success in detecting QCC's in deuterium, ^2H, at natural abundance (Edmonds and Mailer),[26] and this problem presents many of the same features found in the salt problem. It therefore appears that sufficient resolution is available.

The experimental procedure in this case will present a number of challenging problems, one of which is that all the species present will

possess multiple energy levels which will collapse and cross over when the field is switched off in a complex way (Figure 4).

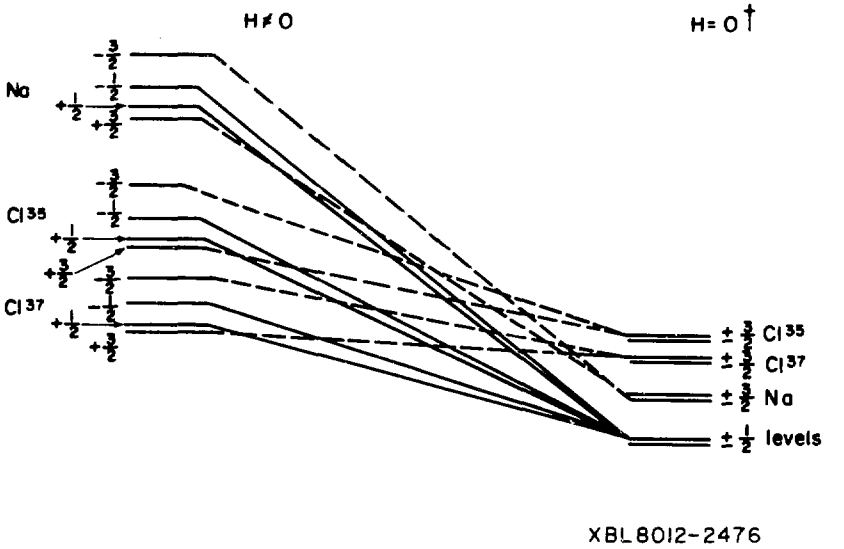

Figure 4. NaCl level crossing diagram.

†The earth's field is always present, of course, producing splittings on the order of a few hundred hertz in the pure quadrupole frequencies.

Although these multiple crossings as the energy manifolds collapse present considerable theoretical difficulties to analyze in detail, it is not obvious that it makes the experiment any more difficult nor the extraction of the information need to determine stress. The "central" $+\frac{1}{2} \rightarrow -\frac{1}{2}$ transition in the sodium spectrum can be monitored as the "abundant" species to detect the low quadrupole frequencies in the chlorines. Because of the overlap, the observed spectrum will be a superposition of three lines as shown in Figure 1.

The continuous coupling procedure differs from a level crossing experiment (DRLC) only subtly. In the latter, a partial polarization in the R spin magnetization is introduced as the spin multiplets collapse to their zero-field values. If during the irradiation phase ω_R corresponds to an allowed R spin transition frequency, power is absorbed, changing the R spin level populations. When the H ≠ 0 state is restored, additional level crossings take place allowing a transfer of energy ("heat") between the R and A spins.

The so-called zero-field energy levels are not in fact in a strictly H = 0 state. For one reason, the earth's magnetic field is still present, which gives energy levels of a few hundred hertz. More important is the dipolar coupling between the spins, which may produce effective internal fields of several gauss, and thus produce energy levels extending up to tens of kilohertz. (In fact, it is this internal dipolar coupling which makes energy transfer between the spins possible and thus is essential to the whole experiment.) Thus, at very low values of the coupling constant, the two spin systems make continuous thermal contact in zero applied field owing to partial overlap of their absorption spectra. Irradiation at ω_R then also causes transitions among the A spin levels. Hence, there is a competition at a given frequency between direct absorption by the A spins and absorption by the R spins and subsequent transfer of power to the A spins by mutual spin flips which conserve the total spin energy. The relative probability of these two absorption mechanisms depends on many factors e.g. the density of A spin states at the irradiation frequency compared with that of the R spins, the relative magnitudes of the matrix elements which govern photon absorption, and spin diffusion effects. The competition between direct absorption by the A

spins and indirect absorption through the R spins has been shown not to be a problem. For example, in the case of 5% enriched D_2O in H_2O, it was possible to destroy virtually all the proton magnetization by irradiating the deuteron quadrupole resonance with such a low power level that almost no proton absorption occurred. The ultimate limitation on the sensitivity, therefore, is the competition offered by direct A spin absorption (Edmonds).[25] This can only be answered by laboratory experiments.

The foregoing discussion suggests that the two most promising approaches are quadrupolar perturbed NMR and double resonance by continuous coupling (DRCC). Both schemes present some difficulties, but they do seem surmountable using existing technologies. These include the following: (a) A magnetic field produced by a coil generates heat owing to ohmic losses. A cooling system capable of dissipating a few kilowatts will, therefore, have to be provided. (b) For DRCC, it will be necessary to turn the magnetic field off and on in short times, less than about 1 sec, and this requires careful but realizable engineering design. (c) Any magnetic field generated in a borehole will fall off in intensity with penetration depth and thus only the nuclei in an annulus, not more than 1 cm wide, can be effectively in the same field. The resulting field inhomogeneity makes a more complex NMR signal or FID, and decreases the linewidths of the FID and echo, thus requiring fast electronics. (d) The field inhomogeneity limits the amount of material which can be sampled at any one time. This can be partially compensated for by making an oval-shaped rf coil, perhaps 1/10 of the borehole circumference as its small diameter and up to about 150 cm long. This would encompass a volume of several liters (>5 kg of salt).

(e) The last problem is the intrinsic overlap of the Na^{23}, Cl^{35}, and Cl^{37} (and possibly H^{1}) signals in the spectrum, if DRCC is used. This factor, plus the fact that the lineshapes will depend on the stress field, the orientation of the crystals, and the orientation of the rf exciting field to both of the foregoing, means that it is unlikely that there will be any simple one-to-one correspondence between visually recognizable features in the spectrum and the stresses. However, mathematical treatments of the spectra, e.g. Fourier transforms,[27] together with a sufficient laboratory data base, make it possible to process the input information in the computer and output a value directly related to stress. Thus field measurements could be related to the stress by reference to model spectra obtained from careful laboratory measurements. This phase of the work must be begun before detailed elaboration on this point can be given. There will also be contributions to the NQR spectra from lattice defects which must be studied.

Based on extent knowledge the LBL and LLNL technical staffs believe the DRCC method has a high chance of success. As a back up, the NMR perturbation method can be considered. Most of the equipment items will remain the same between these two system technologies, so the cost of switching from one to the other will be minimal.

D. CHOICE OF MEASUREMENT TECHNIQUE

Several major choices have been made in designing and predicting the potential of a borehole NQR stress/strain sensor.

1) Choice of Measurement Technique

The pure NQR stress-induced absorption in NQR occurs at a few kHz frequencies, where transitions saturate at extremely low power levels, 1/f

noise becomes a severe problem, the sensitivity of electronics and receiver coils is much reduced, and spatial and directional resolution is limited.

By going to the double resonance method as discussed in Section II.C.3, the NQR excitation is measured as a perturbation of an NMR signal observed at a higher frequency in the presence of a strong magnetic field. The inconvenience of having to furnish this field is far less than the difficulties associated with solving the above problems. On the other hand, field nonuniformity restricts the effective sample volume more the higher the center frequency, for a given bandwidth. After detailed calculation, however, the S/N levels for pure NQR measured directly and via the double resonance are 37 and 320, respectively. This represents a substantial gain for the double resonance technique even while disregarding its engineering virtues.

Occasions have been reported in the literature where the S/N gain of the double resonance is not realized because energy transfer does not occur rapidly enough, and the various magnetizations relax to thermal energy before being measured. Here we must remember that these energy transfer rates show order of magnitude increases when the NQR and NMR energies are exactly equal (resonance) as will happen at some point as the field drops, since NMR energies are field dependent and NQR ones are not. However, since the field spends equal time at all intermediate values, it must either spend too much time in the resonance region or too much in the entire process of reducing the field. Either way, sensitivity losses occur. In the present situation, however, we know exactly at what field level the resonance is expected, because for a particular NQR irradiation frequency there is a specific matching magnetic field. We thus can irradiate at a specific NQR frequency and follow this by a double resonance measurement in which the falling field

drops rapidly to the resonance levels, waits there an optimum time, and then completes its drop.

2) Choice of Mapping Method

Because the principal stress contours perpendicular to the direction of the cylindrical hole produce a dipolar field, it is theoretically possible to map this field by measuring the strain distribution and calculating the direction and magnitude of the stress causing the observed strain.

Two methods can be used for measuring stress/strain in salt formations. The first one generates a three-dimensional map of NQR transition frequencies (and thus stress/strain) in the strata around the sample, and carries this map far enough from the borehole to get out of the region of stress/strain disturbances produced by the borehole. The other measures the integral signal at each azimuth from the surface layers of the borehole, and measures the azimuthal variation produced by the borehole stress/strain disturbance. The measured disturbance is linked to the original stress/strain by a functional relationship that is then inverted.

3) Mapping the Surrounding Strata by NQR

The spectrometer will be tuned to the specific frequency of the Na^{23} NMR line at the magnetic field used. The measurement technique will be spin echo NMR, in which the sample gives a delayed "echo" pulse a few milliseconds after irradiation with a radio pulse, for which the field-intensity pulse-duration product has a specific value. Since the radiofrequency magnetic field falls away rapidly with distance from the transmitting coil, only points along a specific radial distance element around the borehole axis will contribute to the signal for a given power in the coil. By changing the power

in the transmitting coil, this radial distance will change, and maps of the NQR signal as a function of radius can be made by scanning the coil power (Figure 5).

A similar technique can be used to discriminate the radial direction. By using appropriate coil shapes (supplemented if necessary by ferrite inserts) the field it produces can be made completely circularly asymmetric, so that the proper field is reached at different ranges in different directions. Three possible configurations are; a "horseshoe", Figure 6, a canted transmitter loop with receive loops above and below, Figure 7, and an array of three or more half wave dipoles, Figure 8.

The "horseshoe" provides some control of close-in fields with and without high permeability cores, but may not provide any significant directivity even at a small number of multiples of the pole spacing. Figure 9 is an heuristic illustration of the magnetic field for this kind of configuration. The length l is long compared to the diameter d. Magnetic field strength vs. distance and angle, centered on the length in a plane perpendicular to the faces, can be calculated. If this directional transmitting coil is now combined with a rotating, directionally-sensitive receiver coil, a map of NQR signals as function of azimuth and radius vector can be constructed.

The vertical scan can now be provided by simply moving the coils and their associated electronics up and down.

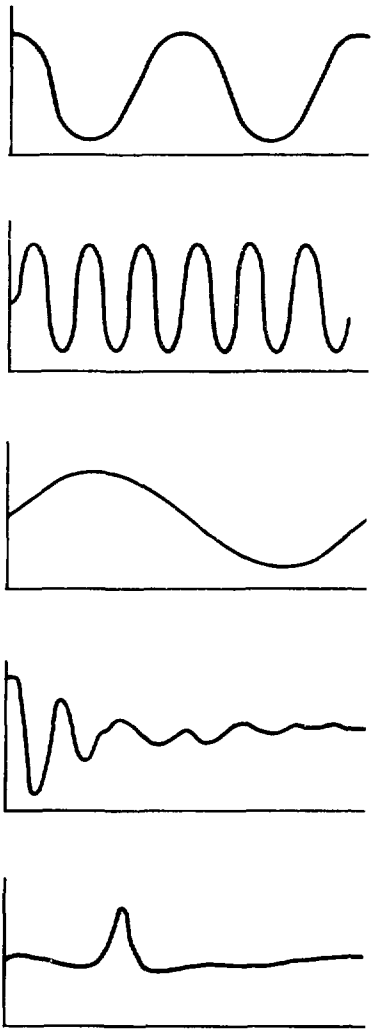

XBL 8012-2485

FIGURE 6 RANGE RESOLUTION IN SPIN ECHO MEASUREMENTS

FIGURE 6

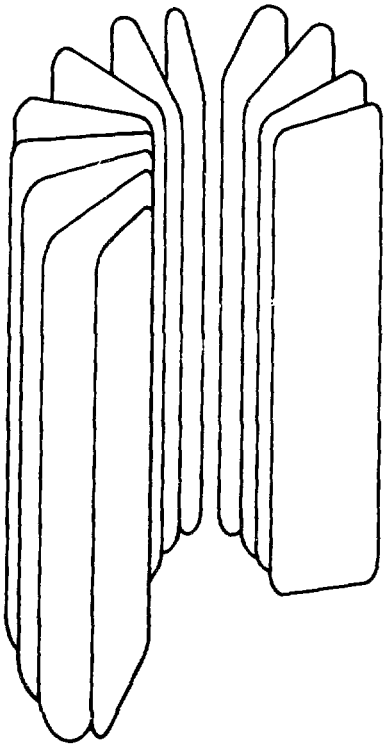

XBL 8012-2480

FIGURE 6. HORSESHOE COIL FOR DIRECTIONAL TRANSMITTER

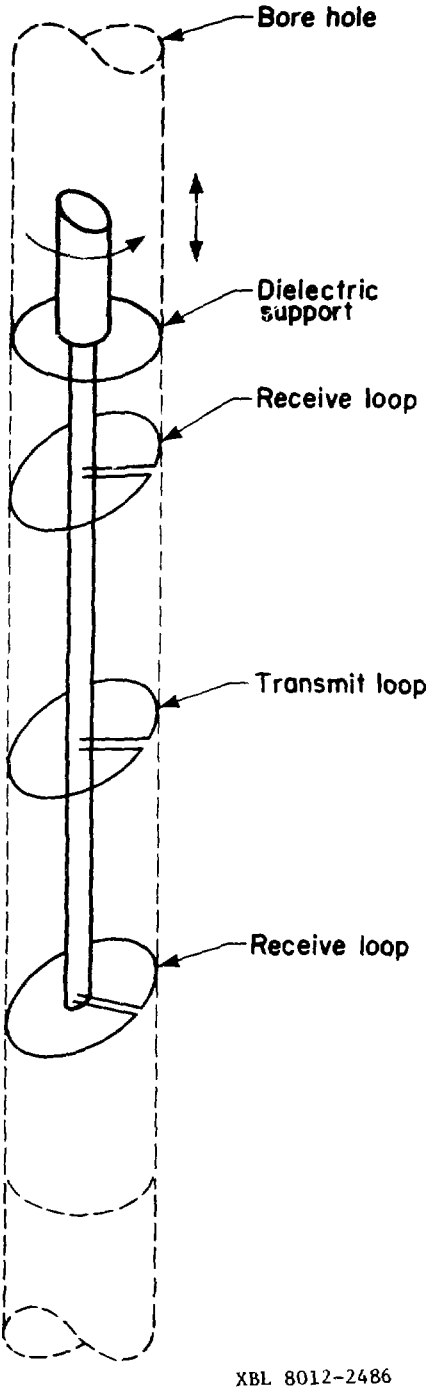

XBL 8012-2486

FIGURE 7. CANTED TRANSMITTER/RECEIVER LOOPS FOR SPATIAL RESOLUTION

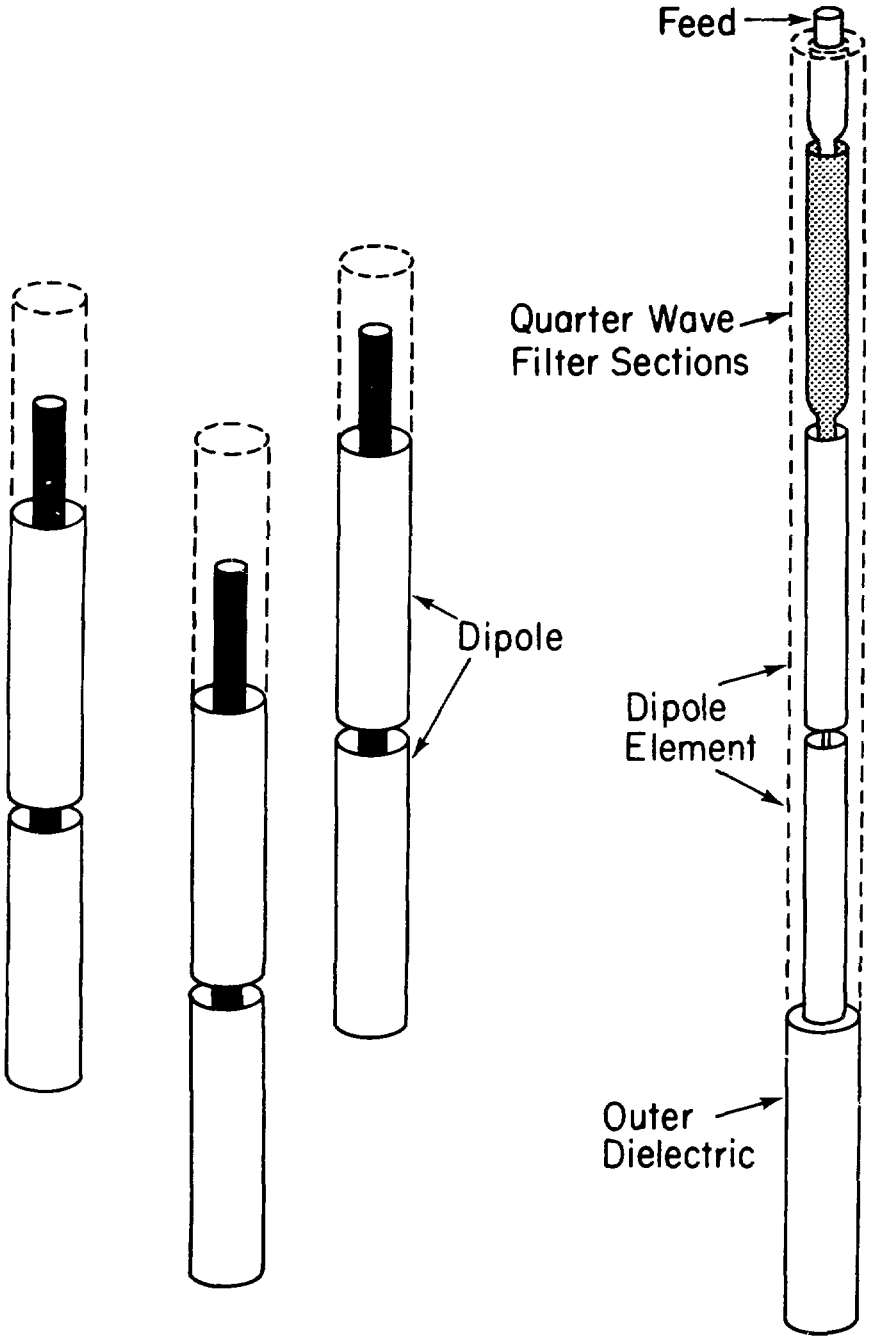

XBL 8012-6544

FIGURE 8. ARRAY OF HALF-WAVE DIPOLES FOR SPATIAL RESOLUTION

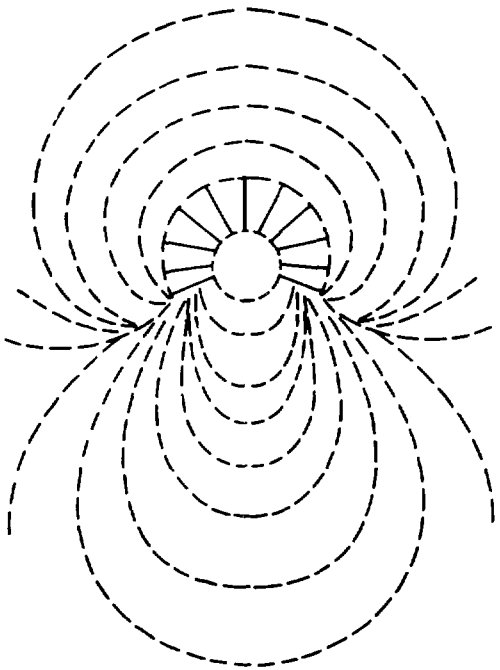

XBL 8012-2479

FIGURE 9. MAGNETIC FIELD LINES OF HORSESHOE COIL

4) Mapping the Borehole Perturbation by NQR

To use the borehole perturbation approach, the details of the borehole stress/strain field interaction must be considered. The stress tensor can be revolved into three orthogonal principal stresses, σ_1, σ_2 and σ_3, the planes containing any two being those of zero shear stress, and the three principal shear stresses, Σ_1, Σ_2, and Σ_3. It is normally assumed that one of the principal stresses acts vertically and is due to lithostatic pressure, and that the remaining two are oriented horizontally. This is not always the case but for the purpose of this discussion, is first assumed to be so. A more general case, in which this orientation does not hold, can be taken into account quite readily. According to Cook,[2] "many mine excavations such as boreholes, shafts, and drifts can be approximated closely by a cylindrical hole. The most useful single analytical solution in rock mechanics is, therefore, that for the region outside a circular hole with given principal stresses at infinity. If the principle stresses at infinity normal to the axis of the hole are σ_v and σ_h and the radius of the hole is R, the state of stress outside the hole is given by

$$\sigma_r = \frac{1}{2}(\sigma_v + \sigma_h)(1 - \frac{R^2}{r^2}) + (\sigma_v - \sigma_h)(1 - \frac{4R^2}{r^2} + \frac{3R^4}{r^4})\cos 2\theta \tag{30}$$

$$\sigma_\theta = \frac{1}{2}(\sigma_v + \sigma_h)(1 + \frac{R^2}{r^2}) - \frac{1}{2}(\sigma_v - \sigma_h)(1 + \frac{3R^4}{r^4})\cos 2\theta \tag{31}$$

$$\tau_{r\theta} = \frac{1}{2}(\sigma_v - \sigma_h)(1 + \frac{2R^2}{r^2} - \frac{3R^4}{r^4})\sin 2\theta, \tag{32}$$

for any radius, r, and direction, θ, measured counterclockwise from the vertical.

"Equations (30-32) above define the total state of stress. The change from the original state of stress induced by excavating the hole is given by the following components of these equations.

$$\sigma_r' = \frac{1}{2}(\sigma_v + \sigma_h)\left(-\frac{R^2}{r^2}\right) + \frac{1}{2}(\sigma_v - \sigma_h)\left(-\frac{4R^2}{r^2} + \frac{3R^4}{r^4}\right)\cos 2\theta \tag{33}$$

$$\sigma_\theta' = \frac{1}{2}(\sigma_v + \sigma_h)\left(\frac{R^2}{r^2}\right) - \frac{1}{2}(\sigma_v - \sigma_h)\left(\frac{3R^4}{r^4}\right)\cos 2\theta \tag{34}$$

$$\tau_{r\theta} = \frac{1}{2}(\sigma_v - \sigma_h)\left(\frac{2R^2}{r^2} - \frac{3R^4}{r^4}\right)\sin 2\theta. \tag{35}$$

Equations (33-35) show that the induced changes in stress are confined to the rock adjacent to the hole, as would be expected from St. Venant's principle. At the boundary of the hole, r = R, these induced stresses have an important property: they are equal in magnitude and direction but opposite in sign to the virgin state of stress acting on that boundary before the excavation of the hole. The sum of the induced state of stress and the virgin state of stress yields that total state of stress everywhere including the stress-free boundary. This is the basis of integral methods for numerical solutions described later.

"In Figure 10 a solution to equations (30-32) is illustrated in the form of principal stress contours and trajectories, for $\sigma_v = 1$ and $\sigma_h = 1/2$, in the upper right and left quadrants, respectively."

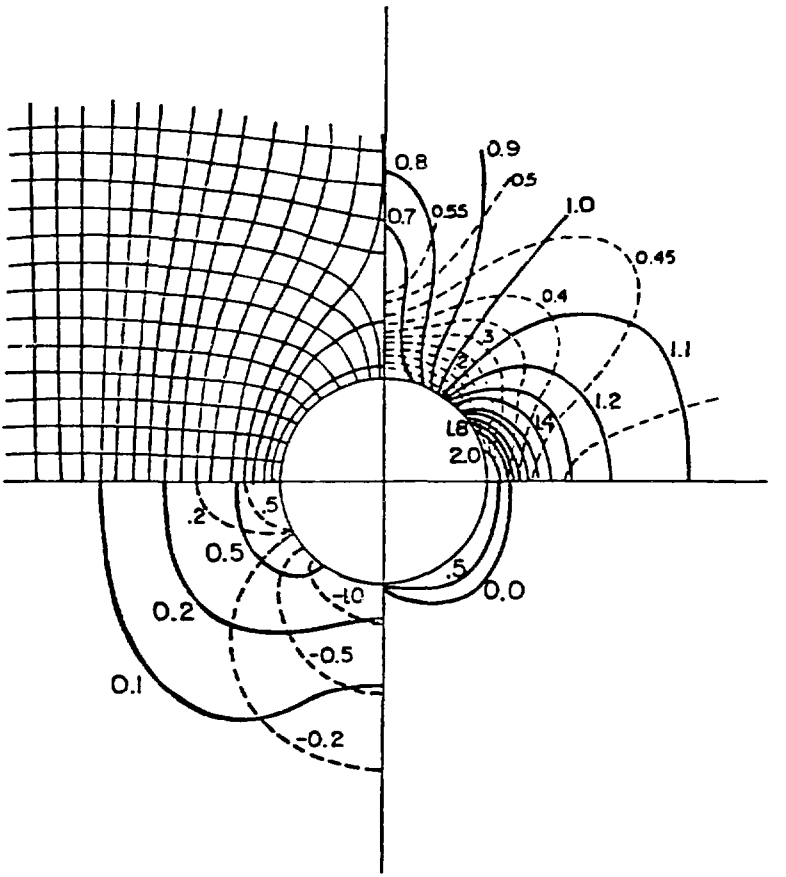

FIGURE 10. A sketch showing the results of Kirsch's solution for the stresses around a long circular hole subjected to a vertical principal stress with unit value and a horizontal principal stress of half this value. Contours of the values of the principal stresses are drawn in the left quadrant. In the lower right quadrant, are drawn contours of σ_1-$5\sigma_2$, and in the left quadrant contours of the sums of, and differences between the principal stresses.

These equations can be numerically inverted by generating a lookup table of their predicted results and then determining the initial stress/strain curve in the salt bed by interpolation.

This method has several advantages over the full mapping one:

1) Instead of experiencing the borehole distortion as a difficulty, it actually is used as the detection mechanism.

2) The measured regions are much closer to the coil with an inverse cube signal gain.

3) A considerable sample volume is integrated rather than only a small region as used in mapping.

4) The directionality requirements on the coil are released, owing to the high symmetricity of the borehole distortion pattern.

5) No need for computationally-complex, signal-to-noise reducing, zeugmatographic range resolution.

6) The volume of data is sharply reduced.

3) Operational Scenario

To pinpoint the wavelength to an accuracy of a fraction of a line, one needs at least two measured samples per bandwidth, high S/N, and a good interpolation routine. This reduces the necessity for scanning a great many points in the spectrum to determine the correct peak frequency.

A further cut in the number of separate measurements needed (each of which consumes about 1/2 min) can be accomplished by using approximate estimates for the stress/strain and thus the frequency value. If one extrapolates from either the previous azimuth or depth, these estimates become fairly indicative unless the stress/strain has rapid spatial variations. In

these cases, as little as 2-3 measurements are enough to accurately pinpoint the center frequency if the initial estimate came within ±25 atmospheres of the correct value.

To resolv the azimuthal pattern may then require 4 to 8 measurements, but this again may be reduced by extrapolation from a different depth. In any case, 10-30 measurements, involving 10-15 minutes elapsed time, seem sufficient to characterize a given depth element, and a complete stress/strain map of a borehole would take under a day.

E. Description of an NQR Stress Sensor for Borehole Operation

The main subsystems of an NQR borehole stress sensor are (Figure 11):

1) A magnetic field generator, containing
   a) A field solenoid
   b) A power supply
   c) A cooling system
2) An NMR-NQR double resonance transmitter-receiver, comprising
   a) An NQR irradiator
   b) A rotating transmit/receive coil
   c) A matched, switched network and preamplifier
   d) An NMR transmitter/receiver
   e) A data system

1) Magnetic Field Generator

(a) Field solenoid. The purpose of this is to generate a ~1000 gauss field within the sodium chloride bed in the immediate vicinity of the borehole wall. This coil must be moderately long, to achieve reasonable axial

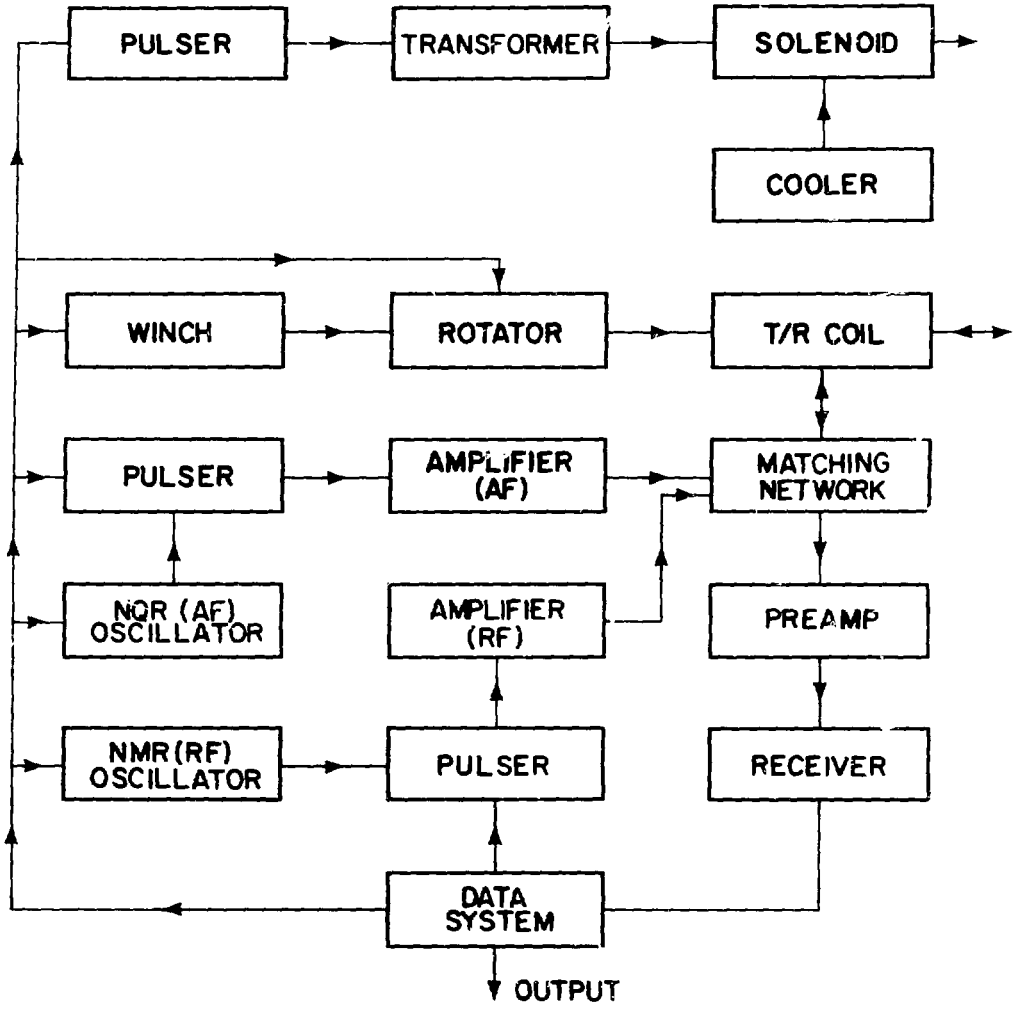

FIGURE 11. BLOCK DIAGRAM OF NQR BOREHOLE STRESS SENSOR.

homogeneity of the field around its center. In practice, further improvement in this homogeneity may be possible by increasing the winding density or layering near the ends. A longer coil also increases the size of the instanteously observed sample volume and thus the signal-to-noise ratio (S/N). Eventually, the increased power requirement, which goes as the square root of the coil length, the physical dimensions of the system, the required depth resolution of the measurement, and the progressively closer approach of the coil to resonance with its on-off switching frequency, limits the total length. A detailed calculation of power requirements in the coil, assuming a 10 cm borehole diameter, indicates that for a coil length of 150 cm the peak power requirement will be 100 kW. Here the duty cycle including high, zero, and transfer field wait times will be 25%, indicating an overall power consumption of 25 kW.

This power consumption is based on using standard, circular cross-section wire, with an optimum diameter of 5 mm. A better solution uses spiral wound foil, giving not only reduced power consumption but a much higher resistance and thus a better match to a power source. Consider a coil wound of such strips with width u, thickness v, and length l. The number of turns, n, is given by

1) $$n = \frac{\ell}{v} \tag{37}$$

and the resistance, R, is

2) $$R = \frac{2\pi r_B n \rho}{uv} \tag{38}$$

where r_B is the radius of the strip and ρ is the specific resistance.

Substitution of 1/v for n gives

3) $$R = \frac{2\pi r_B \ell \rho}{uv^2} \tag{39}$$

Then from basic theory,

4) $$I = \sqrt{P/R} = v\left(\frac{Pu}{2\pi r_B \ell \rho}\right)^{1/2} \tag{40}$$

where I is the current and P is power.

The central field of the solenoid, H, is

5) $$H = \frac{\pi u I}{5 r_B h} \tag{41}$$

where h is the height of the coil, while the field immediately exterior to its winding, H_0, is

6) $$H_o = \frac{\pi}{5}\frac{1}{v} \tag{42}$$

which further gives

7) $$H_o = \frac{\sqrt{\pi}}{5\sqrt{2}}\left(\frac{Pu}{r_B \ell \rho}\right)^{1/2} \tag{43}$$

from which it can be shown that the input power required, W, is

8) $$W = \frac{50}{\pi}\left(H_0^2\right)\left(\frac{r_B \ell \rho}{u}\right) \tag{44}$$

If we use here the value

$$u = 1.5 \text{ cm}$$

and the same values for the other variables as used for wire windings, then

$$W = 28 \text{ kW}.$$

This is a slightly more favorable value, which after application of the duty cycle, becomes

$$W = 7 \text{ kW}$$

Alternatively, higher values of H_0 for better S/N may be considered by using a 25 kW input to the ribbon windings.

On the other hand, the effect of this change on R, I and V is large. The former values, for circular conductors, were

$$R = 0.166\ \Omega$$
$$I = 776 \text{ A}$$
$$V = 129 \text{ V}$$

For this improved conductor, and choosing

$$v = 0.20 \text{ mm}$$

we obtain

$R = 27.2\ \Omega$

$I = 32$ A (or 1/4 of this average)

$V = 865$ V,

a much more favorable electrical condition, avoiding the need for a down-hole transformer and allowing simple power feeds via a reasonably low current cable.

Calculation of the inductance and self-resonance of such a coil shows it still to be compatible with rapid on-off switching.

Such coils do not, of course, give radially homogeneous fields, which limits the observation volume V to the small values described above. These, however, are still large enough to give the desired S/N with a substantial safety margin.

If even lower power consumption appears desirable (for which there is little demand) or higher H_0's are wanted (conservative design led to adoption of an easy to reach H_0), ferromagnetic inserts such as ferrites appear workable. An alternative, having no power consumption, but requiring a powerful winch for spatial rather than electrical switching, is a large permanent magnet. Here the required field is obtainable with greater simplicity but equal cost (large permanent magnets are expensive).

(b) Power supply. Transmitting power to the bottom of a borehole is much easier at the reasonable current and lower voltage of the strip wound coil. 1100V power is readily available, being one of the standard power distribution voltages for which small, vehicle-mountable transformers are available if the

motor generator operates at some other voltage. Complete with all necessary insulation, an armored cable for this voltage and peak current, capable of carrying the required current for 1-2 miles, is about 1/2" in diameter, and produces power losses not exceeding 20%.

To generate the necessary power, a generator having about 50 kW power is necessary to cover the power losses, remaining electronic systems, etc. Mobile, vehicle-rated military power sources in this range typically operate at 440 Hz to achieve small size and low cost. Of course, the power supply to this coil must be rectified.

A much smaller power supply can be built using a resonant accumulator topside. This would allow using a 15 kW power supply for the same job, but would require storage of about 100 kJ of electrical energy and be counterproductive in cost. A few kW of additional electrical power will be required at the sensor for operating all other systems and could best be provided by sending down electrical AC power over the same cable, and separating them with a small filtering transformer in the borehole. This filtering would be aided by the high impedance of the coil.

This power source must furnish power at two levels to the coil; one enough to produce H_0=1000 gauss, as discussed previously, as well as a "trickle" level of 5-25 gauss during which the NQR excitation transfers to the NMR domain. This trickle level is adjusted to scan from one stress/strain range to another. The switching between power levels must occur rapidly, roughly as fast as the coil ringdown time. During the NQR excitation, the coil will be completely shut off.

(c) Cooling system. The dissipation of an average of ~10kW power at the bottom of the borehole would constitute an appreciable problem, as heating of the sample will shift its NQR frequencies as well as create new stresses. To avoid this, a coolant flow must extract this heat, mainly from the field solenoid.

To do this via water cooling, the coolant flow can be calculated by

$$G = 0.004 \frac{\bar{P}}{\Delta t} \tag{45}$$

where Δt is the water temperature increase, G its flow rate in liters/min, and P the average power. If we now take

$$\Delta t = 10^{o}C$$

we arrive at

$$G = 4 \text{ liters/min.},$$

a quite comfortable flow rate.

2. NMR/NQR Double Resonance Transmitter -- Receiver

(a) NQR Irradiator. This essentially audiofrequency oscillator-pulser amplifier chain serves to irradiate the NQR absorption frequencies in the sample. The absorbed energy then interacts with the NMR energy levels, during the transfer time, at which point the magnetic field is held at a level at which both transitions are at the same energy and resonate.

The frequency coverage required here is limited by the maximum pressure to be measured. If we assume this to be about 1000 atm, some tens of kHz will be adequate. Since the bandwidth of the system is ~1 kHz, to measure the actual transition frequency a scan through about 40 resolution elements would be required for a stress/strain measurement.

In practice, each measurement will show some correlation with those taken at the previous azimuth and the same depth or the same azimuth and a previous depth, so that on the average a 3-5 point scan will be enough. The high pressure resolution of the measurement will actually come from high accuracy location of the NQR line center.

The power required here will be small, as saturation is easy to achieve at these low frequencies. Typically fields of a few gauss, requiring powers of a few hundred watts, will be enough.

(b) A rotating transmit/receive coil. This toroidal coil is wrapped around the main solenoid, and can rotate to produce a two-lobed cylindrical response pattern in the surrounding material. The orientation of this rotating coil at the maximum stress signal will fix the orientation of the borehole stress distortion pattern and thus of the original stress/strain. A typical configuration of such a coil is shown in Figure 12.

The toroidal coil must avoid self resonance at 1.1 MHz, the resonant frequency of sodium in 1 kG (in order to have some slight tunability) and must achieve at the same time a Q value higher than the ~1100 limit imposed by the bandwidth and frequency of the measurement. The bandwidth, in turn, is imposed by the residual fluctuating magnetic field produced by the crystal lattice. The appendices describe this optimization in detail. For a radius of 10 cm, a coil having resonance frequences >>1MHz and Q > 1000 can be

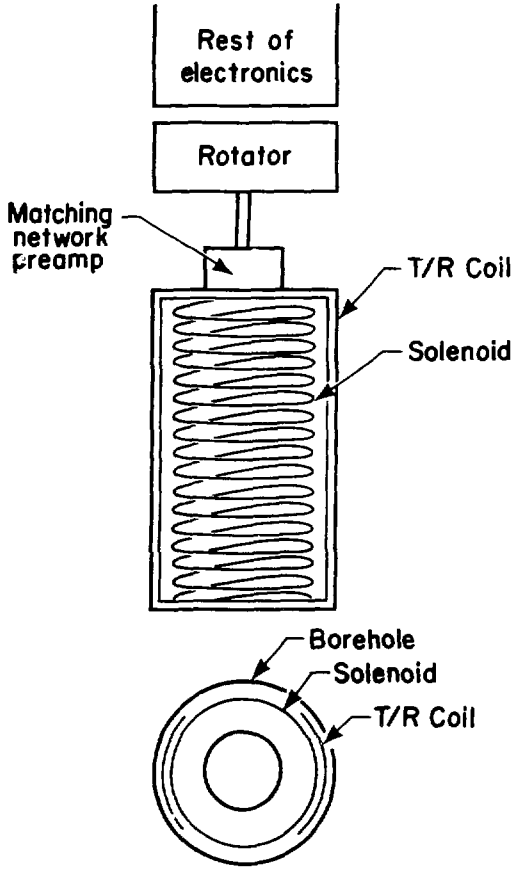

XBL 8012-2482

FIGURE 12. BOREHOLE CONFIGURATION FOR ROTATING TRANSMIT/RECEIVE COILS AND SOLENOID FOR GENERATING A MAGNETIC FIELD

built. Such Q's were obtained in previous work under contract with the U.S. Navy to develop an NQR landmine detector.[28]

There is no requirement for special guard coils to discriminate against background radiation. The coil will be well shielded from atmospheric noise deep underground. However, the need for rotating this coil in the gap between the solenoid and the wall is a strong mechanical constraint. Since this coil must work both as a receiver and a transmitter it is coupled to an appropriate switching system.

(c) A matched switching network and preamplifier. Duplexing and recovery time of the transducer (switching) and circuit elements cannot be readily separated since the circuit elements usually must be considered as part of the same network. The duplexing function cannot be considered complete until the effects of the transmit signal are reduced to a level below the received signal, or to a level where the two may be separated. The duplexing must limit the transmit signal to some maximum safe level specified at the receive terminals. The receiver isolation required by the duplexer is then directly proportional to transmitted power. In addition, the duplexer must provide a low loss path between the transmitter and the transducer during transmission and a low loss path to the receiver during reception.

As transmit power is increased, duplexing networks become more complex. Switching elements have some minimum realizable impedance and maximum power/current limitations. At the present no switching device is available suitable for series use in low level, low noise applications. Present devices are only low noise in the open state.

High power duplexing circuits are fairly complex band-pass-band-reject filters. Figure 13 illustrates some variations based on a simple filter

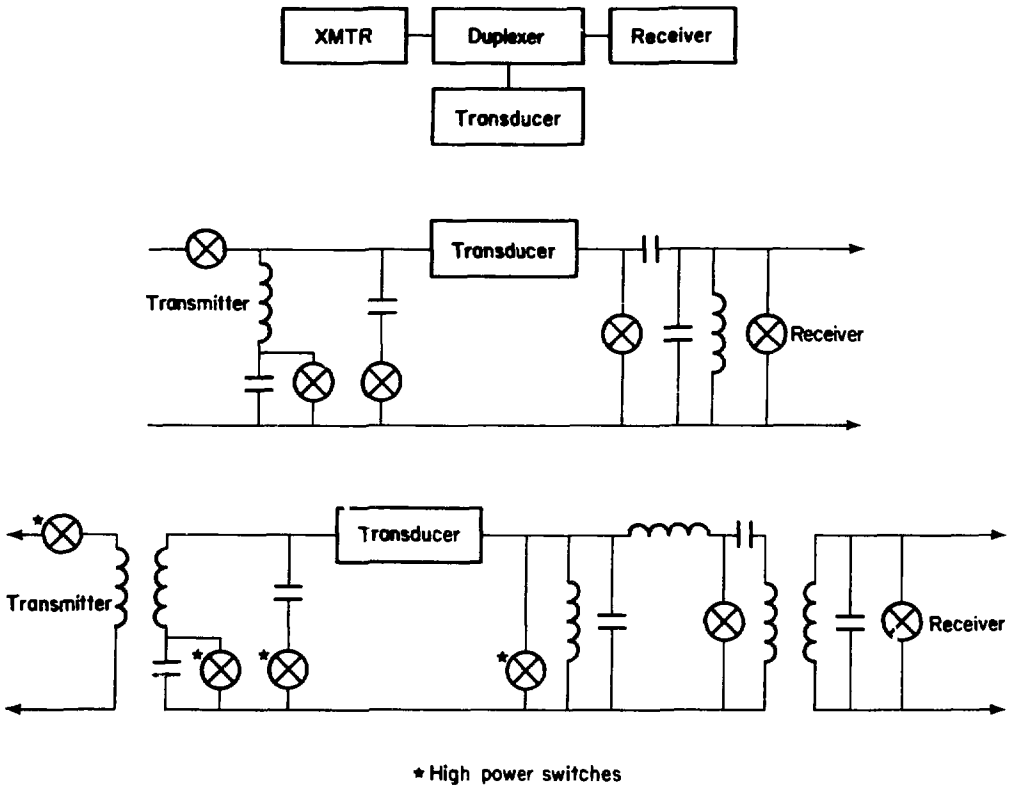

FIGURE 13. SEVERAL DUPLEXING CIRCUITS

design. Because of the increased complexity required for higher powers, losses are greater, affecting sensitivity and Q.

Gas discharge devices (TR's and ATR's) using hydrogen and water vapor are commonly employed in radar and in transmission line or wave guide analogues of the circuits illustrated. These are about the only devices presently available capable of handling the power levels probably required for the borehole instrumentation in the 10 MHz region, and, particularly, in high Q coil configurations. The hydrogen-water-vapor gas discharge devices also have fast recovery time (~5 to 10 microseconds for multi-megawatt usage) but must be operated above the freezing point of water and certainly are not suitable for low temperature application. They are triggered when the voltage applied across the device exceeds the breakdown of the low pressure gas in them. In modern devices tritium is used to provide a low level ionization to reduce the breakdown voltage. When the applied voltage drops below the ionization potential, the discharge is extinguished. The addition of water vapor to the hydrogen decreases the deionization time.

The high power, high Q circuits present a dequeing problem. A switching device is required with a hold-off voltage greater than the voltage present during transmission, but which can be rapidly turned on at the end of transmission and remain on while the circuits decay to a suitable level. Here either a modified hydrogen thyratron or a design using a longer recovery time gas discharge device (with a series resistor in parallel with it) can be used. Figure 14 is a simplified circuit illustrating this approach. Various circuit elements have shunting resistors switched in to critically damped conditions during the dequeing time.

Figure 15 is a simplified series resonant circuit with the turn-to-turn and other parasitic capacitances shown as one shunt capacitance across the

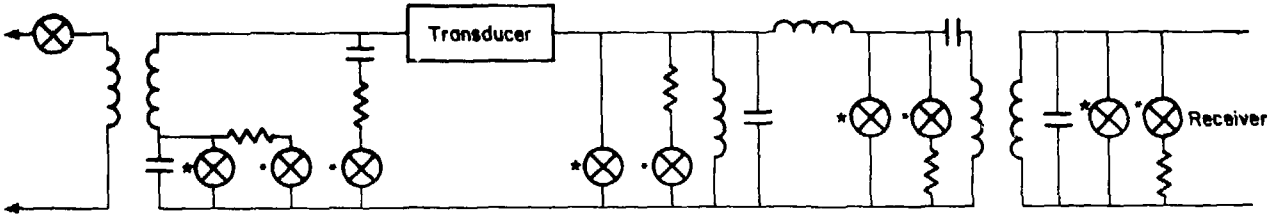

FIGURE 14. A HIGH POWER DEQUEING CIRCUIT

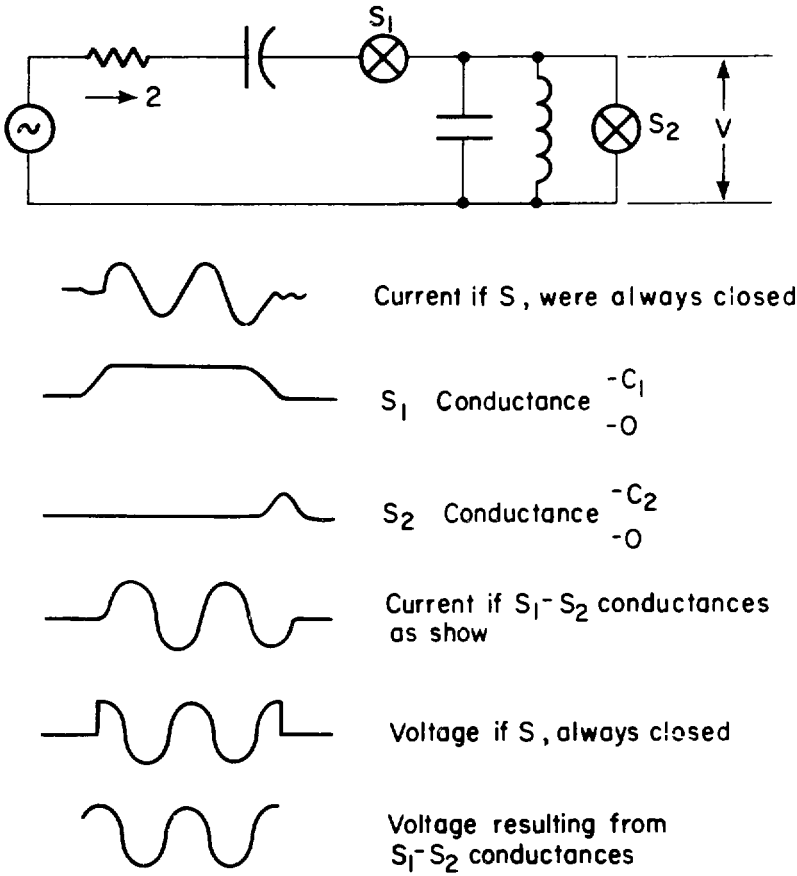

FIGURE 15. A SERIES DEQUEING CIRCUIT

inductance. If the driving impedance is greater than the inductive reactance, the current through the circuit without a series switch would be as indicated. Some ringing is shown since this would be the case with any realizable source. With finite switching time and switch conductances controled so that conductances of the form indicated are realized, currents and voltages of the forms illustrated will be attained. Residual ringing and other non-ideal behavior is obviously going to be present, but should be at greatly reduced levels.

Series switching could be employed with higher Q circuits, but for the most part it is not necessary in laboratory instrumentation. For higher power applications it becomes very much a part of the transmitter design. Substantially better current waveforms should result from a series circuit that is at least critically damped without the switches.

The receiver canceling coils discussed previously accomplish essentially the same action as the series switch so that shunt dequeing is used to discharge the shunt circuit elements. Separate dequeing windings may be employed if good coupling can be obtained. In a particular design the benefits of DC isolation could be large.

Transmitter waveform through the switches must be such that no large low frequency component in the magnetic field is generated either by the series elements or by the dequeing action. The exciting magnetic field must be essentially an integral number of cycles or have leading and trailing matched positive and negative components so that there is not a low frequency or D.C. skew introduced. The Fourier transform of the exciting field should be symmetric about the center frequency in the main lobe portion of the spectrum and there should be no zero-frequency component.

Wide bandwidth fast-recovery-time designed circuits should be employed in the receiver ahead of base-band conversion and band-limiting filters. Gating should be done as much as possible at wide bandwidths. Gating and limiting before filtering usually reduces the effects of large signals on the small signals immediately following and is a common technique used to reduce the effects of very large interfering signals.

Given these precautions in the switching systems, and the absence of background rf noise far underground, a preamplifier whose noise is much lower than the coil's Johnson noise is practical, as can be seen in the Appendices.

(d) NMR transmitter/receiver system. This system embodies standard NMR technology with the following three exceptions:

1) It is designed for unusually low frequencies, which after the preamplfier imposes no significant system requirements.

2) It is designed to do time-gated NMR intensity measurements in a cyclical mode, instead of frequency scan or FFT operations in the pulsed mode. Actually, there is no NMR band to observe, since the inhomogeneity of the magnetic field spreads the NMR signal out over the entire spectrum. Specifically, the taking of one frequency sample by the filter bandpass in the system defines a volume in space which is the only one sampled since nowhere else does H_0 have the right value to put the Na^{23} resonance in the bandpass of the measurement. This is what makes the calculated volume so much smaller than the entire volume of sample near the coil, and is included in our sensitivity calculations.

The time-gating in the NMR signal occurs at two levels. The first of these is that successive NMR measurements are taken at intervals, the cycle being exposure to high field, saturation of the NMR magnetization by an NMR

pulse train, magnetic field shutoff, NQR irradiation, field increase to NMR-NQR resonance point, waiting for the exchange, and then going back to the full field, and completing the NMR measurement.

3) The NMR measurement is performed by a continuous train of very fast pulses following the SLSE sequence[29], which sharply reduces the effect of T_1, and increases signal levels by allowing extensive signal averaging. This is the second level of timing control in the experiment.

(e) Data system. The data system must accomplish a number of tasks:

1) Clock, control, and monitor the pulsing sequence for the magnetic field solenoid, the NMR irradiation pulse sequence, and the NMR magnetization and readout pulse sequences.

2) Aid the operation of the switching transmit/receive network by real-time calibration and compensation of residuals.

3) Log depth, azimuth, temperature, and system field levels for function monitoring, data reduction, and calibration.

4) Accumulate repetitive signal for S/N enhancement.

5) Sequence azimuth, rotate the coil, and initiate depth changes.

6) Control the "hill-climbing" routine to zero in on an exact NQR frequency with a minimal number of tries.

7) Correlate the azimuthal reading pattern with value tables constructed from the borehole perturbation equations to reconstruct the original stress/strain values and directions.

8) Format all of the above for logging.

F. Predicted Sensitivities on Stress/Strain Determinations

The calculations presented below refer specifically to sodium chloride and will have to be modified for other geologic specimens. The NMR signal from the three nuclei present in sodium chloride at a field of 1000 gauss occurs at frequencies of

Na^{23} - 1126 kHz
CL^{35} - 417 kHz
CL^{37} - 347 kHz

Since signals in this frequency region tend to have an intensity that is linear in frequency, the Na^{23} NMR signal is the observable of choice for the double resonance measurements. The NMR sensitivity which is modified by the NQR transition can be calculated.

The signal induced in the sensing coil of an NMR spectrometer driven by an rf voltage V_0, and having a quality factor Q, to which the sample is coupled with an efficiency ϵ, is

1) $$\bar{V}_s^2 = -4\pi\epsilon Q\chi_2 \bar{V}_0^2 \tag{46}$$

where χ_2 is the absorptive component of the nuclear magnetization.

Here, since the driving voltage is sinusoidal, we can substitute

2) $$\bar{V}_0^2 = V_0^2/2 \tag{47}$$

Furthermore, we can substitute

3) $$Q = \omega L_0 / R_0 \tag{48}$$

where ω is the frequency, L_0 the coil inductance, and R_0 its resistance, and we also have

4) $$V_0 = I_0 R_0 \tag{49}$$

where I_0 is the coil current. Since the electric and magnetic fields in the coil store equal amounts of energy, we have

5) $$L_0 I_0^2/2 = V H_1^2/2\pi \tag{50}$$

where V is the sensed volume and H_1 the rf magnetic field intensity. We can now calculate

6) $$V_0^2 = \frac{V H_1^2 R_0^2}{\pi L_0} \tag{51}$$

and by substitution

7) $$\bar{V}_s^2 = 2\pi Q V R_0 \omega (2\epsilon H_1 \chi_2)^2 \tag{52}$$

Here we have

8) $$2H_1\chi_2 = \frac{\chi_0 \omega_0 H_1 (\omega_0 - \omega) T_2^2}{1 + (\omega_0 - \omega)^2 T_2^2 + \gamma^2 H_1^2 T_1 T_2} \tag{53}$$

where χ_0 is the static nuclear susceptibility, ω_0 the resonant frequency, T_1, the spin-lattice relaxation time, T_2 the spin-spin relaxation time (equal approximately to the reciprocal of the intrinsic line width), and γ is the magnetogyric ratio of the nucleus used.

Equation 53 peaks at

9) $$\omega_0 - \omega = \frac{\sqrt{1 + \gamma^2 H_1^2 T_1 T_2}}{T_2} \tag{54}$$

where

10) $$2H_1\chi_2 = \frac{\chi_0 \omega_0 H_1 T_1}{2\sqrt{1 + \gamma^2 H_1^2 T_1 T_2}} \tag{55}$$

In practice, to optimize the signal we saturate its intensity by letting H_1 grow until

11) $$H_1^2 = \frac{1}{\gamma^2 T_1 T_2} \tag{56}$$

at which point

12) $$\omega_{0PT} = \omega_0 \tag{57}$$

13) $$2H_1\chi_2 = \frac{\chi_0 \omega_0 T_2}{2\gamma\sqrt{T_1 T_2}} \tag{58}$$

giving by substitution

14) $$\overline{V_s^2} = \frac{\pi Q V R_0 \omega_0 \epsilon^2 \chi_0^2 H_0^2 T_2}{2T_1} \tag{59}$$

This noise must be detected against the receiver noise, which if well designed, is Johnson-noise limited by the receiver coil. This is given by

15) $$\overline{V_n^2} = 2R_0 kT_c F/t \tag{60}$$

where V_n is the noise voltage, k is Boltzman's constant, T_c the coil temperature, t the measurement time, and F is the factor by which the receiver noise exceeds the sensing coil's Johnson noise. This gives

16) $$\overline{V_s^2}/\overline{V_n^2} = \frac{\pi Q V \omega_0 \epsilon^2 \chi_0^2 H_0^2 T_2 t}{4kT_c F T_1} \tag{61}$$

Here we can calculate the DC nuclear paramagnetic susceptibility

17) $$\chi_0 = \frac{N4\pi^2\gamma^2 I(I+1)h^2}{3kT_s} \tag{62}$$

where I is the nuclear spin of the target nucleus, T_s the sample temperature, N the number density of the target nucleus, and h is Planck's constant.

From the above we can calculate the rms S/N ratio as

18) $$\overline{V_s}/V_n = \frac{Q^{1/2} V^{1/2} \epsilon h^2 N \gamma I(I+1) t^{1/2}}{6\sqrt{2}\, k^{3/2} T_s T_c^{1/2} F^{1/2}} \; (T_2/T_1)^{1/2} f_0^{3/2} \tag{63}$$

where f_0 is the resonant frequency. We can also express this as

19) $$\overline{V_s}/V_n = \frac{Q^{1/2}V^{1/2}\epsilon h^2 N\gamma^{5/2}I^{1/2}I(I+1)}{24(\pi k)^{3/2}T_s T_c^{1/2}F^{1/2}}\,(T_2/T_1)^{1/2}H_0^{3/2} \qquad (64)$$

In order to calculate Q, we must refer to the coil design description in the appendices, where it is shown as a function of coil diameter. In practice, of course, loading of the coil by the receiver and the cross coupling filters required limits Q, but values >1000 should be attainable at these low frequencies.[28]

The useable volume, on the other hand, is determined not by the effectively infinite sample volume, but by the magnetic field gradient around the exciting solenoid. In the immediate vicinity of the solenoidal field coil's periphery, the field falls off with the inverse square of the radius, making the radial depth element sampled equal to

20) $$\Delta_r = \frac{r_B B_W}{2\gamma H_0} \qquad (65)$$

where r_B is the borehole radius and B_W is the bandwidth.

From here we get the total sampled volume as

21) $$V = \frac{r_B^2 B_W \alpha \ell}{4\pi\gamma H_0} \qquad (66)$$

where α is the utilized fraction of the circumference, and ℓ is the length of the sampled region.

We can now tabulate a few of the relevant properties of Na^{23}:

$I = 3/2$

$\gamma = 1126$ Hz gauss^{-1}

$N = 2.23 \cdot 10^{22}$ cm^{-3}

A further substitution possible is

22) $$T_2 = 1/B_w \tag{67}$$

In order to calculate the value of ε, the geometry of the sensing coil must be taken into account. This must lie outside the solenoid which generates H_0, which, in order to generate the largest possible H_0 with a reasonable current, must fill the borehole. This restricts the coil to a flat loop surrounding the solenoid. To maximize the efficiency with which we generate H_0, and to maximize the sample volume V, we elongate the solenoid and give the receiver coil a rectangular cross section. In order to increase the coupling of the coil to the sample, its solid angle as perceived from the sample must be maximized. This can be done by giving the coil a toroidal cross section utilizing more of the borehole's circumference. The limit to this improvement is reached when the restriction on α by this procedure begins to dominate the total signal. Actual integration of the resulting function shows an optimum toroid width equal to the borehole radius. As perceived by the sample, the transmit/receive coil is then a short on-axis rectangular solenoid.

The extent of the coupling of the sample to such a coil is the exact inverse problem of calculating the field induced by the coil at the sample's location. The ratio of the field produced by the coil at its center (at which

location $\epsilon \rightarrow 1$) to that produced at the actual sample location is thus the inverse of ϵ.

We can now write for the axial field of a circular solenoid (an approximation adequate for these purely relative calculations) of radius a, length b, at a distance c from its center along the axis

23) $$H_s(c) = \pi/5 \; nI\,b \left[\frac{0.56 + c}{\sqrt{a^2 + (0.56 + c)^2}} + \frac{0.5\ell - c}{\sqrt{a^2 + (0.56 - c)^2}} \right] . \qquad (68)$$

In the above case, we can write at the sample

24) $$a = \sqrt{3}/2 \; r_B \qquad (69)$$

25) $$b = c = r_B \; . \qquad (70)$$

giving

26) $$H_s(c) = \pi nI/r_B \, (\sqrt{3} - 1)/10 \qquad (71)$$

while for $c \equiv 0$ we have

27) $$H_s(0) = \pi nI/5r_B \qquad (72)$$

giving for the efficiency

28) $$\epsilon = (\sqrt{3} - 1)/2 = 0.366 \qquad (73)$$

In order to calculate H_o, we calculate the field of the main DC solenoid along the outer edge of its winding by

29) $$H \simeq \frac{\pi n I}{10 r_B h} \tag{74}$$

where h is the solenoid's length/diameter ratio and h>>1. Then

30) $$h = \ell / 2 r_B \ . \tag{75}$$

If we now assume this solenoid contains closely-wound layers of wire having a diameter d and a resistivity ρ, we have

31) $$R = \frac{8 \rho r_B n}{d^2} \tag{80}$$

and

32) $$n = \frac{\ell m}{d} \tag{81}$$

where m is the number of coil layers, giving

33) $$R = \frac{8 \rho r_B \ell m}{d^3} \tag{82}$$

This number will usually be low enough to require a downhole transformer rectifier. If we now substitute the above and

34) $$I = \sqrt{P/R} \tag{83}$$

where P is the peak power during the high field portion of the double resonance cycle, we have

35) $$H_0 = \frac{\pi}{10\sqrt{\tau}} \left(\frac{Wd}{\rho r_B \ell m}\right)^{1/2} \quad (84)$$

To calculate the proper value of T_1 to use in the calculations, the precise pulse sequence used in the NMR measurement is of importance. An optimal sequence for use here is the SLSE multiple spin-locked spin-echo method described in the appendices, which does better than the pure T_1 limited system by the factor.

36) $$I = \eta^{1/2} \quad (85)$$

where η, the number of pulses in the train, is of the order of $10^2 T_2$. Finally, Q will generally be limited by the signal bandwidth at

37) $$Q < \frac{\gamma H_0}{B_w} \quad (86)$$

Combining all of the above, we can write for equation (64)

38) $$(S/N)_{NMR} = \frac{\sqrt{3}-1}{1920\pi^{5/2}} \frac{r_B^2 a(h^2 N \gamma^{5/2} \tau^{1/2} I(I+1) H_0^{3/2}}{k^{3/2} T_s T_c^{1/2} F^{1/2}} \quad (87)$$

Here it is reasonable to assume $T_s = T_c = 300^0$K. F can be assumed to be of order unity, although slight adjustments for finite measuring times, as described in the appendices, would be required.

The actual NQR signal, detectable as a modification of the NMR one, has a S/N proportional to the latter. Here the extent of the perturbation if the

measured quantity, and it is desirable to bias this into the range where convenient measurements can be done.

For the present application the energy transfer between NQR and NMR must be optimized, by providing enough time for this transfer to occur within the overall time constraint imposed by the T_1 relaxation. Here we take advantage of the resonant enhancement of this transfer process at the intermediate magnetic field where the NQR and NMR energies are identical. For this purpose the "DC" magnetic field used is switched in a 3-level cycle containing this intermediate value as well as 0 and the high one (1,000 gauss), with fast transition in between. At this optimum coupling the S/N in NQR would still be 1/e that of its NMR carrier. The optimum value of t is limited to somewhat less than T_1, and for the T_1 values expected would be of the order of 10 sec.

The meaning of the above equations can now be clarified through an example. Consider a situation where

H_o = 1000 gauss

r_B = 10 cm

B_w = 10^3 Hz

α = π (for a bilaterally-symmetric measurement)

ℓ = 150 cm

γ = 1126 Hz gauss^{-1}

σ = 1.73×10^{-6} Ω cm^{-1} (copper)

T_1 = 30 sec

T_2 = 10^{-3} sec

$m = 1$

$d = 0.5$ cm

Then

$\omega_0 = 1.126$ MHz

$H_1 = 0.005$ gauss

$Q \geq 1126$

$V = 3.33$ cm^3

$S/N_{NMR} = 880$

$S/N_{NQR} = 320$

Our ability to locate precisely the center of a peak, E_f, depends on the S/N, and is approximately

39) $$E_f = \frac{B_W}{S/N} \tag{88}$$

giving in our example

40) $$E_f = 3.0 \text{ Hz} \tag{89}$$

which even for the lowest stress coefficients represents a pressure noise of 0.16 atmospheres.

This is, of course, a mere calculation, and conservative engineering practice requires a margin of safety of 10 above this, leading to a pressure noise level of 1.6 atm.

III. CONCLUSIONS AND RECOMMENDATIONS

A. Conclusions

The research and development performed to date yielded some very basic information:

(1) The NQR technique should be able to resolve changes in triaxial pressures in salt of 25 psi or smaller and determine their principal directions.

(2) There are no obvious theoretical problems at this time.

(3) Downhole instrumentation, suitable for in-situ determination of pressure appears to be within the state-of-the-art.

(4) Detailed laboratory measurements on salt, under known pressures (magnitude and direction), are needed to refine the theoretical calculations and to permit the design of fieldable hardware.

B. Recommendations

Based on work done to date, the recommendations can be divided into two catagories -- additional work with salt and initiation of research on aluminum-27 containing rocks. For salt the suggestions are:

(1) Sufficient laboratory measurements on salt to permit data to be statistically evaluated on the effect of pressure and its direction on the NQR spectrum.

(2) For measurements in the borehole, existing calculations will have to be transformed from Cartesion to polar coordinates.

(3) Calculation of line shapes associated with salt under various applied pressures and comparison of these with data from controlled laboratory experiments.

(4) Evaluate the effect of point defects and dislocations on the electric field gradient and the line shape.

(5) Finalize the design of a laboratory NQR system which will permit optimi. measurements of salt under applied directional pressure.

(6) Construct the instrument defined by (III.B.5)

(7) Determine the effects of such variables as temperature, chemical, and crystallographic inhomogeneities and plastic flow on the accuracy of the stress/strain NQR measurements.

For aluminum-27 containing geologic samples the following must be done:

(8) Locate the aluminum-27 NQR resonances in Al-O and Al-O-Si type compounds.

(9) Measure the NQR spectra of select Al-O-Si compounds as a function of direction and pressure applied to the sample.

(10) Make a preliminary calculation as to the feasibility of measuring stress/strain in aluminum-27 compounds using data from (III.B.9).

(11) Evaluate contributions of such factors as multiple aluminum-27 compounds, temperature, crystallographic inhomogeneities, and defects and dislocations on stress/strain measurements.

(12) Repeat (III.B.5 and 6) for the aluminum-27 system.

It should be noted that the most beneficial and cost effective program is one where the NaCl and aluminum-27 investigations are done in parallel. Inasmuch as the salt studies are far ahead of the aluminum ones, and will, in all probability stay that way, the results for the less complicated salt system can be used as a guide for the more complex aluminum-27 research and development.

IV. REFERENCES

1. Love, A.E.H. A Treatise on the Mathematical Theory of Elasticity, Dover, New York (1944).

2. Jaeger, J.C. and Cook, N.G.W. Fundamentals of Rock Mechanics, Chapman and Hall, London (1976).

3. Leeman, E.R. Rock Mechanics 3, 25-60 (1971).

4. Rocha, M. and Silverio, A. Geotechnique 19, 116-132 (1969).

5. Blackwood, R.L. Proc. Internl. Symp. of Field Measurements in Rock Mechanics, Zurich, Vol. I, pp. 137-150 (1977).

6. Duncan-Fama, M.E. and Pender, M.J. Internl. J. Rock Mech. Min. Sci. and Geomech. Abstr. 17, 137-146 (1980).

7. Baar, C.A. Applied Salt - Rock Mechanics, I. The In-Situ Behavior of Salt - Rocks, Elsevier, New York (1977).

8. Marsh, J.L., Jr. and Casabella, P.A. Phys. Rev. 150, 546-551 (1966).

9. Schempp, E. and Bray, P.J. "Nuclear Quadrupole Resonance Spectroscopy" in Physical Chemistry, and Advanced Treatise, Vol. 4, Eyring, Jost and Henderson, eds., Academic Press, New York (1970).

10. Nye, J.F. Physical Properties of Crystals, Clarendon Press, Oxford (1972).

11. Shulman, R.G., Wyluda, B.J. and Anderson, P.W. Phys. Rev. 107, 953-958 (1957).

12. Kanert, O. and Mehring, M. "Static Quadrupole Effects in Disordered Cubic Solids" in NMR Basic Principles and Progress, Vol. 3, Diehl, Fluck, and Kosfield, eds., Springer-Verlag, New York, (1971).

13. Lucken, E.A.C. Nuclear Quadrupole Coupling Constants, Academic Press, New York (1969).

14. Muehlberger, W.R. "Internal Structure of the Grand Saline Salt Dome, Van Zandt County, Texas." Univ. Texas Bus. Econ. Geology Dept. Inv. 38, 18p (1959).

15. Kern, H. Tectonophysics 39, 103-120 (1977).

16. Carter, N.L. and Heard, H.C. Am. J. Sci. 269, 193-249 (1970).

17. Kamb, W.B. J. Geology 67, 153-170 (1959).

18. Nichols, E.A. Am. Inst. Min. Metall. Petroleum Engineers, Petroleum Devel. and Tech. Trans. 170, 44-50 (1947).

19. Moses, P.L. World Oil 152, 79-82 (1961).

20. Anderson, L.O. and Forslind, E. Arkiv Fysik 28, 49-64 (1964).

21. Cohen, N.H. and Reif, F. "Quadrupole Effects in Nuclear Magnetic Resonance of Solids," Solid State Physics, Vol. 5, Seitz and Turnbull, eds. Academic Press, New York (1957).

22. Lowe, I.J. and Norberg, R.E. Phys. Rev. 107, 46-52 (1957).

23. Koo, J.C. Ph.D. Thesis, Univ. of California, Berkeley (unpublished), (1970).

24. Hahn, E.L., Koo, J.C., and Hsieh, Y. Chem. Phys. Letters 13, 563-566 (1972).

25. Edmonds, D.T. Phys. Reports C29, 233-290 (1977).

26. Edmonds, D.T. and Mailer, J.P.G. J. Mag. Resonance 26, 93-99 (1977).

27. Klainer, S.M., Hirschfeld, T.B., and Marino, R.A. Fourier, Hadamard, and Hilbert Transforms in Chemistry, A. Marshall, ed., Plenum, New York (in press).

28. Harding, J., Hirschfeld, T. B., Klainer, S. M., Wade, D., and Marino, R. A. "NQR Detection Studies", Final Report to Naval Electronics Laboratory Center, San Diego, March, 1976.

29. Marino, R. A. and Klainer, S. M., J. Chem. Phys. 67, 3388-89 (1977).

V. APPENDICES

A. Practical Applications of FT-NQR Spectroscopy

(to be published as Ref. 27)

(The Appendices which follow give some very specialized and technical discussions. Appendix A provides a general overview of recent developments in NQR FT spectroscopy. Appendices B-H are the result of highly complex calculations on coil and antenna designs and may be of interest only to the specialist. Whether all these results will be immediately applicable to the borehole-stress problem has not been determined because the final system has not been completed.)

PRACTICAL APPLICATIONS OF FT-NQR*

by

Stanley M. Klainer,** Tomas B. Hirschfeld+
and Robert A. Marino++

I. INTRODUCTION

FT-NQR (Fourier Transform Nuclear Quadrupole Resonance) spectroscopy is one of the newer analytical tools. Although nuclear quadrupole coupling constants were first observed in atoms by Schmidt and Schuler[1] in 1935 and in molecules by Kellog[2] and coworkers in 1936, it was the discovery of pure quadrupole coupling transitions in solids by Dehmelt and Kruger[3][4] in 1950 and 1951 that initiated the understanding of the NQR phenomenon as presently utilized.

During the past 30 years the growth of NQR has been anything but phenomenal. A great quantity of theoretical work has been reported but the experimental investigations have been restricted primarily to nitrogen-containing and halogenated compounds. How, then, can an application paper, such as this be justified? The answer lies in responding to two specific questions:

(a) What has hindered the growth of NQR to date and can this be overcome with present day technology?

---

*This work was supported in part by the U. S. Department of Energy under Contract No. W-7405-ENG-48 and U. S. Army Research Office under Contract No. DAAG-29-79-0025.

**Lawrence Berkeley Laboratory, 90/1140, Berkeley, CA 94720.

+Lawrence Livermore National Laboratory, L325, Livermore, CA 94550.

++Hunter College of CUNY, 695 Park Avenue, New York, N.Y. 10021.

(1)H. Schuler and T. Schmidt, Z. Phys. 94, 457 (1935).

(2)J. M. B. Kellog, I. I. Rabi, N. F. Ramsey and J. R. Zacharias, Phys. Rev. 55, 728 (1936).

(3)H. G. Dehmelt and H. Kruger, Naturwiss. 37, 111 (1950).

(4)H. G. Dehmelt and H. Kruger, Naturwiss. 38, 921 (1951).

(b) Why is it important that NQR be developed as a practical analytical technique at this time?

In responding to these queries, it is possible to show that FT-NQR is both needed and implementable.

This paper is directed at the applied scientist, and, therefore, it does not contain the in-depth theoretical and mathematical information of interest to the research scientist. Texts by Schempp and Bray[5], Lucken[6], Slichter[7] and Biryukov, Voronkov and Safin[8] can supplement the information on NQR presented in this paper. There is, however, no primer on FT-NQR and the basic concepts of this specific area will be addressed in this discussion.

II. NQR SPECTROSCOPY

Nuclear Quadrupole Resonance (NQR) is a branch of radio-frequency spectroscopy. The NQR spectrometer detects the interaction of a nuclear quadrupole moment with the electric field gradient (EFG) produced by the charge distribution in a solid state compound. The quadrupole moment arises because the nuclear charge distribution is nonspherical. Resonance occurs when transitions from one spin state to another are excited by radio-frequency electro-magnetic oscillations. In this way, NQR is quite similar in principle to nuclear

---

(5) E. Schempp and P. J. Bray, "Nuclear Quadrupole Resonance Spectroscopy", Physical Chemistry, an Advanced Treatise, Volume 4, Academic Press, New York (1970).

(6) E. A. C. Lucken, "Nuclear Quadrupole Coupling Constants", Academic Press, New York (1969).

(7) C. P. Slichter, "Principles of Magnetic Resonance", Second Edition, Springer Series in Solid-State Sciences 1, Springer-Verlag, Berlin, Heidelberg, New York (1978).

(8) I. P. Biryukov, M. G. Voronkov and I. A. Safin, "Tables of Nuclear Quadrupole Resonance Frequencies", Israel Program for Scientific Translations, Jerusalem (1969).

magnetic resonance (NMR). In NQR, however, the energy levels depend on the coupling of the nuclear moment to the internal electric field gradient, whereas in NMR they are primarily dependent on the coupling of the nuclear magnetic moment with an external magnetic field. Since the EFG is a very sensitive function of the molecular and crystal structure, the resonance frequencies and band shapes are specific to each compound, and NQR data can be used for determining unambiguous sample identification, local electronic structure, atomic arrangement, order/disorder phenomena, and crystal phase transformations. In addition, molecular dynamics in the solid state can be studied. Furthermore, since NQR data are sensitive to changes in temperature and pressure, there is the possibility of obtaining strain information.

A. Basic Concept of NQR

In order to understand the origin of nuclear quadrupole resonance, it is usual to visualize the nucleus as a classical distribution of positive charges, $\rho_N(\vec{r})$, over a volume of characteristic dimensions on the order of nuclear radii, i.e. 10^{-13} cm (Figure 1). On the other hand, a charge cloud extending over a volume on the order of several angstroms (10^{-8}cm) generates an electrostatic potential $\phi(\vec{r})$ which can be considered as varying slowly over the region occupied by the nucleus. The electrostatic energy W of the system can be expressed (7) as:

$$W = \int \rho_N(\vec{r})\phi(\vec{r})d\vec{r} \ , \tag{1}$$

which can be expanded in terms of the moments of the nuclear charge distribution:

$$W = -\phi(0)q_N + \vec{p}\cdot\vec{E}(0) - \frac{1}{6}\sum_{ij} q_{ij}Q_{ij} + \cdots \tag{2}$$

where (o) means evaluated at the origin, the center of mass of the nucleus, and

$q_N = \int \rho_N(\vec{r})\vec{dr}$ nuclear charge

$\vec{p} = \int \rho_N(\vec{r})\vec{r}\ \vec{dr}$ nuclear dipole moment vector

$Q_{ij} = \int \rho_N(\vec{r}) x_i x_j \vec{dr}$ nuclear quadrupole moment tensor

$\vec{E} = -\vec{\nabla}\phi$ external electric field vector

$q_{ij} = (\partial E_i/\partial x_j)_o$ external electric field gradient tensor

From quantum mechanical considerations it can be proven that the only non-vanishing terms in Eqn. 2 are the first, third, and other odd-ordered ones. The first term is simply a constant, and, therefore, the orientationally-dependent term in the energy is the quadrupolar energy (hexadecapole interactions are extremely small if they exist at all):

$$W_Q = \frac{1}{6} \sum_{ij} q_{ij} Q_{ij} \tag{3}$$

Q_{ij} is diagonal and is related to the components of the nuclear spin I_i according to:

$$Q_{ii} = \frac{eQ}{I(2I-1)} \left[3I_i^2 - I(I+1) \right] \tag{4}$$

where $I = \left(\sum I_i^2\right)^{1/2}$ is the nuclear spin and $\underline{eQ}$ is defined as the nuclear quadrupole moment. Since $\nabla^2\phi = 0$ by the Laplace equation, we have

$$\sum_i q_{ii} = 0 .$$

The quantum mechanical expression for the quadrupole energy (the Hamiltonian) takes the particularly simple form:

$$H_Q = \frac{eQ}{2I(2I-1)} \sum_i q_{ii} I_i^2 , \tag{5}$$

which can also be expressed in the form:

$$H_Q = \frac{e^2qQ}{4I(2I-1)}\left[\left(3I_z^2 - I^2\right) + \eta\left(I_x^2 - I_y^2\right)\right] \qquad (6)$$

where I and I_j are spin operators.

The quantity e^2qQ is called the quadrupole coupling constant of the system and η is defined as the asymmetry parameter of the electric field gradient (EFG):

$$\eta \equiv \frac{q_{xx} - q_{yy}}{q_{zz}}, \text{ and}$$

$$eq \equiv eq_{zz} \quad \text{so} \quad e^2qQ = (eQ)(eq_{zz}) \qquad (7)$$

when the axes are labelled

$$|q_{zz}| \geq |q_{yy}| \geq |q_{xx}| \qquad \text{by convention.}$$

For nitrogen-14, with nuclear spin I = 1, the solution of the Schroedinger equation $H_Q \Psi_N = E_N \Psi_N$, where Ψ_N is the nuclear wave function, can be shown to lead to a three level system of energies given by

$$E_z = e^2qQ/2$$
$$E_x = -E_z(1-\eta)/2$$
$$E_y = -E_z(1+\eta)/2 \qquad (8)$$

Transitions between these levels can be induced with oscillating magnetic fields of the proper (resonant) frequencies (Figure 2). The frequencies of these transitions are

$$\nu_+ = \frac{e^2qQ}{4h}(3+\eta)$$

$$\nu_- = \frac{e^2qQ}{4h}(3-\eta)$$

$$\nu_d = \frac{e^2qQ\eta}{2h} = \nu_+ - \nu_- \qquad (9)$$

Determining any two of the three NQR frequencies completely describes the magnitude of the EFG in the vicinity of the nitrogen nucleus:

$$e^2qQ = \frac{2}{3}(\nu_+ + \nu_-)$$

$$\eta = \frac{2(\nu_+ - \nu_-)}{e^2qQ} \tag{10}$$

As another example, for nuclei of spin I = 5/2, such as aluminum-27, the solution of the Schroedinger equation can be shown to lead to a three-level system of energies[6] given by solutions of the secular equation[9]

$$E^3 - 7(3 + \eta^2)E - 20(1 - \eta^2) = 0, \tag{11}$$

where E is in units of $e^2qQ/20$. For the case, $\eta = 0$, the energies of the three eigenstates are:

$$E\left(\pm \frac{1}{2}\right) = -4\,\frac{e^2qQ}{20}$$

$$E\left(\pm \frac{3}{2}\right) = -1\,\frac{e^2qQ}{20}$$

$$E\left(\pm \frac{5}{2}\right) = +5\,\frac{e^2qQ}{20} \tag{12}$$

The frequencies of the resultant allowed transitions are given by:

$$\nu_1 = \nu\left(\frac{3}{2} \rightarrow \frac{1}{2}\right) = \frac{3}{20}\,\frac{e^2qQ}{h}$$

$$\nu_2 = \nu\left(\frac{5}{2} \rightarrow \frac{3}{2}\right) = \frac{6}{2}\,\frac{e^2qQ}{h} \tag{13}$$

For the general case, $\eta \neq 0$, no solution in closed form can be written down. However, tables of the results of numerical solution of the eigenvalue

---

[9] T. P. Das and E. L. Hahn, "Nuclear Quadrupole Resonance Spectroscopy," Solid State Physics, Supplement 1, Academic Press, New York (1958). (Note that the error in the secular equation for spin 5/2 given on page 13 has been corrected.)

problem for $0 \leq \eta \leq 1$ in steps of .001 are available[10], so that observation of two NQR frequencies uniquely determines both the quadrupole coupling constant, e^2qQ, and the asymmetry parameter, η, of the site under study. For large values of η, it becomes theoretically possible to observe the "forbidden" transition corresponding to the sum of ν_1 and ν_2 in Equation 10. This may be especially useful to do in situations of low quadrupole coupling.

As an additional example, for nuclei of spin I = 7/2, such as uranium-235, the solution of the Schroedinger equation can be shown to lead to a five-level system of energies given by solutions of the secular equation[5],

$$E^4 - 42\ (1 + \eta^2/3)\ E^2 - 64\ (1 - \eta^2)\ E + 105\ (1 + \eta^2/3)^2 = 0$$

where E is in units of $e^2qQ/28$.

For the general case, $\eta \neq 0$ no solution in closed form can be written. However, tables of the results of numerical solution of the eigenvalue problem for $0 \leq \eta \leq 1$ in steps of .001 are also available[10], so that observation of two identified NQR frequencies again uniquely determines both the quadrupole coupling constant, e^2qQ, and the asymmetry parameter, η, of the site under study.

B. Experimental Techniques

Experimental techniques for the determination of NQR spectra can be divided into three categories:

a. Continuous-wave (CW) methods,

b. Transient methods, and

c. Double resonance techniques.

CW methods have enjoyed great popularity for they are simple and inexpensive. The limitations of these techniques are so severe, however,

---

[10] R. Livingston and H. Zeldes, "Tables of Eigenvalues for Pure Quadrupole Spectra, Spin 5/2 and 7/2," Oak Ridge National Laboratory Report ORNL-1913 (1955).

that in the low MHz region they are rarely used anymore. Transient methods include the superregenerative technique (unproductive at the low frequencies of interest in many applied problems) and pulsed methods. Double resonance techniques are essentially pulsed methods that monitor the resonance of one type of nuclear species while another is being perturbed.[7] When applicable, these methods are extremely sensitive and are very convenient for locating unknown resonances, although lineshapes are not always reliable. Interested readers are referred to the excellent review by Edmonds.[11]

Pulsed techniques that operate in the so-called spin-echo mode are particularly good for applied NQR and they naturally lend themselves to remote detection.[12]

To understand the reasons for the advantage of the pulsed method (13-17) it is necessary to begin by defining some basic magnitudes that describe an NQR line. In the frequency domain an NQR line is fully described by its frequency and by a normalized shape function $S(\omega)$. For example:

$$S(\omega) = \frac{2}{\pi\Delta\omega} \frac{1}{1 + \left(\frac{\omega - \omega_o}{\Delta\omega}\right)^2} \qquad (14)$$

---

(11) D. T. Edmonds, Physics Reports 29, 233 (19 ..

(12) T. Hirschfeld and S. M. Klainer, J. Mol. Struc. 58, 63 (1980).

(13) A. Zussman and S. Alexander, J. Chem. Phys. 49, 3792 (1968).

(14) G. Petersen and T. Oja, "Advances in Nuclear Quadrupole Resonance", (J. A. S. Smith, Ed.) 1, 179, Heyden, London (1974)

(15) Y. Abe, Y. Ohneda, M. Hirota and S. Kojima, J. Phys. Soc. Japan 37, 1061 (1974).

(16) A. Colligiani and R. Ambrosetti, Gazz. Chim. It. 106, 439 (1976).

(17) A. A. V. Gibson, R. Goc and T. A. Scott., J. Mag. Res. 24, 103 (1976).

However, spin-echo techniques operate in the time domain; here there are three parameters that describe an NQR absorption line:

a. Spin-lattice relaxation time, T_1. The characteristic time with which a bulk magnetization is established and energy can flow between the spin system and the lattice.

b. Spin-spin relaxation time, T_2. The characteristic time which describes the coupling between nuclei and which establishes the time scale for the observation of spin echoes.

c. A spin-echo shape function, G(t). The "width" of this function is defined as $2T_2^*$. G(t) is the Fourier transform of the line-shape function, $S(\omega)$; thus $T_2^* \propto \frac{1}{\Delta\omega}$.

Continuous-wave (CW) and superregenerative methods are poor techniques for lines with large T_1 and/or large $\Delta\omega$ values (short T_2) associated with the NQR line (to avoid saturation in CW, the input power level has to be reduced to very small values). Broad lines, expected to be important in applied NQR, are weak since their areas are constant. Spin-echo wide-line methods are not only unaffected by long T_1 values, but since G(t) and $S(\omega)$ are related by a Fourier transformation, the equality

$$G_{MAX} = \int_{-\infty}^{\infty} S(\omega)\, d\omega = 1 \qquad (15)$$

holds (Fig. 3). Thus, broad lines in the frequency domain do not affect the maximum intensity of the echo signal.

The NQR spectrum of a substance is determined by placing about 25 grams of sample inside the inductor of a tank circuit, which is then subjected to a series of radio-frequency pulses of frequency f. Whenever the frequency of of these pulses satisfies the resonance condition $f = \nu_Q$, where ν_Q is one

of the quadrupole frequencies, absorption of energy takes place and is re-transmitted as a series of signals [free induction decay (FID) or spin echo]. Therefore, by monitoring and detecting the transmitted signals as a function of the frequency of the pulses, the energy levels of the quadrupole nucleus are completely determined. A number of different pulse sequences are possible; this results in more or less efficient signal production, depending on the values of the relaxation times.

III. NQR INSTRUMENTATION AND DATA HANDLING

For applied NQR spectroscopy pulsed techniques are used in conjunction with a variety of pulse sequences and FT data processing. This approach provides for maximum sensitivity and versatility.

A. Pulsed NQR Spectrometer

The most advanced pulsed NQR spectrometer in the nitrogen frequency region presently in operation was described by Harding et al.[18] in 1979. A block diagram of this instrument is shown in Fig. 4. This is an FT-NQR spectrometer which operates from 0.5 to 5MHz. The features of this instrument are:

(a) The use of heterodyne techniques throughout to eliminate carrier feed through.

(b) A matching network design that allows one-knob tuning of both the transmitter and receiver.

(c) The choice of several excitation sequences (Carr-Purcell, Meiboom-Gill modified Carr-Purcell, spin-locked spin-echo and the standard sequence of $\pi/2$ pulses) for generation and collection of signals at high data rates.

(d) Fast Fourier transform routines for studying line shapes, for

---

[18] J. C. Harding, D. A. Wade, R. A. Marino, E. G. Sauer and S. M. Klainer, J. Mag. Res. 36, 21 (1979).

facilitating spectral searches, and for improved sensitivity.

(e) Ability to handle small samples (0.1cc).[19]

The specifications for this instrument are given in Table I, column 1. This instrument, although state-of-the-art and much more versatile and sensitive than previous spectrometers, is not optimally suited to many applied NQR uses. A new system suited for practical NQR use is presently under design and scheduled for construction in early 1981. It's anticipated specifications are shown in Table I, column 2. When this instrument is operational, many of the obstacles which hinder NQR growth should be overcome.

B. Pulse Sequences

In order to optimize the NQR data format, it is necessary to choose the pulse sequence most suited for the measurement. Several of these exist and each has its benefits.

1) Free Induction Decay

The NQR response of a single crystal to a resonant pulse of rf irradiation is completely analogous to the spin 1/2 NMR case. One difference is that the intensity of the free induction decay (FID) response depends on the orientation of the radio-frequency field H_1 with respect to the EFG principal axes system. For a spin I = 1 system, the three resonance lines ν_+, ν_- and ν_d can be observed only when the field H_1 is oriented, respectively, along the x,y, and z principal axes of the EFG tensor. As an example, for a ν_- line, the expected value of the magnetization along the y axis is proportional to:

$$\frac{h\nu_-}{3kT} \sin(\sqrt{2}\omega_1 t_w) \cos(2\pi\nu_- t), \qquad (16)$$

---

[19] R. A. Marino, J. C. Harding and S. M. Klainer, J. Mol. Struc. 58, 79 (1980).

Table I

PULSED FT-NQR SPECTROMETER

Specification	Existing System[a]	System Under Design
Frequency Range	0.5 to 3MHz	0.5 to 64 MHz
Sample Volume	40 to 0.1cc[b]	100 to $5x10^{-4}$cc
System Sensitivity(SLSE)[c] S/N = 3, 1 sec integration	200 mg	1 mg
System Recovery Time (Sample Q=120)	150 µsec @ 3MHz	<15 µsec @ 1MHz
π/2 Pulse Width	50 µsec	10 µsec
Sample Coils	1 per octave	Same
Matching Networks	1 per octave	Same
Sample Operating Temperature	77°K to 350°K	4°K to 350°K
Remote Detection	Yes, non-directional	Yes, directional
Automatic Spectral Search	No	Yes, programmed sequence

a) Reference (18)

b) Reference (19)

c) Reference (21)

where $\omega_1 = \gamma H_1$ measures the intensity of the irradiation, and t_w is the duration of the irradiating pulse. The maximum response is obtained when:

$$\sqrt{2}\omega_1 t_w = \sqrt{2}\gamma H_1 t_w = \pi/2 \qquad (17)$$

in analogy with the NMR case.

In NQR, however, the sample usually consists of a polycrystalline powder. Then a convolution for all orientations must be made. The result[20] is that the $\sin(\sqrt{2}\omega_1 t_w)$ function in the expression for the expectation value of the magnetization becomes a Bessel function, $J_1(\sqrt{2}\omega_1 t_w)$. This function has its first maximum, analogous to a "90° pulse" at $\sqrt{2}\omega_1 t_w = 0.66\pi$ and not at $0.5\ \pi$ like the sine function. Similarly, the first null, corresponding to a "180° pulse" occurs for a value of the argument equal to 1.43π rather than simply to π.[20]

2) Spin Echo and Carr-Purcell (CP) Sequence

Following a FID experiment in a case where T_2 (spin-spin relaxation time) $>T_2^*$ (spin echo shape function) it is possible to recall part of the magnetization not lost through T_2 processes by applying a "180° pulse" at a time τ after the first pulse. As is well known, an echo will form at a time 2τ and this echo can be repeatedly recalled at integral multiples of this time $2n\tau$ by the application of additional "180° pulses" at times $(2n-1)\tau$. The amplitude of the resultant echo train decays with time constant T_2 (Fig. 5). Signal-to-noise enhancement can be obtained by coherently adding successive echoes in the sequence. The optimum time for co-addition is easily shown to be $1.26T_2$. Due to the generally small value of T_2 in solids, however, this method does not result in an appreciable enhancement of the signal-to-noise ratio.

---

[20] G. L. Petersen, Ph.D. Thesis, Brown University (1975).

3) Spin-Lock Spin-Echo (SLSE)

A major advance in S/N enhancement was made by Marino and Klainer[21] when an adaptation of the Ostroff-Waugh sequence[22] was made to NQR. The sequence needed is essentially a Meibrom-Gill-modified-CP sequence where all the pulses have the same flip angle of "90°", which means 0.66π in the NQR of an $I = 1$ nucleus. In Fig. 6 ($NaNO_2$ at 77°K, on resonance) and Fig. 7 ($NaNO_2$ at 77°K, slightly off resonance) it can be seen that the spin echo train in this sequence persists for times of order T_1 (spin lattice relaxation time, actually $T_{1\rho}$) and not the much shorter T_2. Coherent addition of the echoes in this case results in considerable enhancement of the S/N, since $T_{1\rho} >> T_2$ is the typical situation in these solids. Marino and Klainer showed that the optimum enhancement is $0.64\ (T_{2\varepsilon}/2\tau)^{1/2}$ where $T_{2\varepsilon}$ is the effective decay constant of the echo train and 2τ is the spacing between echoes, or equivalently the spacing between pulses of the excitation sequence. It was further shown that the NQR effect was completely analogous to the spin 1/2 NMR case discussed by Waugh[23] in that the decay constant $T_{2\varepsilon}$ tends to $T_{1\rho}$ as τ is reduced to values less than T_2. Furthermore, for intermediate values of $T_{2\varepsilon}$, this parameter is proportional to τ^{-5}, again in analogy to NMR. Fig. 8 shows this functional dependence for $NaNO_2$ at 77°K. Recently, Cantor and Waugh[24] have developed a theory to explain the main features of this NQR effect using a model of a polycrystalline solid with each nitrogen site having one nearest neighbour.

---

[21] R. A. Marino and S. M. Klainer, J. Chem. Phys. 67, 3388 (1977).

[22] E. D. Ostroff and J. S. Waugh, Phys. Rev. Letters, 16, 1097 (1966).

[23] J. S. Waugh, J. Mol. Spec. 35, 298 (1970).

[24] R. S. Cantor and J. S. Waugh, J. Chem. Phys. 73, 1054 (1980).

4) Strong Off-Resonance Comb (SORC)

Recently a new pulsed NQR experiment has been used by one of the authors (RAM) which can have considerable advantages in enhancing the S/N ratio of weak lines. This represents new and yet unpublished information.

The steady state response of an ensemble of nuclear spins, I = 1/2, in high magnetic field H_o to a strong radio-frequency field H_1, applied off resonance by Δf, has long been known[7]. When all the conditions for the establishment of a spin temperature in the rotating frame are met[7], the x-component of the magnetization, which is experimentally observable, is given by the expression:

$$M_x = M_o \left[\frac{H_1 (2\pi \Delta f/\gamma)}{H_1^2 + H_{loc}^2 + (2\pi \Delta f/\gamma)^2} \right] \qquad (18)$$

where M_o is the equilibrium longitudinal magnetization, γ is the magnetogyric ratio of the nucleus, and H_{loc} is a measure of the local field at the nuclear site due to its neighbors. Results analogous to Eqn. 18 have also been derived and observed for a quadrupolar system[25] with nuclear spin I = 3/2 when subjected to the same strong, long, off-resonant irradiation H_1.

The preliminary results obtained, when the irradiation field H_1 is applied in a long train of equally-spaced identical pulses, are presented here. Although the SORC experimental data reported here are for a quadrupolar I = 1 system, analogous effects in a magnetic system or a quadrupolar system with spin different from unity can be expected.

Fig. 9a defines the parameters of the SORC sequence. Here a train of radio-frequency pulses of duration t_w and spacing τ is applied, Δf

---

[25] J. C. Pratt, P. Raghunathan and C. A. McDowell, J. Chem. Phys. 61, 1016 (1974) and J. Mag. Res. 20, 313 (1975).

away from exact resonance, to a pure nuclear electric quadrupole system in zero external magnetic field.

The variation of the signal amplitude vs. Δf, the distance from exact resonance, shows two features as depicted in Figs. 9b and 9c. First, the signal amplitude is modulated by a sinusoid of period $1/\tau$, the pulse repetition rate. This phenomenon is best understood by considering that the Fourier transform of the transmitter pulses has periodicity $1/\tau$. This leads to successive maxima and minima in the NQR signal (Figs. 9b and c) as the transmitter frequency is changed, i.e., Δf is varied. Alternatively, and more naively, this modulation can be interpreted as the destructive interference of type I signals (immediately following the rf pulse) and type II signals (immediately preceeding the rf pulse) in their overlap region as the frequency, Δf, is slowly varied.

Another feature shown in Fig. 9c is the shape of the envelope, possibly conforming to a function of the type $\Delta f/(A^2 + \Delta f^2)$, such as Eqn. 18. Insufficient data have been taken so far to ascertain the degree of agreement with theory on this last point.

The nuclear induction signals present in the observation window between successive pulses of the SORC sequence are shown in Figs. 10a-j as a function of the pulse separation τ. All data were taken on the ν_- line of $NaNO_2$ at 77°K. The magnitude of the type I signal is then plotted vs. τ in Figure 11. Note that for $\tau \geq 8$ msec the magnitude of type I signals increases with τ as might be expected for a FID signal subject to spin-lattice relaxation. On the other hand, for $\tau \leq 5$ msec, signals at both ends of the observation window are of a comparable size and they grow exponentially with decreasing τ. This is the region of interest.

Fig. 12 shows the variation of the type II signal vs. $\langle H_1 \rangle$ for τ = 3 msec. The experimental points are obtained for four different values of the instantaneous field H_1 obtained by changing the pulse width t_w at constant "flip angle" $\sqrt{2}\ \gamma\ t_w H_1$. The dotted line is the curve $F = \langle H_1 \rangle / [\langle H_1 \rangle^2 + B^2]$ with B = 0.05 G. The fact that $\langle H_1 \rangle$, the average value, rather than H_1, the peak value, is the important parameter and that there is good agreement of the data with the form of Eqn. 18 is strong evidence that the ensemble of spins is responding to the time-average field of the SORC sequence in a manner analogous to the conventional long, strong, off-resonant pulse.

The size of the parameter B is found to be about 0.05G which is approximately two orders of magnitude too small for the value expected from the contribution of Δf to Eqn. 18. This discrepancy is reduced by a factor of 5 when the experiment is repeated for τ = 1 msec, as shown in Fig. 13. Comparison of Figs. 12 and 13 suggest that the pulse nature of the experiment is still very important for τ = 1 msec and that quantitative agreement cannot be expected until τ is reduced further.

The potential of this technique appears to be great since signals can be obtained at essentially 100% duty cycle. However, further experimentation is needed to completely understand the operational parameters of SORC.

C. FT Considerations

There are three main reasons for doing FT spectroscopy:

a. Enchancement of signal-to-noise over CW methods is given by the square root of the ratio of the total width of the spectrum to the typical line width, $\sqrt{T_2^* \Delta}$.

b. Pulsed methods are singularly well-suited to data processing.

c. The line shape is readily obtained directly from the output.

Of these, the first reason, probably the most important in other disciplines, is not nearly as important in NQR, because the ratio defined above is not large and can often be close to unity. This is so because in solids line widths are relatively large (a few kHz) while the bandwidths which can be suitably irradiated are in the 10-100 kHz range. The other two advantages, however, have provided the impetus toward the growth of FT-NQR.

(1) Comparison with High Resolution NMR (HR-NMR)

In HR-NMR the width of the spectrum Δ is much less than the carrier frequency f_o; $\Delta/fo \leq 10^{-3}$ can be expected even in worst cases. In NQR however, the ratio Δ/f_o is often of order unity.

This implies that the NQR spectrum must be obtained one frequency interval at a time and cannot usually be displayed in one operation as in the case in HR-NMR.

2. Processing Techniques

Once FID or echo signals have been obtained, the proper FT treatment for each will yield the desired lineshape spectrum.[26,27] In this section the procedures the authors found most satisfactory are discussed.

The problem of phase correction for NQR spectra presents a particular problem not found in fixed-frequency spectrometers. The fact that the NQR spectrometer operates at variable frequencies means that instrumental phase shifts will be present for NQR signals which are not corrected for before final data collection. These phase shifts can be considerable and are of course also present in echoes, where the receiver dead time problem present for FID signals does not occur. In Table II the mathematical results

---

[26] R. Lenk and E. A. C. Lucken, Pure Applied Chem. 40, 199 (1974).

[27] A. Colligiani and R. Ambrosetti, Gazz. Chim. Italiana 106, 439 (1976).

for Lorentzian lineshapes are collected as guides to the solution of this problem.

The results in the Table show that the presence of phase shifts produces an admixture of absorption and dispersion modes in the case of FID signals, and a possible loss of intensity in echo signals. This problem can be avoided while at the same time the true Lorentzian line shape is preserved, if the modulus squared transform is computed for FID signals, and the modulus transform is computed for echoes. Thus the proper line shapes are obtained in each case regardless of the degree and source of phase shift without need for a separate "phase correction" subroutine.

In Figs. 14-21 the results of computer-simulated spectra are shown. An echo and a FID signal have been simulated for both Lorentzian and Gaussian lineshapes. Cosine, sine, the square of the modulus, and modulus transforms are computed and displayed. Figs. 14-17 are for no phase shift, while Figs. 18-21 have a phase shift of 30° in the time domain signals. Note that in all cases the conclusions discussed for proper data processing are borne out, mainly that the modulus squared transform should be used for FID signals, and the modulus transform should be used for echo signals.

Figs. 22-24 show experimental spectra that demonstrate the foregoing arguments. Figs. 22(a) and 23(a) are the Nitrogen-14 NQR FID signals at 77°K from hexamethylenetetramine (HMT) and urea, respectively. The cosine and sine transforms of HMT, Figs. 22(b) and (c), clearly show the admixture of adsorption and dispersion expected when phase shifts exist in the time-domain data. This effect is much less evident in the cosine and sine transforms of urea, Figs. 23(b) and (c), which occurred with only a small phase shift. Finally, the proper lineshapes are shown in Figs. 22(d) and 23(d), the modulus squared

TABLE II

Lorentzian FID and echo complex signals and their Fourier transforms

FID

Time domain: $f(t) = e^{-\alpha t} e^{i\omega_0 t} e^{-i\phi} \quad t \geq 0$

C, Cosine transform $= \frac{1}{\alpha^2+(\omega-\omega_0)^2}\left\{\alpha\cos\phi - (\omega-\omega_0)\sin\phi\right\}$

S, Sine transform $= \frac{1}{\alpha^2+(\omega-\omega_0)^2}\left\{\alpha\sin\phi + (\omega-\omega_0)\cos\phi\right\}$

C^2+S^2, Modulus squared transform $= \frac{1}{\alpha^2+(\omega-\omega_0)^2}$

$[C^2+S^2]^{\frac{1}{2}}$, Modulus transform $= \left[\frac{1}{\alpha^2+(\omega-\omega_0)^2}\right]^{\frac{1}{2}}$

ECHO

Time domain: $f(t) = \begin{cases} e^{\alpha t} e^{-i\omega_0 t} e^{-i\phi} & t < 0 \\ e^{-\alpha t} e^{i\omega_0 t} e^{-i\phi} & t \geq 0 \end{cases}$

C, Cosine transform $= \frac{1}{\alpha^2+(\omega-\omega_0)^2} 2\alpha\cos\phi$

S, Sine transform $= \frac{1}{\alpha^2+(\omega-\omega_0)^2} 2\alpha\sin\phi$

C^2+S^2, Modulus squared transform $= \left[\frac{2\alpha}{\alpha^2+(\omega-\omega_0)^2}\right]^2$

$[C^2+S^2]^{\frac{1}{2}}$, Modulus transform $= \left[\frac{2\alpha}{\alpha^2+(\omega-\omega_0)^2}\right]$

transforms of the time-domain signals. Note the fine structure on the HMT line, first reported by Colligiani and Ambrosetti.[28] The modulus transforms, Figs. 22(e) and 23(e), are shown for comparison and they are visibly broader than the true lineshapes.

An example of an echo signal is shown in Fig. 24(a), a doublet of ν_- lines from the monoclinic phase of TNT at 77°K. Figs. 24(b) and (c) are, respectively, the cosine and sine transforms of this signal. Note that, as expected, both of these transforms yield valid lineshapes with fractional amplitudes, and that the modulus transform, Fig. 24(e), yields the correct lineshape.

IV. APPLICATIONS

The current intense interest in the chemistry, physics, and crystallography of solids is responsible for the renewed activity in NQR. In 1964 Grechishkin and Soifer[29] suggested specific applied categories into which NQR could be divided. These have been updated and include:

a. Investigation of the nature of chemical bonds in solids. (The NQR frequency is directly dependent upon the type of hybridization and the degree of ionization of the chemical bond.)

b. Establishment of nonequivalence of the location of resonant atoms in crystal lattices and molecules.

c. Qualitative analyses (each chemical compound has a definite NQR spectrum).

d. Inspection of purity of chemical synthesis products (The NQR line

---

[28] A. Colligiani and R. Ambrosetti, J. Chem. Phys. 60, 1871 (1974).

[29] V. S. Grechishkin and G. B. Soifer, Pribory i Tekhnika Eksperimenta 1, 5, (1964) (Russian).

intensity is directly dependent on the amount of soluble impurities in a sample.)

e. Structural analysis of crystals. (NQR is a valuable compliment to x-ray methods.)

f. Detection of phase transitions in crystals and the investigation of their kinetics.

g. Measurement of average rotary vibration frequencies and average moments of inertia of molecules in crystals, from the temperature dependence of NQR lines.

h. Measurement of strain.

i. Determination of temperature.

Table III lists some of the capabilities of NQR. These examples have been chosen because they represent real, current-day problems which have been presented for possible solution using NQR.

Table III

Suggested Applications of FT-NQR*

Characterization of new compounds (drugs, chemicals, explosives, liquid crystals, etc.).

Degree of crystal order (in clays, solid solutions, etc.).

Locus of aluminum atoms in plagioclase minerals.

Shelf life of materials (drugs, chemicals, explosives, etc.).

Determination of in-situ strain (salt domes, hard rock, etc.).

Detection of contraband (drugs, explosives).

Identification of contaminants (i.e. nature of N, S and O in coal).

Measurement of temperature.

Radiation damage in solids.

Crystalline polymorphism studies (i.e. relationship of TNT crystalline forms to impact stability, etc.).

Measurement of organic complexes (i.e. V, Cu, Ni in crude oil).

Identification of host minerals in bore-holes (i.e. measurement of uranium grade and type).

Characterization of phase transitions (i.e. in rock-forming minerals such as feldspars, pyroxenes, phyllosilicates, etc.).

Interpretation of crystal order with respect to thermodynamic properties (in minerals).

Determination of non-stoichiometric behavior (i.e. minerals, alloys single crystals, etc.).

Identification of small solid samples (i.e. exsolution in alumino-silicates, dangerous materials, rare compounds, etc.).

*In some instances NQR techniques other than FT may prove to be more suitable, i.e., double resonance NQR, acoustic NQR, etc.

V. CONCLUSIONS

It is now possible to answer the two questions posed in the introduction. NQR development has been hindered by:

(a) Lack of proper instrumentation

(b) Inefficient sample excitation techniques

(c) Primitive data handling and processing methods.

It can be shown that solutions have been found for each of these drawbacks:

(a) Sensitive, high resolution, automated, pulsed NQR spectrometers which utilize state-of-the-art electronic, radar, and computer techniques fulfill the instrumentation needs.

(b) The availability and usability of a variety of pulse sequences such as spin-lock spin-echo (SLSE) or strong off-resonance comb (SORC) provide superior sample excitation.

(c) Fourier Transform data processing, using modulus squared or modulus transforms, represents the state-of-the-art procedure for the special NQR conditions.

The need for FT-NQR is clearly demonstrated by the examples given in Table III. The growing interest in understanding the behavior of solids has provided an impetus for analytical techniques suitable for use with solid state systems. Particular emphasis has been directed at natural systems, such as minerals, and military and security applications. Furthermore, the possibility of measuring in-situ strain is of major interest to the rock mechanics community. A technology which can measure both single crystals and polycrystalline materials, which can respond to contaminants or homogeneous small samples, which can operate both in the laboratory or under semi-remote conditions while providing high resolution spectral data for solid samples has

all of the versatility to develop into an important analytical method.

The authors wish to thank Mr. R. Connors of Block Engineering, Cambridge, MA for his assistance in running the NQR spectra. They would also like to recognize Mr. N. Henderson, Office of Nuclear Waste Isolation, Battelle-Columbus, Columbus, OH and Dr. C. Boghosian, U. S. Army Research Office, Research Triangle Park, N.C. for their continued support. Technical editing was done by Dr. Ellory Schempp of Lawrence Berkeley Laboratory, Berkeley, California.

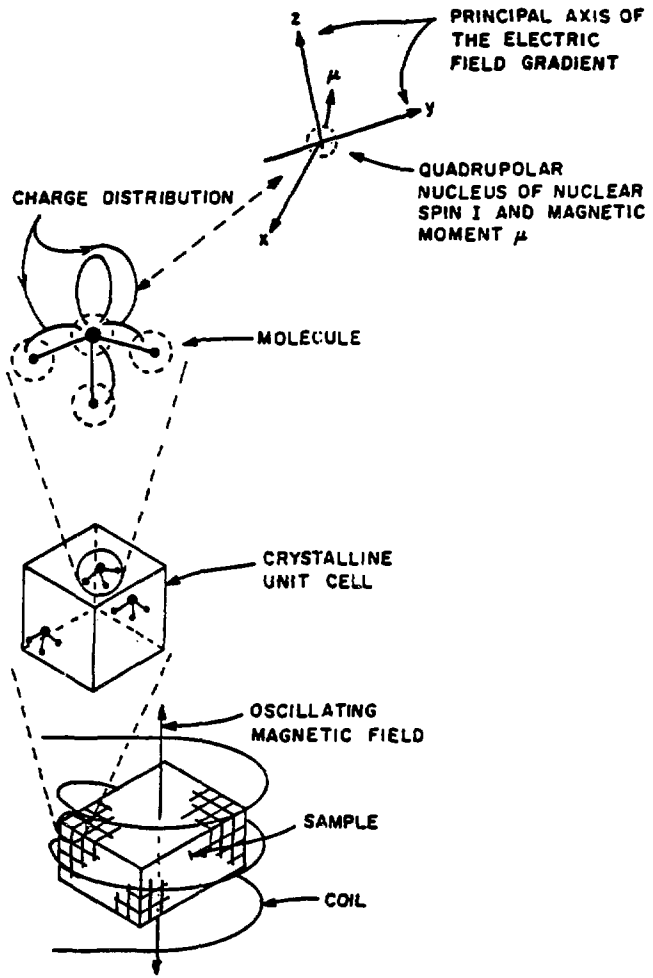

Figure I. Graphic Display for Nuclear Quadrupole Resonances.

XBL 793-8926A

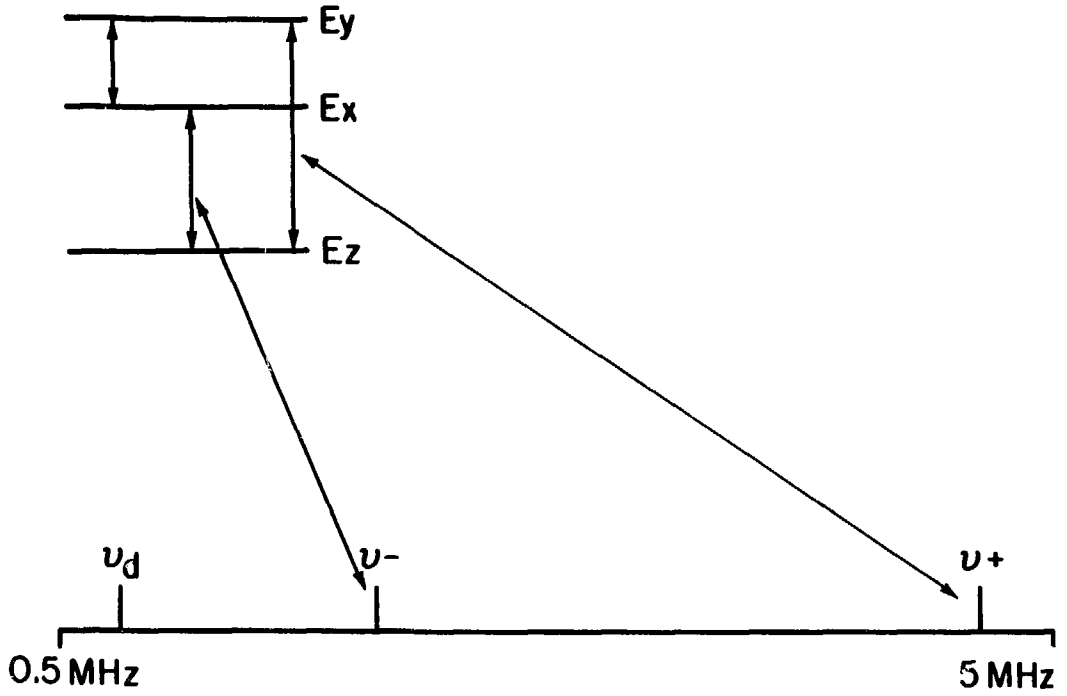

Figure 2. Energy Level Diagram and Approximate Frequency Range for Nitrogen-14 NQR.

XBL 808-2700A

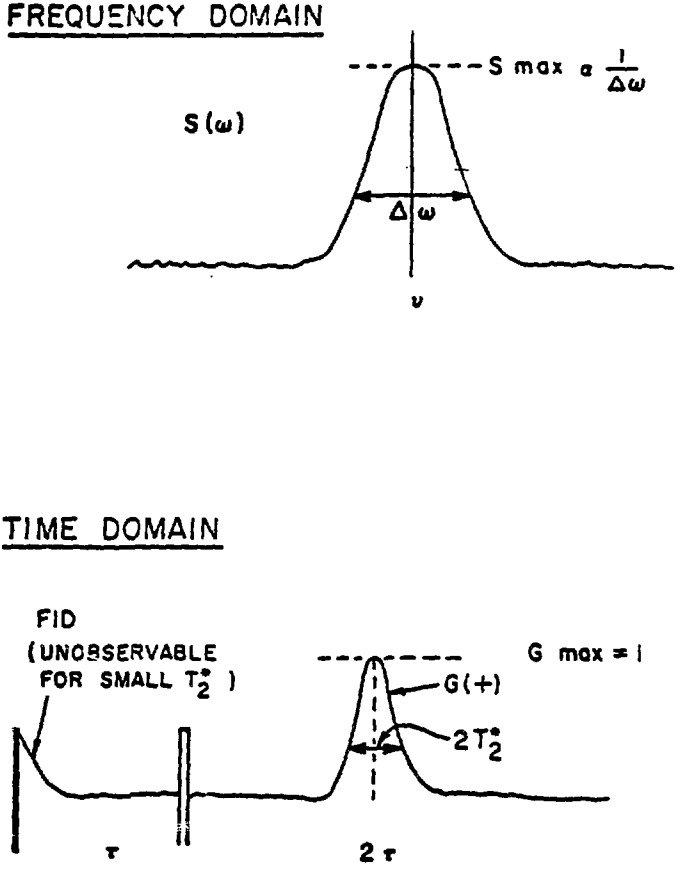

Figure 3. Line Shape Parameters for Spin Echo Sequence.

XBL 808-2701A

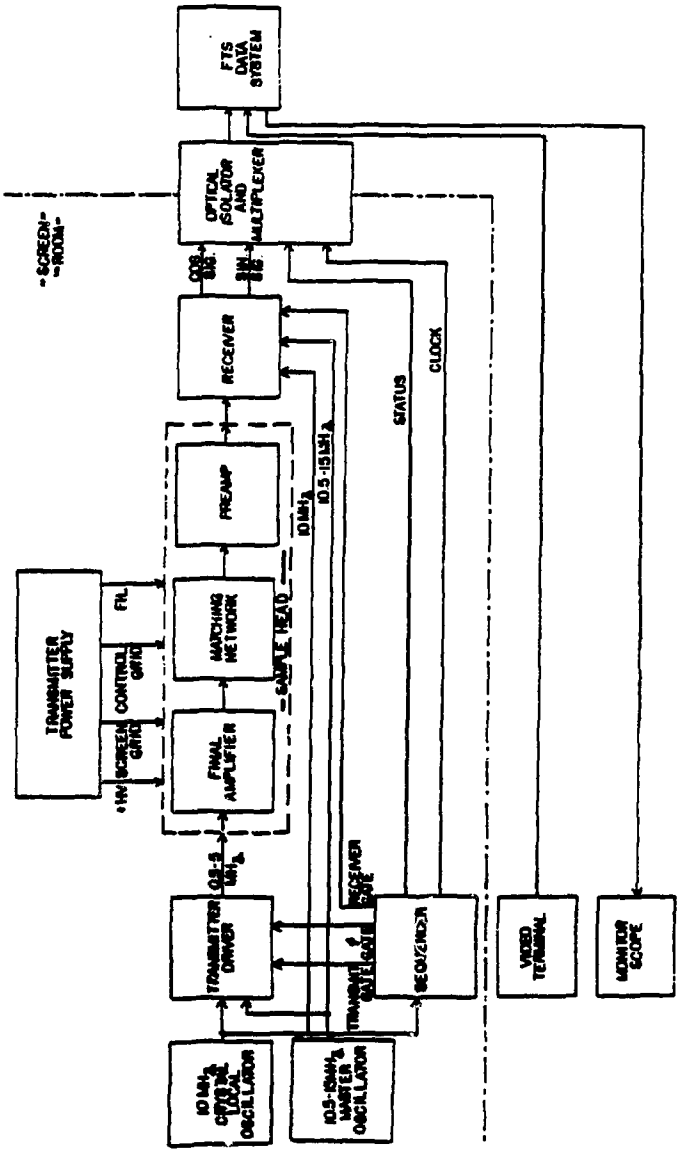

Figure 4. Block Diagram of the FT-NQR Spectrometer.

XBL 808-2702A

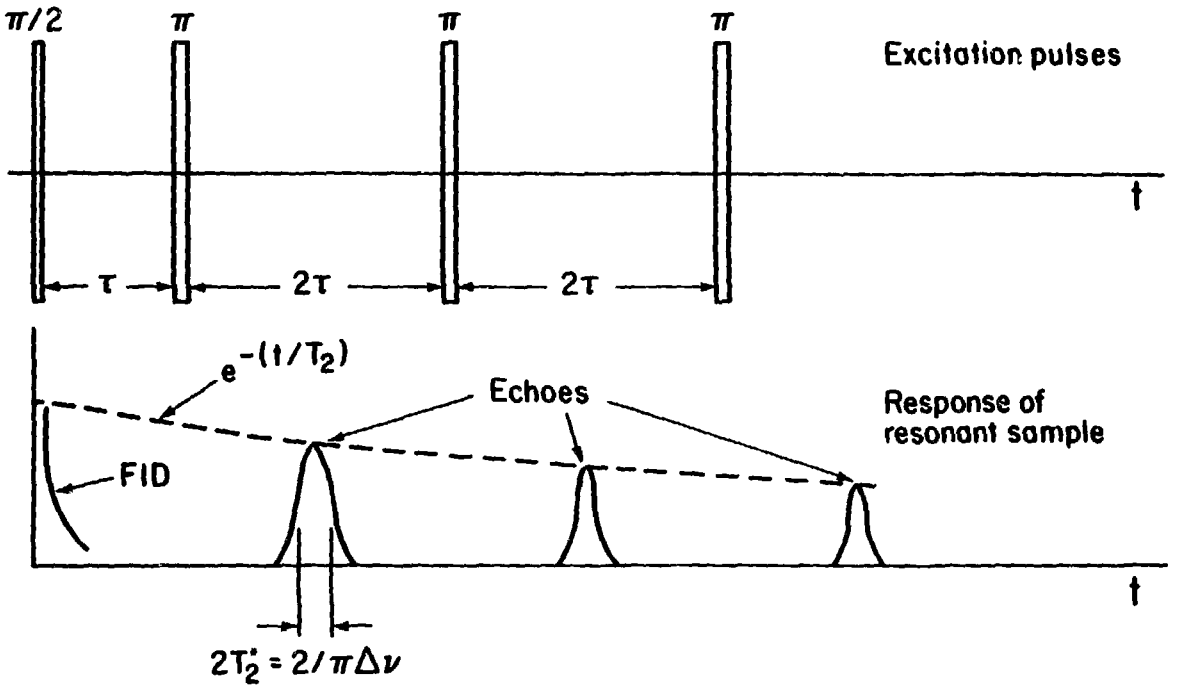

Figure 5. Parameters for the Carr - Purcell Sequence.

XBL 808 - 2703A

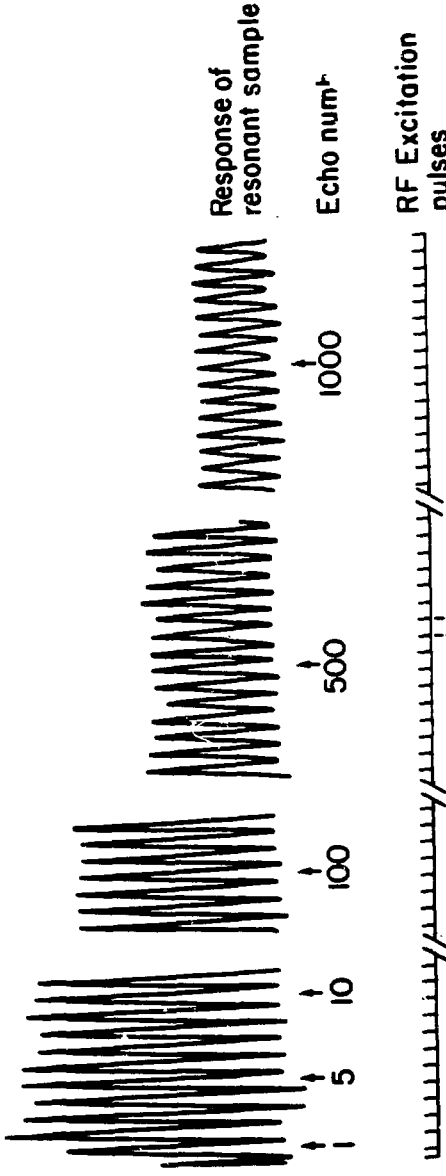

Figure 6. $NaNO_2$, 77 °K ν_- Line, On Resonance SLSE Sequence

XBL808-2710A

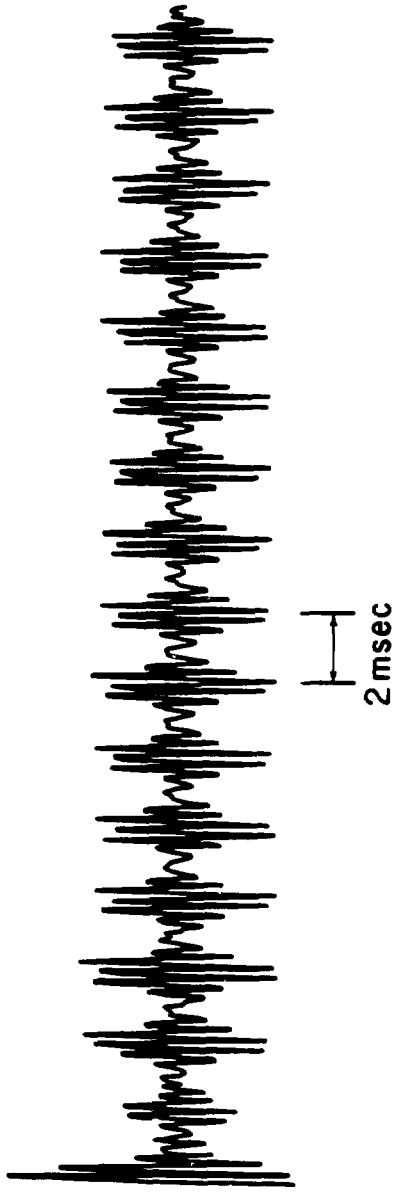

Figure 7. $NaNO_2$, 77 °K $\nu_\perp$ Line, Off-Resonance SLSE Sequence

XBL 808-2711A

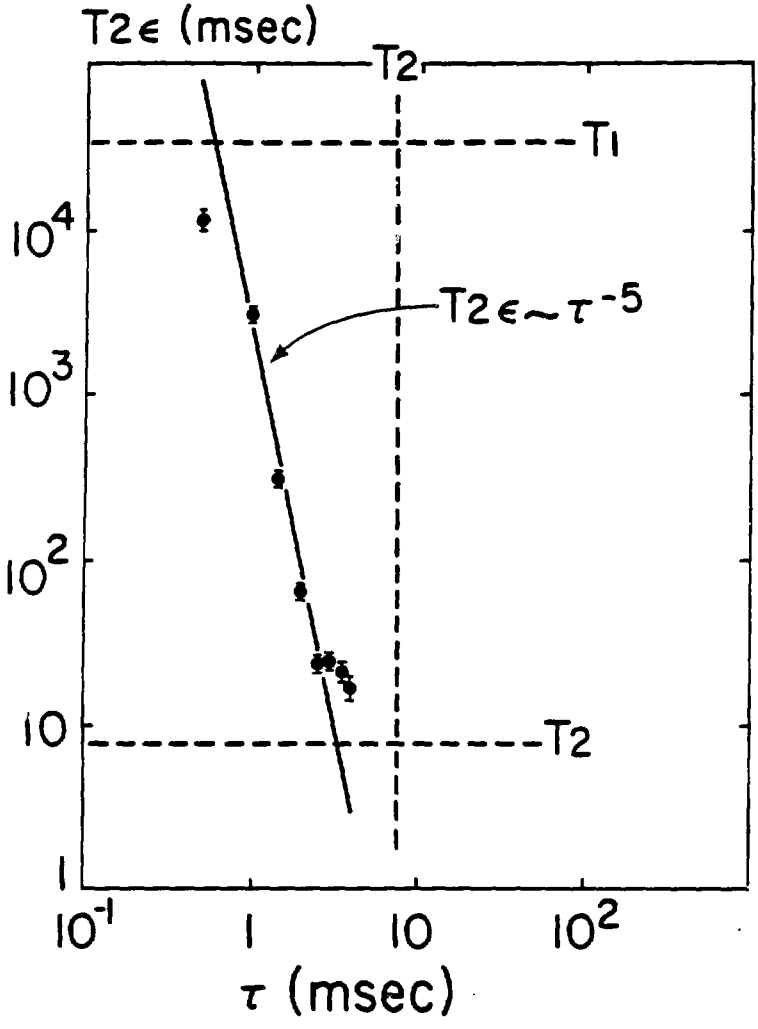

Figure 8. Echo Train Decay Constant, T2ε vs. SLSE Pulse Spacing τ for the ν_- Line of $NaNO_2$ at 77 °K

XBL 808 - 2704A

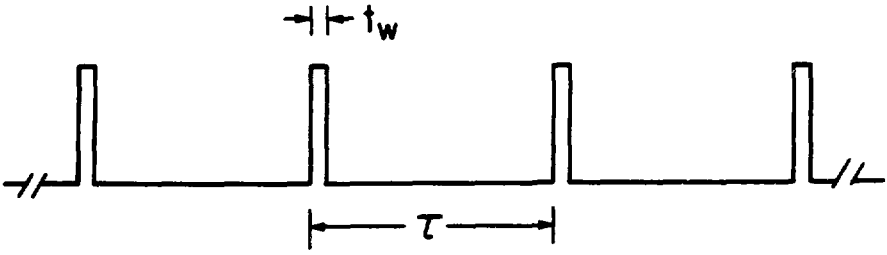

(a) Parameters

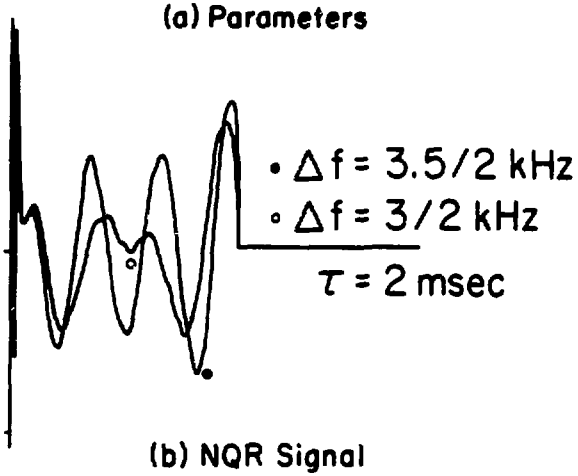

(b) NQR Signal

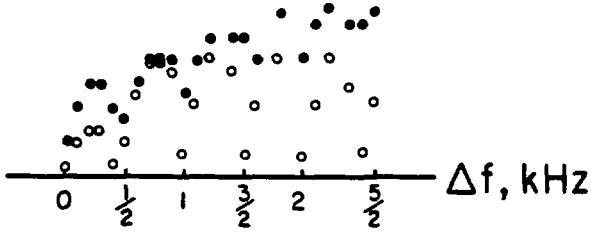

(c) NQR Signal vs. Resonance Offset

Figure 9. SORC Pulse Sequence

XBL 808 - 2705A

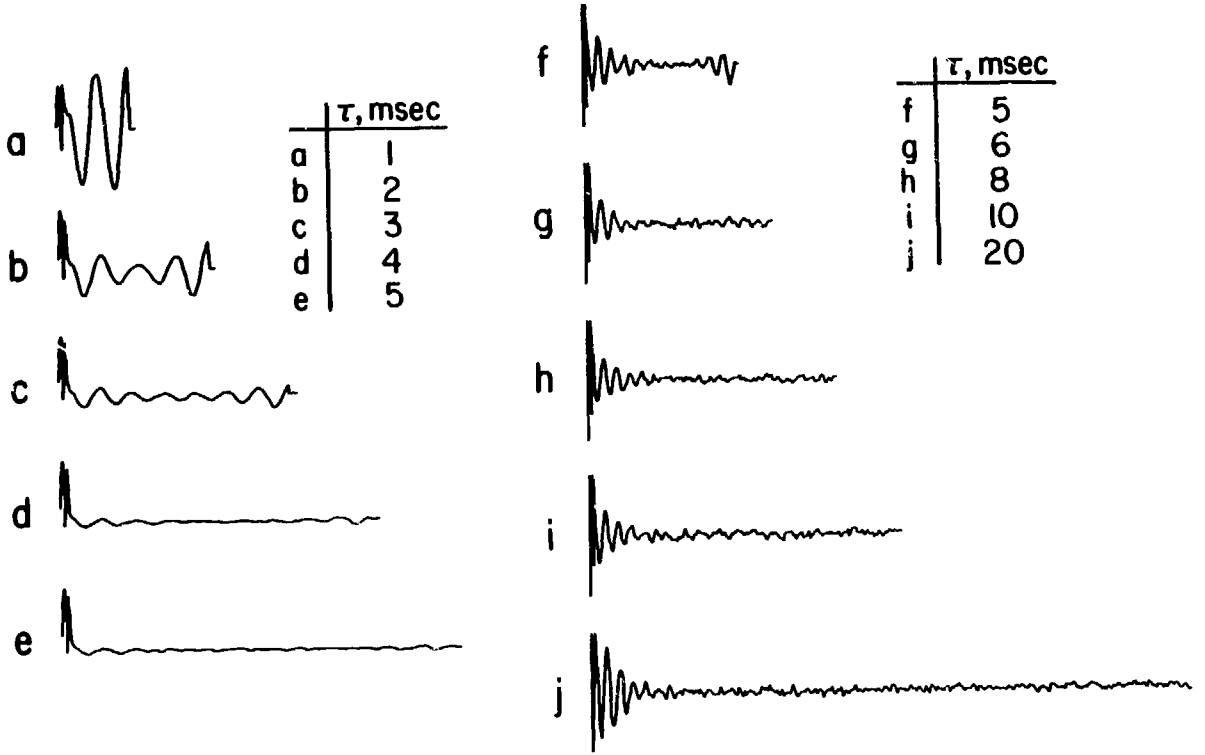

Figure 10. Steady State SORC Signal vs. τ

XBL 808-2706A

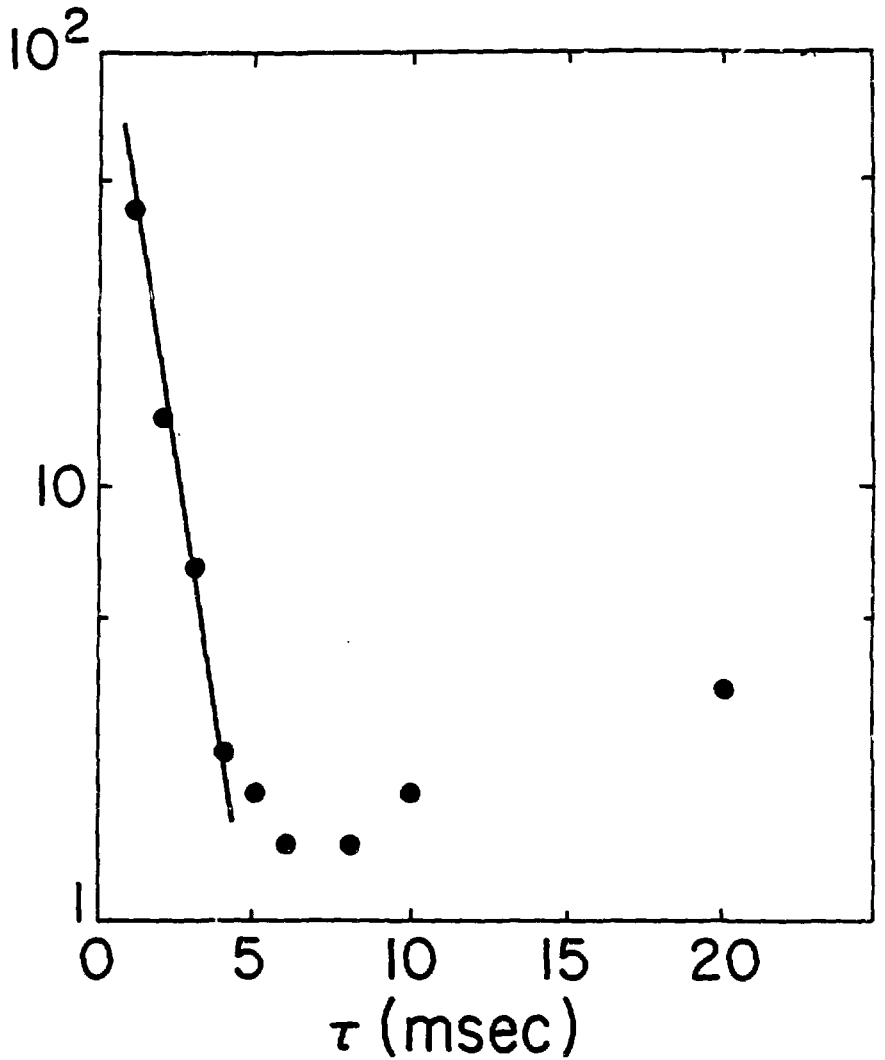

Figure 11 . Semilog Plot of SORC Signal vs. τ

XBL 808-2707A

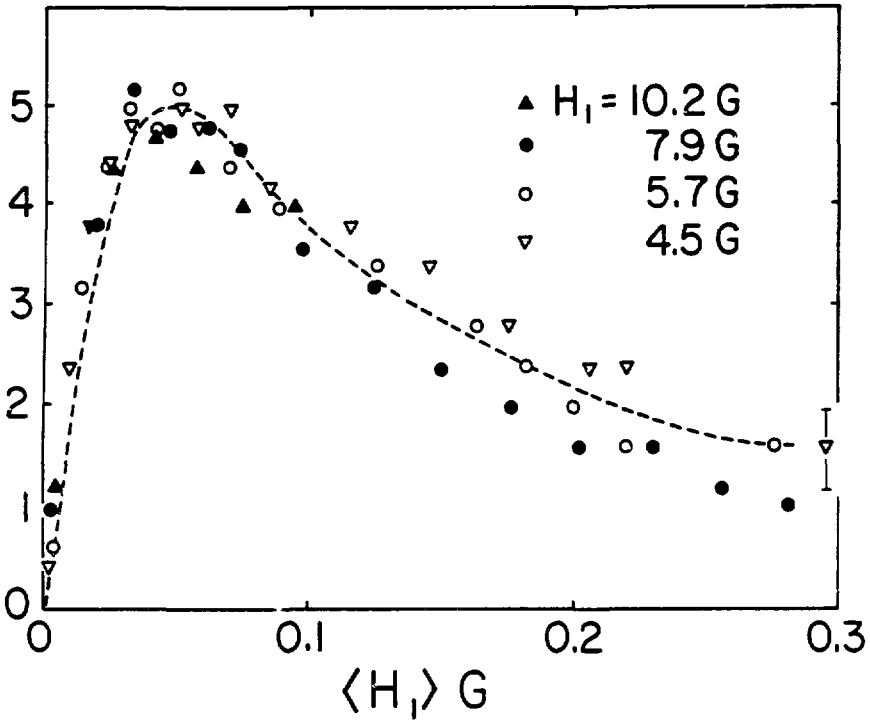

Figure 12. Size of SORC Signal vs. Average Value of H_1 (τ = 3 msec)

XBL 808-2708A

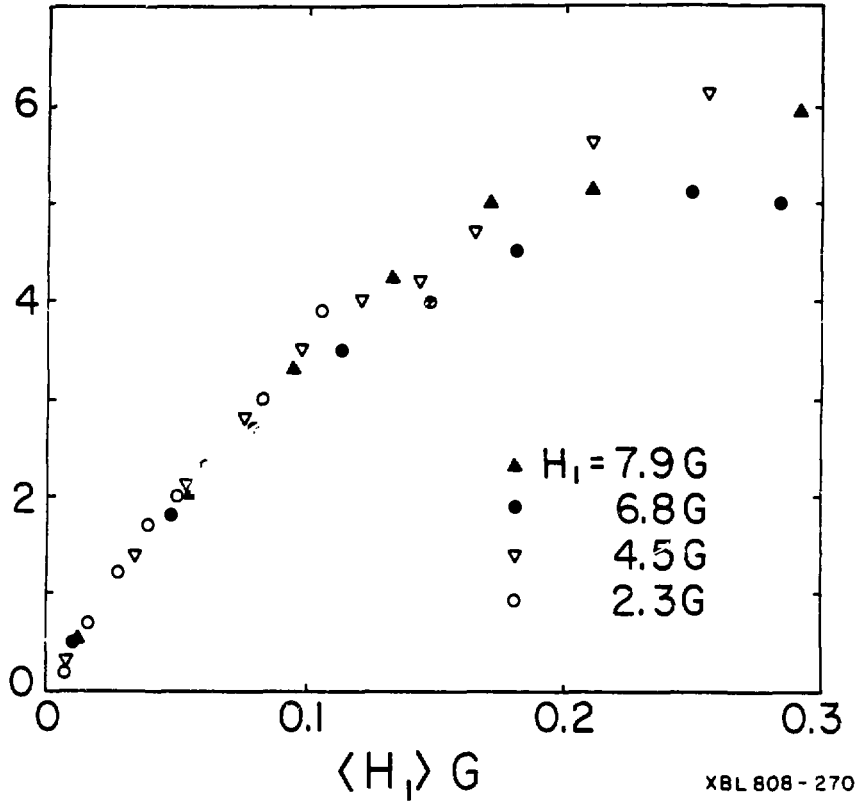

Figure 13. Size of SORC Signal vs. Average Value of H_1 (τ = 1 msec)

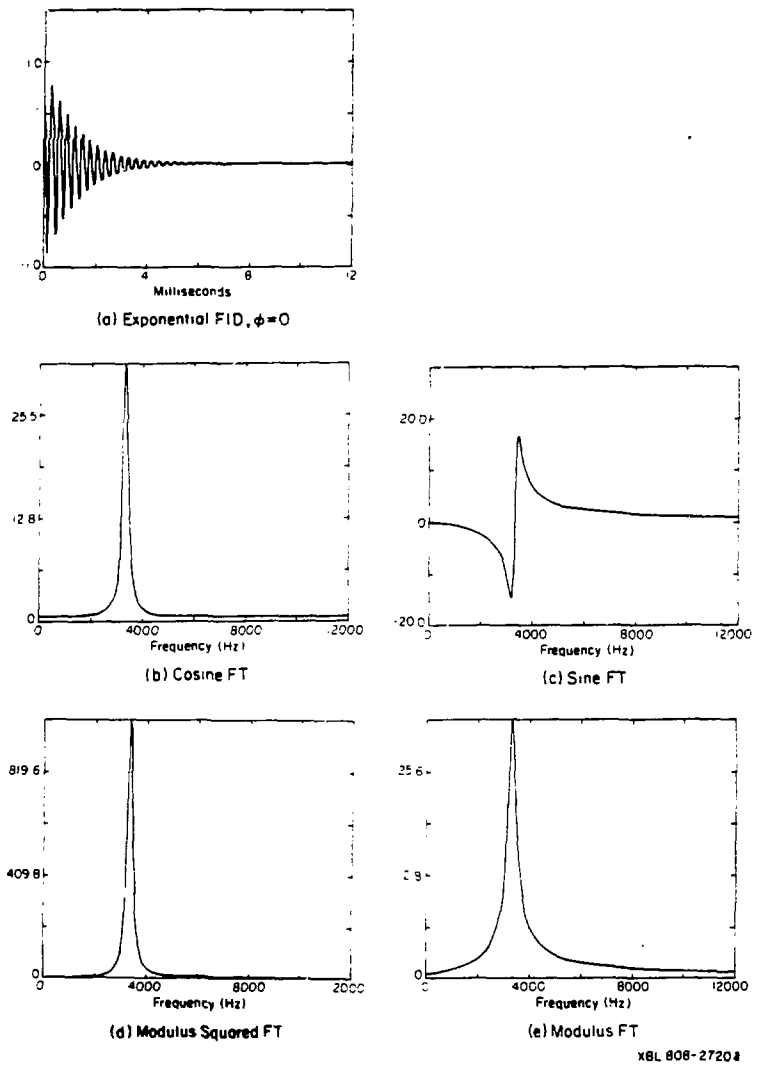

Figure 14. Simulated Exponential FID (ϕ=0) and its Fourier Transforms

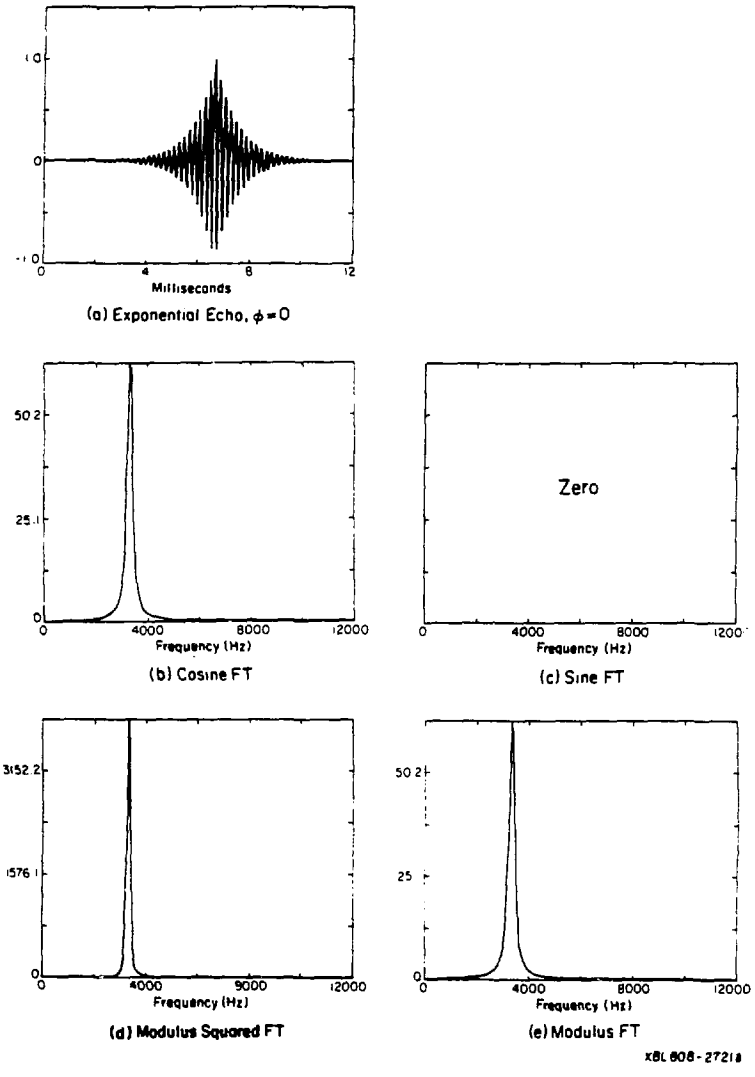

Figure 15. Simulated Exponential Echo ($\phi = 0$) and its Fourier Transforms

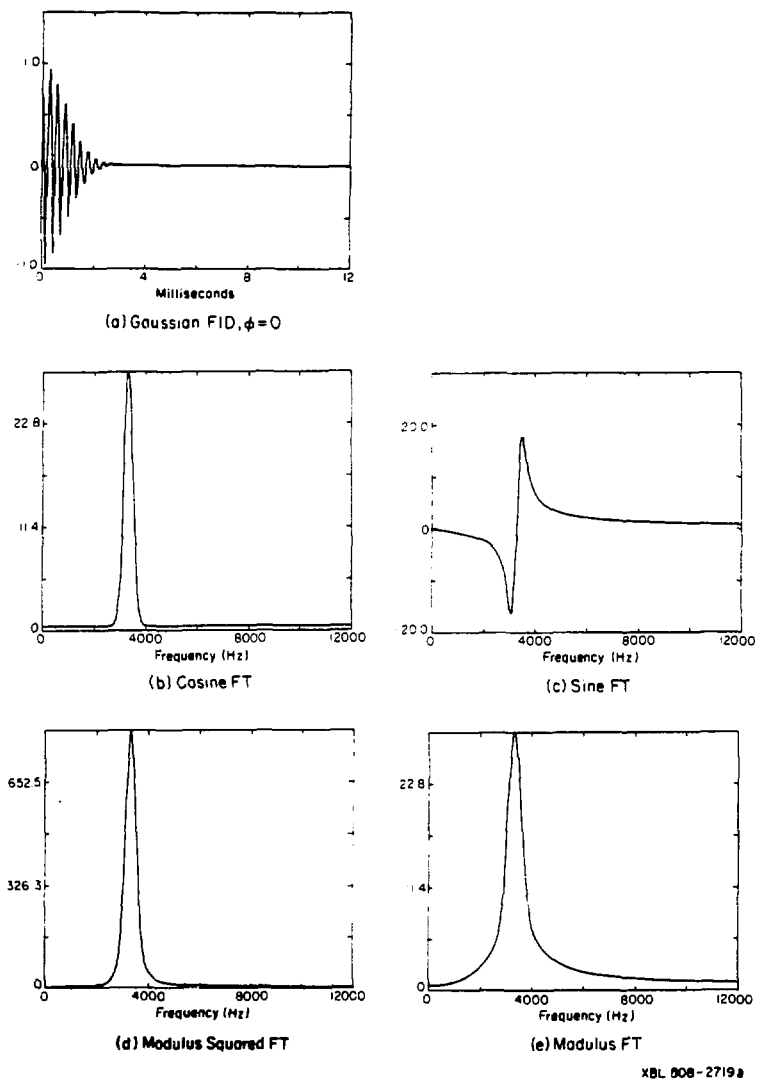

Figure 16. Simulated Gaussian FID ($\phi = 0$) and its Fourier Transforms

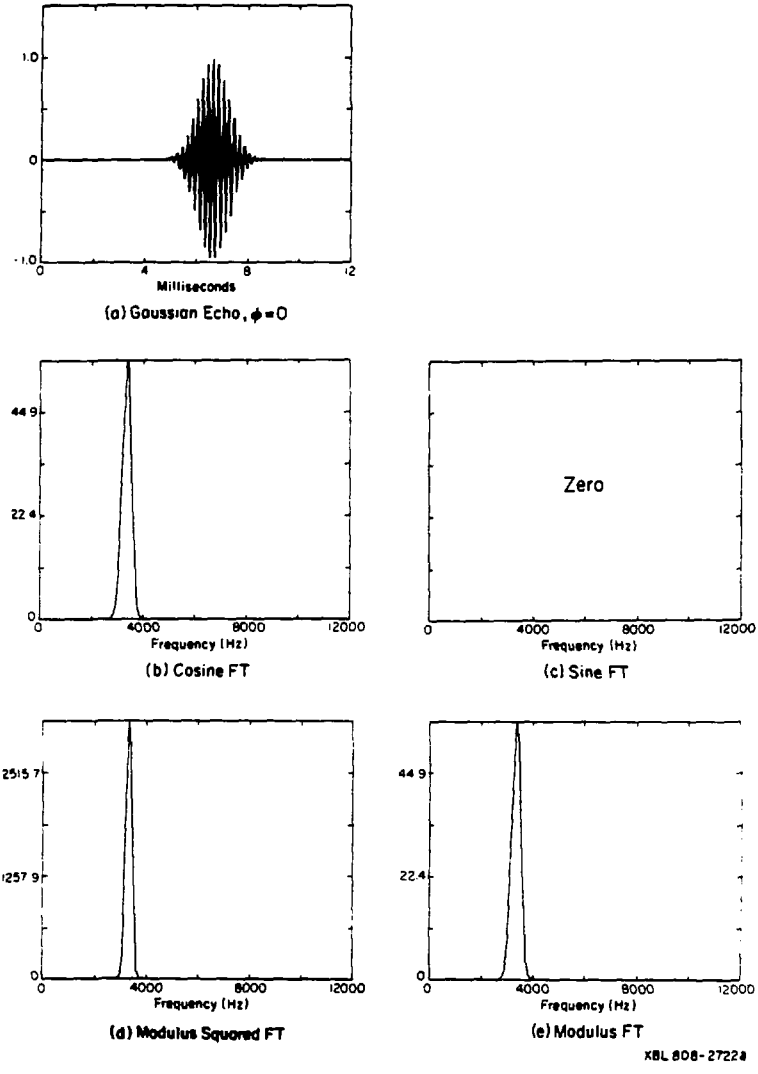

Figure 17. Simulated Gaussian Echo (ϕ=0) and its Fourier Transforms

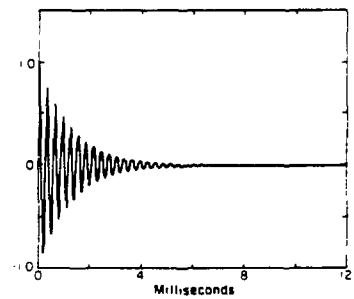

(a) Exponential FID, $\phi \neq 0$

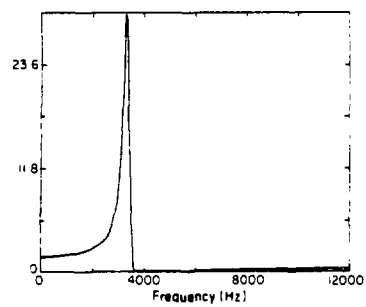

(b) Cosine FT

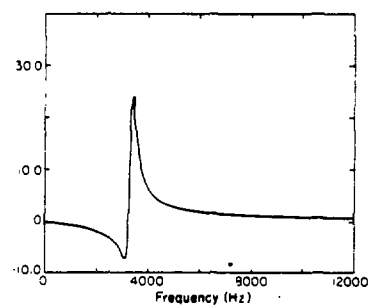

(c) Sine FT

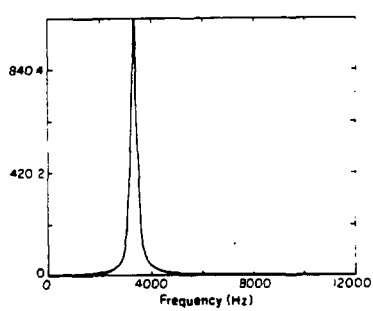

(d) Modulus Squared FT

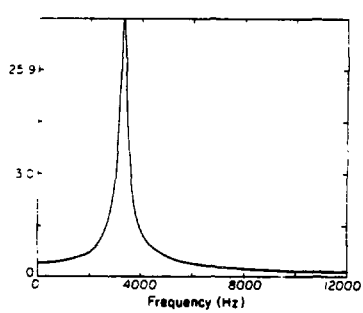

(e) Modulus FT

XBL 808-2712a

Figure 18. Simulated Exponential FID ($\phi \neq 0$) and its Fourier Transforms

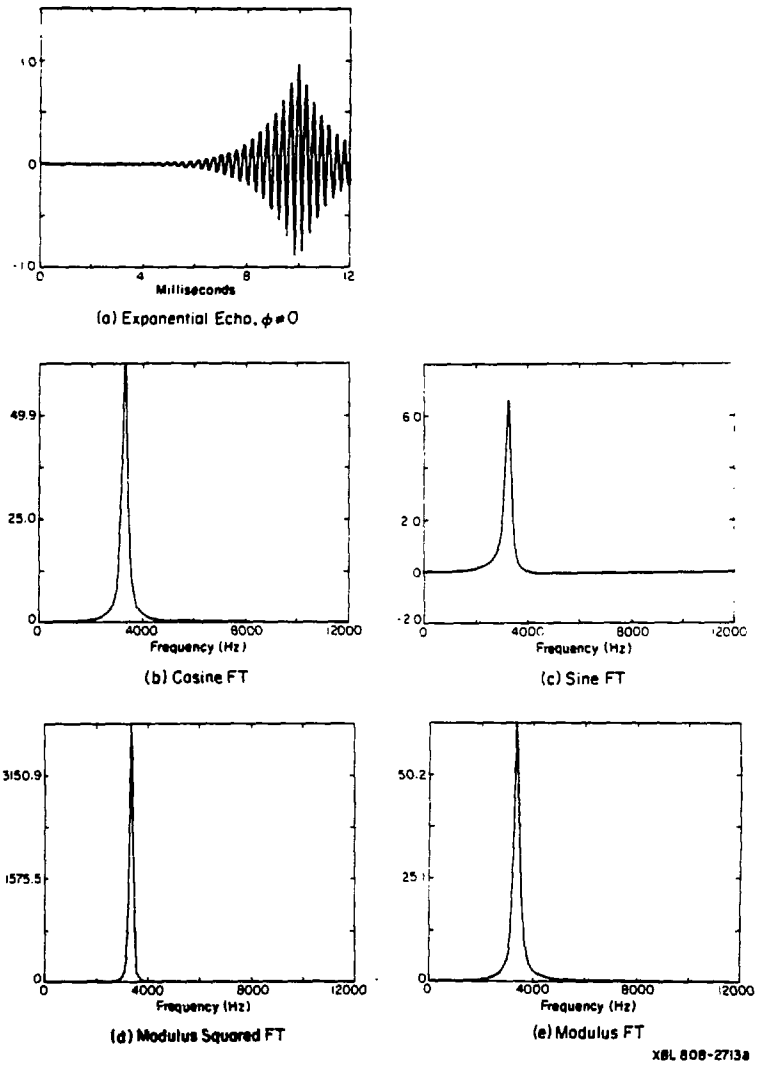

Figure 19. Simulated Exponential Echo ($\phi \neq 0$) and its Fourier Transforms

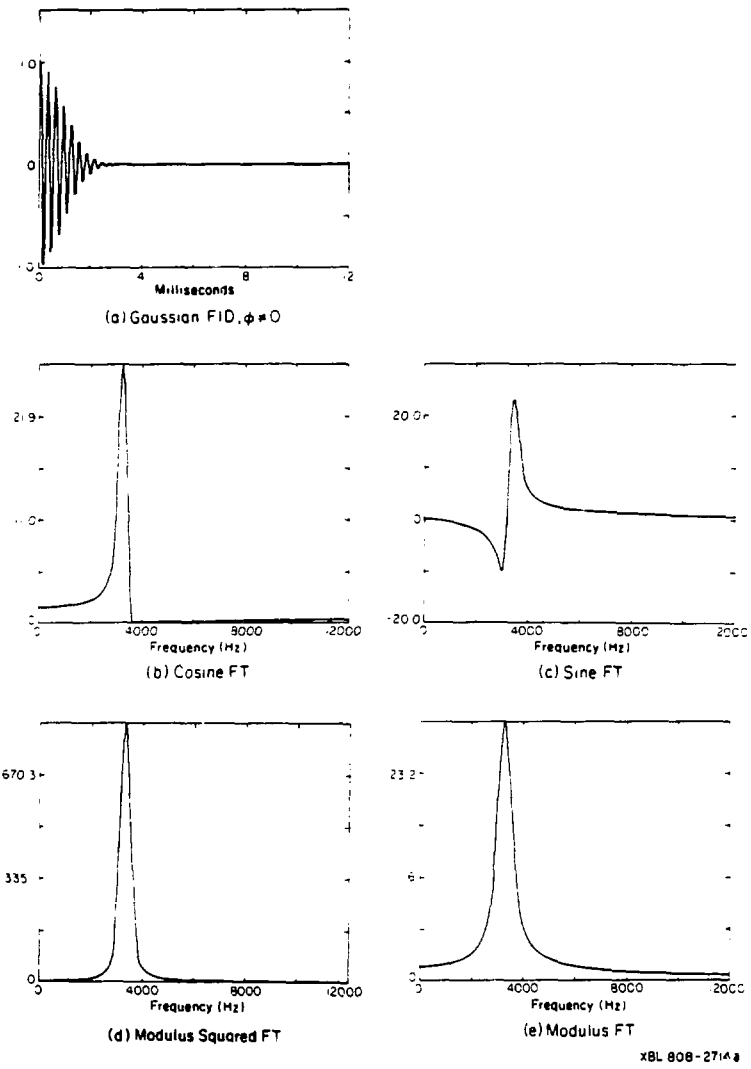

Figure 20. Simulated Gaussian FID ($\phi \neq 0$) and its Fourier Transforms

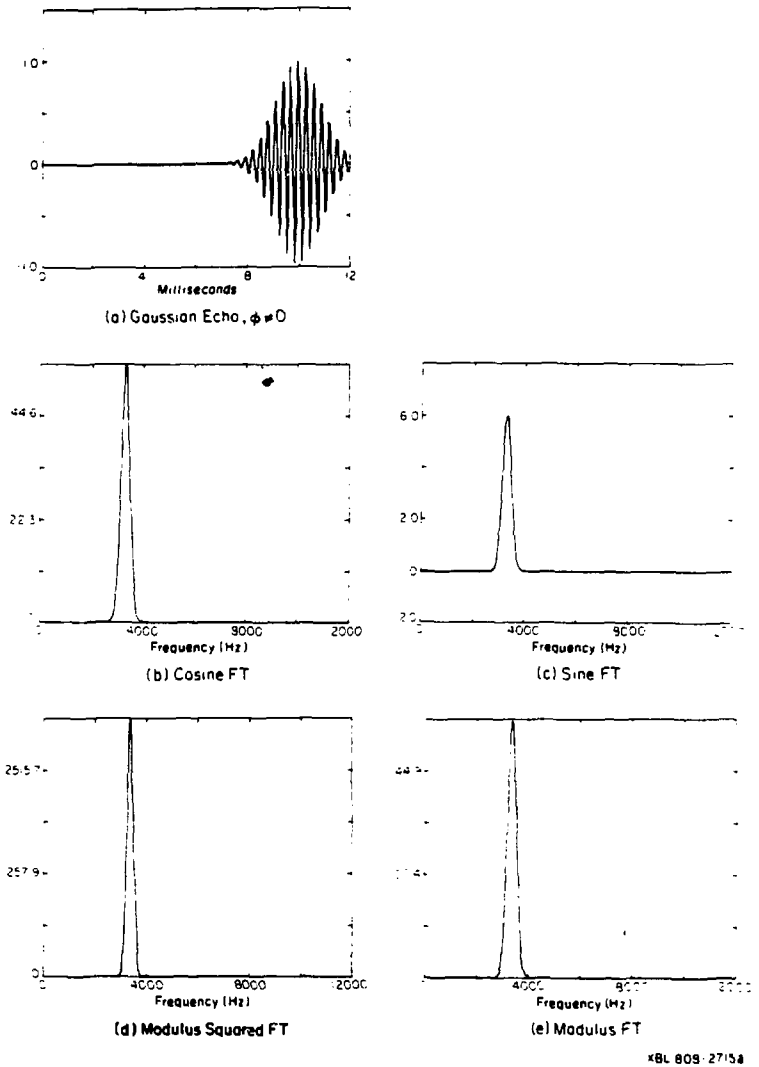

Figure 21. Simulated Gaussian Echo ($\phi \neq 0$) and its Fourier Transforms

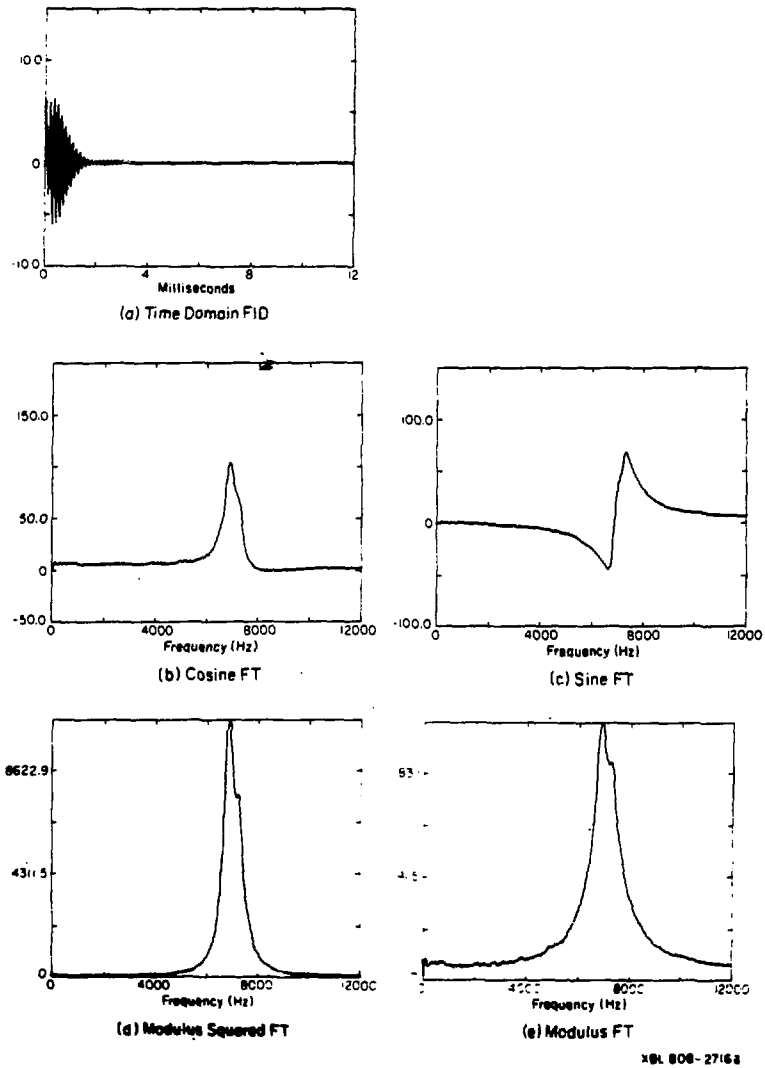

Figure 22. Hexamethylenetetramine, Room Temperature

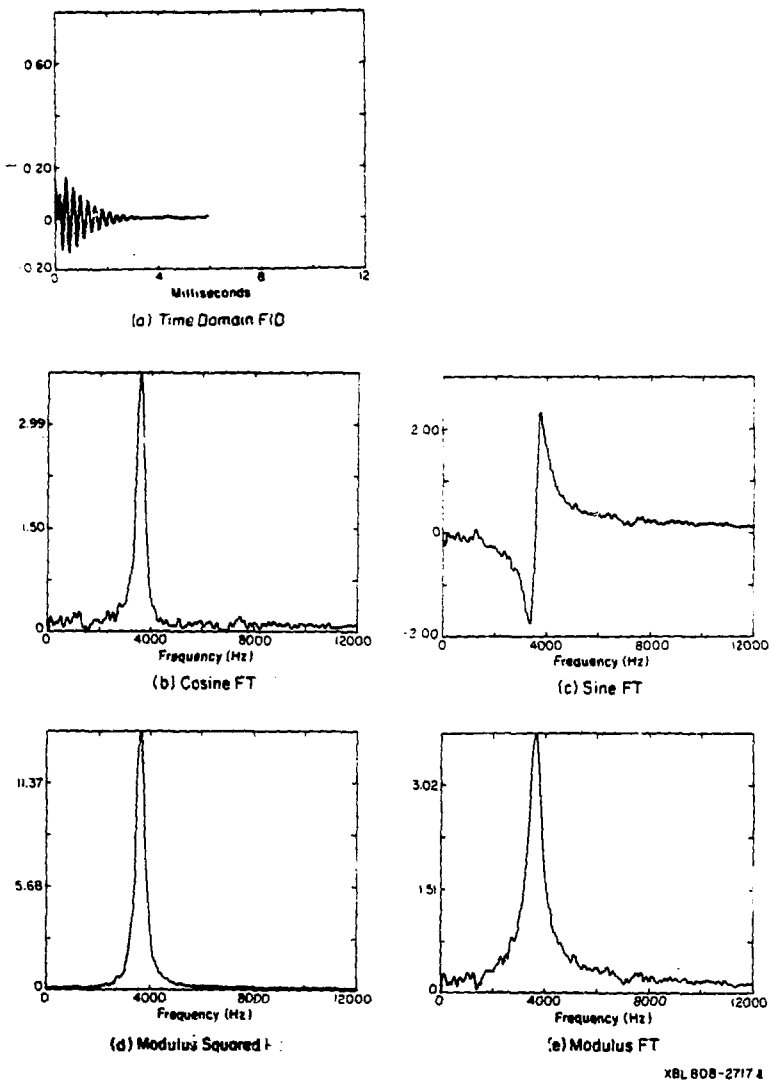

Figure 23. Urea, ν_4 Line at 77 °K

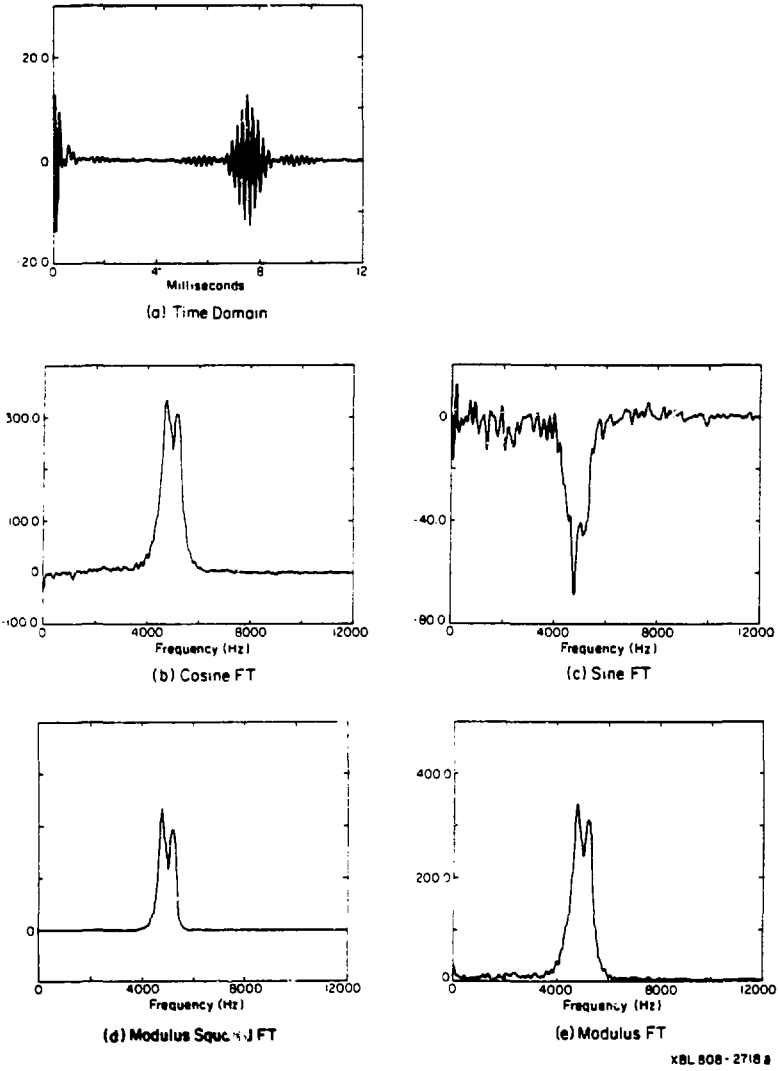

Figure 24. 727 kHz Doublet in Monoclinic TNT at 77°K

B. Axial Field of a Coil of Finite Height and Width

If we define

ℓ = winding half-height, cm

A_r = width of annulus in terms of coil radius

x = axial distance from coil center, cm

H_ℓ = field in coil axis for a given winding height, oerstedt

H_{A_r} = field in coil axis for a given relative annulus width, oerstedt

H_x = field in coil axis for a given axial distance, oerstedt

we have

$$H_{0,0,0} = \frac{\pi}{5} \frac{nI}{r_m} \tag{1}$$

where

n = turns in coil

I = current in coil, amp

r_m = median coil radius, cm

r = coil radius, cm

Furthermore

$$H_{r,\ell,x,} = \frac{\pi}{10} \frac{nI}{\ell} \left[\frac{x+\ell}{\sqrt{r^2 + (x+\ell)^2}} - \frac{x-\ell}{\sqrt{r^2 + (x-\ell)^2}} \right] \tag{2}$$

and, if we make

$$A = \frac{x + \ell}{r_m} \tag{3}$$

$$B = \frac{x - \ell}{r_m} \tag{4}$$

we have

$$H_{\ell,\,h} = \frac{\pi}{5} \quad \frac{nI}{A-B} \quad \left[\frac{A}{(r^2 + A^2 r_m^2)^{1/2}} - \frac{B}{(r^2 + B^2 r_m^2)^{1/2}} \right] \tag{5}$$

Now, we can describe the coil as a current sheet for which

$$\frac{dH_{\ell,x}}{dr} = \frac{\pi}{5} \quad \frac{I}{A-B} \quad \left[\frac{A}{(r^2 + A^2 r_m^2)^{1/2}} - \frac{B}{(r^2 + B^2 r_m^2)^{1/2}} \right] \frac{dI}{dr} \tag{6}$$

where

$\frac{dI}{dr}$ = linear current density in sheet, amp x cmp^{-1}

and we have by integration

$$\frac{dI}{dr} = \frac{nI}{r_m A_r} \tag{7}$$

we can make

$$H_{\ell,\,A_r,x} = \frac{\pi}{5} \quad \frac{nI}{r_m^2 A_r (A - B)} \left[A \int \frac{dr}{(r^2 + A^2 r_m^2)^{1/2}} - B \int \frac{dr}{(r^2 + B^2 r_m^2)^{1/2}} \right]_{r_m (1 - A_{r/2})}^{r_m (1 + A_{r/2})}$$

$$= \frac{\pi}{5} \quad \frac{nI}{r_m^2 A_r (A - B)} \left[A \ell n \left(r + \sqrt{r^2 + A^2 r_m^2}\right) - B \ell n \left(r + \sqrt{r^2 + B^2 r_m^2}\right) \right]_{r_m (1 - A_{r/2})}^{r_m (1 + A_{r/2})} \tag{8}$$

C. EFFECT OF FINITE WINDING HEIGHT ON AXIAL FIELD OF TOROIDAL COIL

The axial field of a solenoidal coil is given by

$$H_\ell = \frac{2\pi}{10}\,\frac{nI}{\ell}\left[\frac{0.5\ell + x}{\sqrt{r^2 + (0.5\ell + x)^2}} + \frac{0.5\ell - x}{\sqrt{r^2 + (0.5\ell - x)^2}}\right] \tag{1}$$

where

H_ℓ = axial field for a given winding height, oerstedt

n = number of turns in coil

I = current in coil, amp

ℓ = winding height, cm

r = coil radius, cm

x = axial distance from coil center, cm

If we make

$$X = \frac{x}{r} \tag{2}$$

where

X = relative axial distance to coil center

and

$$h = \frac{\ell}{2r} \tag{3}$$

where

h = length/diameter ratio of coil

we have by transposition

$$H_\varrho = \frac{\pi}{10} \frac{nI}{r} \left[\frac{1 + X/h}{\sqrt{1 + (h + X)^2}} + \frac{1 - X/h}{\sqrt{1 + (h - X)^2}} \right] \tag{4}$$

and since

$$\lim_{\varrho \to 0} H_\varrho = H_0 = \frac{2\pi}{10} \frac{1}{(1 + X^2)^{3/2}} \tag{5}$$

we can write

$$\frac{H_\varrho}{H_0} = \frac{1}{2} (1 + X)^{3/2} \left[\frac{1 + X/h}{\sqrt{1 + (h + X)^2}} + \frac{1 - X/h}{\sqrt{1 + (h - X)^2}} \right]$$

as the correction term sought.

D. Effect of Finite Annular Width on Axial Field of Toroidal Coil

$$H = \frac{\pi}{5} \quad \frac{In}{1 + h^2/r_m^2)^{3/2} r_m} \tag{1}$$

where

H = axial magnetic field, oerstedt

I = current in coil, amp

r_m = mean coil radius, cm

h = axial distance from plane of coil, cm

n = number of turns

To accomodate an annulus of finite width, we describe it as a current sheet for which

$$nI = \int_{r_m(1 - A_{r/2})}^{r_m(1 + A_{r/2})} I_r dr \tag{2}$$

where

A_r = fractional annular width in terms of radius

I_r = linear current density along radius, amp x cm^{-1}

giving

$$I_r = \frac{nI}{r_m A_r} \tag{3}$$

Then

$$dH = \frac{\pi}{5} \quad \frac{I_r}{r(1 + h^2/r^2)^{3/2}} \quad dr \tag{4}$$

and thus

$$H' = \frac{\pi}{5}\,\frac{nI}{r_m A_r}\int_{r_m(1-A_{r/2})}^{r_m(1+A_{r/2})} \frac{r^2}{(r^2+h^2)^{3/2}}\,dr \qquad (5)$$

where

H' = axial field for finite width annulus. oerstedt

from which

$$H' = \frac{\pi}{5}\,\frac{nI}{r_m A_r}\left[\ln\left(r+\sqrt{r^2+h^2}\right) - \frac{r}{\sqrt{r^2+h^2}}\right]_{r_m(1-A_{r/2})}^{r_m(1+A_{r/2})} \qquad (6)$$

and thus

$$H' = \frac{\pi}{5}\,\frac{nI}{r_m A_r}\left[\ln\frac{1+A_{r/2}+\sqrt{(1+A_{r/2})^2+h^2/r_m^2}}{1-A_{r/2}+\sqrt{(1-A_{r/2})^2+h^2/r_m^2}} + \frac{(1-A_{r/2})}{\sqrt{(1-A_{r/2})^2+h^2/r_m^2}} - \frac{(1+A_{r/2})}{\sqrt{(1+A_{r/2})^2+h^2/r_m^2}}\right] \qquad (7)$$

giving

$$\frac{H'}{H} = \frac{(1+h^2/r_m^2)^{3/2}}{A_r}\left[\ln\frac{1+A_{r/2}-\sqrt{(1+A_{r/2})^2+h^2/r_m^2}}{1-A_{r/2}-\sqrt{(1-A_{r/2})^2+h^2/r_m^2}} + \frac{(1-A_{r/2})}{\sqrt{(1-A_{r/2})^2+h^2/r_m^2}} - \frac{(1+A_{r/2})}{\sqrt{(1+A_{r/2})^2+h^2/r_m^2}}\right] \qquad (8)$$

E. Optimum NQR Coil for Constant Maximum Field

Given

F_{MAX} = maximum allowable electric field between coil terminals, V cm^{-1}

we have

$$V_{MAX} = F_{MAX}\, r A_r F_a \tag{1}$$

where

V_{MAX} = maximum voltage across coil terminals, V

r = coil radius, cm

A_r = fractional width of annulus in terms of radius

F_a = fraction of annulus occupied by air gaps

We also have

$$V_{MAX} = I_{MAX}\, Z = I_{MAX}\sqrt{\frac{L}{C}} \tag{2}$$

where

I_{MAX} = maximum current, in coil, A

Z = impedance, Ω

L = inductance, H

C = capacitance, F

where, for a sample located axially one radius below the coil plane

$$I_{MAX} = \frac{10\sqrt{2}}{\pi}\,\frac{r}{n}\,H_{MAX} \tag{3}$$

n = number of turns in coil

H_{MAX} = maximum magnetic field at sample, oe

in which, for a quasi-rectangular pulse

$$H_{MAX} = \frac{\pi}{2}\,\frac{1}{\gamma t_p} \tag{4}$$

where

γ = gyromagnetic ratio, rad oe^{-1} sec^{-1}

t_p = pulse length, sec

Then

$$I_{MAX} = \frac{10}{\sqrt{2}} \frac{r}{n} \frac{1}{\gamma t_p} \tag{5}$$

and

$$V_{MAX} = \frac{10}{\sqrt{2}} \frac{rL^{1/2}}{hC^{1/2}} \frac{1}{\gamma t_p} \tag{6}$$

Now, the resonance condition

$$f = \frac{1}{2\pi\sqrt{LC}} \tag{7}$$

where

f = frequency, Hz

reduces to

$$\sqrt{\frac{L}{C}} = \frac{1}{2\pi fC} \tag{8}$$

from which

$$V_{MAX} = \frac{5}{\sqrt{2}\ \pi} \frac{r}{nfC} \frac{1}{\gamma t_p} \tag{9}$$

Now, we can also write

$$C = \frac{5 \times 10^8}{c^2} \frac{h_D K_m}{F_c S_c} \tag{10}$$

where

h_D = height of coil ribbon conductor, cm

K_m = mean dielectric constant of gap

F_c = fraction of total capacitance inside coil

S_c = gap width in terms of radius

c = velocity of light, cm sec^{-1}

and also

$$S_c = \frac{A_r F_a}{n} \tag{11}$$

from which

$$C = \frac{5 \times 10^8}{c^2} \frac{n h_D K_m}{F_c A_r F_a} \tag{12}$$

giving

$$V_{MAX} = \frac{10^{-8} c^2}{\sqrt{2}\,\pi} \frac{r A_r F_a F_c}{n^2 h_D K_m f} \frac{1}{\gamma t_p} \tag{13}$$

Combining this with Equation 1 gives

$$n = \frac{10^{-4} c}{2^{1/4} \pi^{1/2}} \frac{F_c^{1/2}}{F_{MAX}^{1/2} h_D^{1/2} K_m^{1/2} f^{1/2}} \frac{1}{\gamma^{1/2} t_p^{1/2}} \tag{14}$$

from which by substitution

$$S_c = \frac{2^{1/4}\pi^{1/2}10^4}{c} \quad \frac{A_r F_a F_{MAX}^{1/2} h_D^{1/2} K_m^{1/2} f^{1/2}}{F_c^{1/2}} \quad \gamma^{1/2} t_p^{1/2} \tag{15}$$

$$C = \frac{5 \times 10^4}{2^{1/4}\pi^{1/2} c} \quad \frac{h_D^{1/2} K_m^{1/2}}{F_c^{1/2} A_r F_a F_{MAX}^{1/2} f^{1/2}} \quad \frac{1}{\gamma^{1/2} t_p^{1/2}} \tag{16}$$

Now, since

$$L = \frac{K r n^2}{F_L} \tag{17}$$

where

K = coil factor, H cm^{-1}

F_L = fraction of inductance in coil

we have

$$L = \frac{10^{-8} c^2}{\sqrt{2\pi}} \quad \frac{r K F_c}{h_D F_{MAX} K_m f F_L} \quad \frac{1}{\gamma t_p} \tag{18}$$

On the other hand, from Equation 7, we have

$$L = \frac{1}{4\pi^2} \quad \frac{1}{f^2 C} \tag{19}$$

and therefore

$$L = \frac{c}{2^{3/4} 10^5 \pi^{3/2}} \quad \frac{F_c^{1/2} A_r F_a F_{MAX}^{1/2}}{h_D^{1/2} K_m^{1/2} f^{3/2}} \gamma^{1/2} t_p^{1/2} \tag{20}$$

from which

$$h_D = 10^{-6} c^2 \sqrt{2\pi} \frac{r^2 F_c f K^2}{A_r^2 F_a^2 K_m F_{MAX}^3 F_L^2} \frac{1}{\gamma^3 t_p^3} \tag{21}$$

We now substitute again and have

$$n = \frac{1}{10\sqrt{2}\pi} \frac{A_r F_a F_{MAX} F_L}{r K f} \gamma t_p \tag{22}$$

$$S_c = 10\sqrt{2}\pi \frac{r K f}{F_{MAX} F_L} \frac{1}{\gamma t_p} \tag{23}$$

$$C = 50 \frac{rK}{A_r^2 F_a^2 F_{MAX}^2 F_L} \frac{1}{\gamma^2 t_p^2} \tag{24}$$

$$L = \frac{1}{200\pi^2} \frac{A_r^2 F_a^2 F_{MAX}^2 F_L}{K r f^2} \gamma^2 t_p^2 \tag{25}$$

$$Z = \frac{10^{-2}}{\pi} \frac{A_r^2 F_a^2 F_{MAX}^2}{r K f} \gamma^2 t_p^2 \tag{26}$$

giving

$$I_{MAX} = 100\pi \frac{r^2 K f}{A_r F_a F_{MAX} F_L} \frac{1}{\gamma^2 t_p^2} \tag{27}$$

There

$$(P_{MAX})_{CIRC} = 50\pi \frac{r^3 K f}{F_L} \frac{1}{\gamma^2 t_p^2} \tag{28}$$

where

$(P_{MAX})_{CIRC}$ = maximum circulating power, W

We now turn to the dissipative losses in the coil, where

$$R = \pi \frac{r n \rho}{h_D \sigma F_R} \tag{29}$$

where

R = resistance, Ω

ρ = conductor resistivity, Ω cm^{-1}

σ = skin depth, cm

F_R = fraction of total resistance in coil

and, in which

$$\sigma = \frac{10^4\sqrt{10}}{2\pi} \frac{\rho^{1/2}}{f^{1/2}} \tag{30}$$

Then

$$R = \frac{\sqrt{10}}{c^2} \frac{A_r^3 F_a^3 F_{MAX}^4 F_L^3 K_m \rho^{1/2}}{r^2 K^3 F_c F_R f^{3/2}} \gamma^4 t_p^4 \tag{31}$$

and since

$$Q = \frac{2\pi f L}{R} \tag{32}$$

where

Q = Q-factor

we have

$$Q = \frac{10^{-3}}{\pi} \frac{10\, c^2}{} \frac{r K^2 F_c F_R f^{1/2}}{A_r F_a F_{MAX}^2 F_L^2 K_m \rho^{1/2}} \frac{1}{\gamma^2 t_p^2} \tag{33}$$

On the other hand, we have

$$(P_{MAX})_{DIS} = \frac{1}{2} I_{MAX}^2 R \tag{34}$$

where

$(P_{MAX})_{DIS}$ = maximum power dissipation rate, W, from which

$$(P_{MAX})_{DIS} = \frac{10^4\sqrt{10}\ \pi^2}{2c^2} \quad \frac{r^2 A_r F_a F_{MAX}^2 F_L \quad K_m \rho^{1/2} f^{1/2}}{K F_c F_R} \tag{35}$$

Furthermore

$$E_{MAX} = \frac{1}{2}\ I_{MAX}^2\ \ L \tag{36}$$

where

E_{MAX} = maximum energy storage in field, J, from which

$$E_{MAX} = 25\ \frac{r^3 K}{F_L} \quad \frac{1}{\gamma^2 t_p^2} \tag{37}$$

Finally, for a quasirectangular pulse

$$(P_{MAX})_{LOAD} = \frac{2}{t_p} \quad E_{MAX} \tag{38}$$

where

$(P_{MAX})_{LOAD}$ = maximum power input into coil, W, from which

$$(P_{MAX})_{LOAD} = 50\ \frac{r^3 K}{F_L} \quad \frac{1}{\gamma^2 t_p^3} \tag{39}$$

As an example, let us take

$A_r = 0.40$

$F_a = F_L = F_c = F_R = 0.90$

$F_{MAX} = 6000\ V\ cm^{-1}$

$K_m = 2.26$

$K = 3.5 \times 10^{-8}$ H cm^{-1}

$\rho = 1.62 \times 10^{-6}$ Ω cm^{-1} (Ag)

$\gamma = 1640$ rad oe^{-1} sec^{-1}

$t_p = 250$ μsec

$f = 3.41$ MHz

We then get

r	10 cm	15	20	25	30
n	15.03	10.02	7.515	6.012	5.010
S_c	2.39×10^{-2}	3.595×10^{-2}	4.790×10^{-2}	5.988×10^{-2}	$7.185 \times 10^{-}$
h_D	4.251 mm	9.565	17.00	26.57	38.26
σ	34.69μ →				
H_{MAX}	3.831 oe →				
L	87.96 μH	58.57	43.93	35.14	29.29
C	24.79 pF	37.19	49.58	61.98	74.37
R	0.5764 Ω	0.2562	0.1441	0.09222	0.06404
Q	3266	4899	6532	8165	9798
V_{MAX}	21.60 KV	32.40	43.20	54.00	64.80
I_{MAX}	11.47	26.42	46.96	73.38	105.7
E_{MAX}	5.784 mJ	19.52	46.27	90.38	156.2
d	2.053 mm	5.389	9.580	1497	21.56
Z	1882 Ω	1255	941.0	752.8	672.3
$(P_{MAX})_{CIRC}$	123.9 KW	418.2	991.2	1936	3345
$(P_{MAX})_{DIS}$	37.92 W	85.32	151.7	237.0	341.3
$(P_{MAX})_{LOAD}$	46.27 W	156.2	370.2	723.0	1249

F. NQR Coil Optimization

Given

n	=	number of turns
A_r	=	relative width of coil annulus in terms of radius
F_a	=	fraction of annulus occupied by gap
F_L	=	fraction of total inductance inside coil
F_c	=	Fraction of total capacitance inside coil
r	=	coil radius, cm
h_D	=	height of ribbon winding, cm
K_m	=	dielectric constant across winding gap
f	=	frequency, Hz
S_c	=	relative width of individual gap in terms of radius
K	=	coil factor, H cm^{-1}
L	=	inductance, H
C	=	capacitance, F
I_{MAX}	=	maximum current, A
V_{MAX}	=	maximum voltage, V
$(P_{MAX})_{CIRC}$	=	maximum circulating power, W
R	=	resistance, Ω
ρ	=	resistivity, Ω cm^{-1}
σ	=	penetration depth, cm
F_R	=	fraction of total resistance inside coil
Q	=	Q-factor
$(P_{MAX})_{DIS}$	=	maximum dissipated power, W
E_{MAX}	=	maximum energy in coil field, J

H_{MAX} = maxiumum magnetic field on coil axis one radius below coil plane, oe

d = gap width, cm

γ = gyromagnetic ratio, rad oe^{-1} sec^{-1}

t_p = pulse length, sec

c = velocity of light, cm sec^{-1}

F_{MAX} = maximum field between coil

z = impedance, Ω

we have, for an axial sample one radius away from the coil plane

$$n = \frac{10^{-3}c^{2/3}}{2^{1/3}\pi^{2/3}} \quad \frac{A_r^{1/3}F_a^{1/3}F_L^{1/3}F_c^{1/3}}{r^{1/3}h_D^{1/3}K_m^{1/3}f^{2/3}K^{1/3}} \tag{1}$$

$$S_c = \frac{10^3 2^{1/3}\pi^{2/3}}{c^{2/3}} \quad \frac{r^{1/3}h_D^{1/3}A_r^{2/3}F_a^{2/3}K_m^{1/3}K^{1/3}f^{2/3}}{F_L^{1/3}F_c^{1/3}} \tag{2}$$

$$L = \frac{10^{-6}c^{4/3}}{2^{2/3}\pi^{4/3}} \quad \frac{r^{1/3}A_r^{2/3}F_a^{2/3}F_c^{2/3}K^{1/3}}{h_D^{2/3}K_m^{2/3}F_L^{1/3}f^{4/3}} \tag{3}$$

$$C = \frac{10^6}{2^{4/3}\pi^{2/3}c^{4/3}} \quad \frac{F_L^{1/3}h_D^{2/3}K_m^{2/3}}{r^{1/3}F_c^{2/3}A_r^{2/3}F_a^{2/3}K^{1/3}f^{2/3}} \tag{4}$$

$$\sigma = \frac{10^4\sqrt{10}}{2\pi}\ \frac{\rho^{1/2}}{f^{1/2}} \tag{5}$$

$$R = 10^{-8}2^{2/3}\sqrt{10}\ \pi^{4/3}c^{2/3}\ \frac{r^{2/3}A_r^{1/3}F_a^{1/3}F_L^{1/3}F_c^{1/3}\rho^{1/2}}{h_D^{1/3}f^{1/6}F_R K_m^{1/3}K^{1/3}} \tag{6}$$

$$Q = \frac{10\sqrt{10}\ c^{2/3}}{\pi^{5/3}2^{1/3}}\ \frac{h_D^{2/3}A_r^{1/3}F_a^{1/3}F_c^{1/3}F_R K^{2/3}}{r^{1/3}F_L^{2/3}\rho^{1/2}K_m^{1/3}f^{1/6}} \tag{7}$$

$$H_{MAX} = \pi\ \frac{1}{\gamma t_p}\ \text{(quasirectangular pulse)} \tag{8}$$

$$I_{MAX} = \frac{10^4\pi^{2/3}}{2^{1/6}c^{2/3}}\ \frac{r^{4/3}h_D^{1/3}K_m^{1/3}K^{1/3}f^{2/3}}{A_r^{1/3}F_a^{1/3}F_L^{1/3}F_c^{1/3}\gamma t_p} \tag{9}$$

$$V_{MAX} = 2^{1/6}10^{-2}c^{2/3}\pi^{1/3}\ \frac{r^{5/3}A_r^{1/3}F_a^{1/3}F_c^{1/3}K^{2/3}f^{1/3}}{h_D^{1/3}K_m^{1/3}F_L^{2/3}\gamma t_p} \tag{10}$$

$$(P_{MAX})_{CIRC} = 50\ \pi\ \frac{r^3 K f}{F_L \gamma^2 t_p^2} \tag{11}$$

$$(P_{MAX})_{DIS} = \frac{\sqrt{10}\,\pi^{8/3}}{2^{2/3}c^{2/3}} \frac{r^{10/3}K_m^{1/3}K^{1/3}\rho^{1/2}f^{7/6}}{h_D^{2/3}A_r^{1/3}F_a^{1/3}F_L^{1/3}F_c^{1/3}F_R\gamma^2 t_p^2} \tag{12}$$

$$F_{MAX} = 2^{7/6}10^{-2}c^{2/3}\pi^{1/3} \frac{r^{2/3}F_c^{1/3}K^{2/3}f^{1/3}}{h_D^{1/3}A_r^{2/3}F_a^{2/3}K_m^{1/3}F_L^{2/3}\gamma t_p} \tag{13}$$

$$E_{MAX} = 25 \frac{r^3K}{F_L\gamma^2 t_p^2} \tag{14}$$

$$(P_{MAX})_{LOAD} = 100\,\pi \frac{r^3K}{F_L\gamma^2 t_p^3} \tag{15}$$

$$d = \frac{10^3\pi^{2/3}2^{1/3}}{C^{2/3}} \frac{r^{4/3}h_D^{1/3}A_r^{2/3}F_a^{2/3}K_m^{1/3}K^{1/3}f^{2/3}}{F_L^{1/3}F_c^{1/3}} \tag{16}$$

$$Z = \frac{10^{-6}c^{4/3}2^{1/3}}{\pi^{1/3}} \frac{r^{1/3}A_r^{2/3}F_a^{2/3}F_c^{2/3}K^{1/3}}{h_D^{2/3}K_m^{2/3}F_L^{1/3}f^{1/3}} \tag{17}$$

$$\frac{V_{MAX}}{n} = 10\sqrt{2}\,\pi\,\frac{r^2 f K}{F_L \gamma t_p} \qquad (18)$$

As an example, for

A_r = 0.40

F_a = 0.90

F_c = $F_R = F_L$ = 0.90

h_D = 1.0 cm

K_m = 2.26

f = 3.41 MHz

K = 3.5×10^{-8} H cm^{-1}

ρ = $1.62 \times 10^{-6}\,\Omega\ cm^{-1}$ (Ag)

γ = 1640 rad oerstedt^{-1} sec^{-1}

t_p = 250 μsec

we have

r	10	15	20	25	30
n	11.30	9.871	8.969	8.326	7.835
S_c	3.185×10^{-2}	3.646×10^{-2}	4.013×10^{-2}	4.323×10^{-2}	4.594×10^{-2}
L	49.67μH	56.86	62.58	67.41	71.64
c	43.85pF	38.31	34.80	32.31	30.40
σ	34.69μ →				
R	0.1843 Ω	0.2415	0.2926	0.3395	0.3834
Q	5773	5043	4582	4254	4003
H_{MAX}	3.193 oe →				
I_{MAX}	15.26 A	26.20	38.45	51.78	66.03
V_{MAX}	16.24 KV	31.92	51.56	74.79	101.3
$(P_{MAX})_{CIRC}$	123.9 KW	418.2	991.2	1936	3345
$(P_{MAX})_{DIS}$	21.47 W	82.95	216.4	455.3	836.1
F_{MAX}	4.511 KV/cm	5.911	7.161	8.309	9.383
E_{MAX}	4.016 mJ	13.55	32.13	62.75	108.4
$(P_{MAX})_{LOAD}$	290.7 W	981.1	2326	4542	7849
d	3.185 mm	5.469	8.026	10.81	13.78
Z	1064 Ω	1218	1341	1444	1535

G. Power Requirements in NQR Coil

The magnetic field generated on axis by a flat coil is given by

$$H = 0.2\pi \frac{nI r^2}{(r^2 + x^2)^{2/3}} \tag{1}$$

where

H = magnetic field,

n = number of turns

I = current, A

r = coil radius, cm

x = axial distance from plane of coil, cm

and its inductance by

$$L = Krn^2 \tag{2}$$

where

L = self-inductance, μH

K = coil constant

provided the number of turns on the conductor diameter are low. Since L is limited by coil resonance considerations, we can substitute it in H to give

$$H = \frac{0.2\pi}{K^{1/2}} \frac{IL^{1/2}}{(r + x^2/r)^{2/3}} \tag{3}$$

In order to optimize r for a given x, we take

$$\frac{\partial H}{\partial r} = \frac{0.3\pi}{\sqrt{K}} I\sqrt{L} \frac{1 - x^2/r^2}{(r + x^2/r)^{5/2}} \tag{4}$$

and, for

$$\frac{\partial H}{\partial r} \equiv 0 \quad \therefore r = x \tag{5}$$

Since

$$\frac{\partial^2 H}{\partial r^2} = - \frac{0.6\pi}{K^{1/2}} I \bar{L} \left[\frac{-(r + x^2/r)\, x^2/r^3 - \frac{1}{10} (1 - x^2/r^2)^2}{(r + x^2/r)^{7/2}} \right] \tag{6}$$

we have

$$\left(\frac{\partial^2 H}{\partial r^2} \right)_{r = x} > 0 \tag{7}$$

thus showing the point r=x to be a maximum, at which

$$H = 0.222 \frac{I L^{1/2}}{K^{1/2} r^{3/2}} \tag{8}$$

a value only $2^{3/2}$ times lower than at the center of the coil. For a given H, then

$$I = 4.50 \frac{H r^{3/2} K^{1/2}}{L^{1/2}} \tag{9}$$

and since

$$P = \left(\frac{I}{Q} \right)^2 \Omega \tag{10}$$

we have

$$P = 20.26 \frac{H^2 r^3 \Omega K}{LQ^2} \tag{11}$$

where

Ω = coil reactance

Q = coil Q-factor

The average power will be given by

$$\bar{P} = P \mu R_p \tag{12}$$

where

μ = pulse repetition rate, HZ

R_p = pulse repetition rate, Hz

An example will now be instructive. Given

H = 40

r = 10 cm

$\Omega = 10^5 \Omega$

L = 40μH

K = 0.04

Q = 100

μ = 160 μsec

R_p = 2 Hz

we have

P = 324 kW

and

$\bar{P}$ = 104 W

The values for the other variables are

n = 10

I = 180 A

Giving for the input current to the coil

$I/Q = 1.8$ A

and for the drive voltage

$I\Omega/Q = 180$ kV

This requirement can be reduced by subdividing the exciting pulse into a pulse train (whose duration must be $<T_1$). Then P, I, I/Q and $I\Omega/Q$ can be divided by the number of pulses in the train.

H. NQR Signal Loss for Finite Length Excitation Pulses

Given a single exciting pulse followed by measurement of the free induction decay, we may define

T_2 = free induction decay time constant, sec

T_p = pulse duration, sec

t = time, sec

$H(t)$ = magnetic field as a function of time, oerstedt

γ = gyromagnetic ratio, rad x sec^{-1} x $oerstedt^{-1}$

To give a maximum signal, a saturated pulse is required, for which

$$\gamma \int_0^{T_p} H(t)\, dt = \frac{\pi}{2} \tag{1}$$

For such a pulse the fraction of the total pulse corresponding to a given instant is

$$f(t) = \frac{2}{\pi} H(t)\, dt \tag{2}$$

If the pulse duration is finite, part of the signal will decay during it; the fractional loss in intensity will be

$$F = \int_0^{T_p} e^{-(T_p - t)/T_2} \; f(t) = \frac{2}{\pi} e^{-T_p/T_2} \int_0^{T_p} H(t)\, e^{-t/T_2}\, dt \tag{3}$$

A few of the more typical cases can be tabulated (See Table H-1). Figure H-1 shows F as a function of T_p for all three cases and for α = 1, 2, and 5. If pulsing schemes requiring q pulses within the thermal equilibration time are used, the actual T_p must be multiplied by q to get the effective one.

TABLE H-1

PULSE SHAPE	H(t)	CONSTANT	F	H_{MAX}
SQUARE	C	$\frac{\pi}{2\gamma T_p}$	$\frac{T_2}{T_p}\left(1 - e^{-T_p/T_2}\right)$	$\frac{\pi}{2\gamma T_p}$
TRIANGULAR	Ct	$\frac{\pi}{\gamma T^2_p}$	$2\left(\frac{T_2}{T_p}\right)^2\left(\frac{T_p}{T_2} - 1 + e^{-T_p/T_2}\right)$	$\frac{\pi}{\gamma T_p}$
EXPONENTIAL DECAY	$C\left(1 - e^{-\alpha t/T_p}\right)$	$\frac{\alpha\pi}{2\gamma T_p\left(1 - e^{-\alpha}\right)}$	$\frac{T_2/T_p\,\alpha e^{-T_p/T_2}}{1 - e^{-\alpha}}\quad\frac{e^{-\alpha + T_p/T_2} - 1}{1 - \alpha T_2/T_p}$	$\frac{\pi\alpha}{2\gamma T_p\left(1 - e^{-\alpha}\right)}$
EXPONENTIAL-ASYMPTOTIC	$C\left(e^{-\alpha t/T_p}\right.$	$\frac{\alpha\pi}{2\gamma T_p\left(\alpha + e^{-\alpha} - 1\right)}$	$\frac{T_2/T_p\,\alpha e^{-T_p/T_2}}{\alpha + e^{-\alpha} - 1}\left(e^{T_p/T_2} - 1 + \frac{1 - e^{-\alpha + T_p/T_2}}{1 - \alpha\frac{T_2}{T_p}}\right)$	$\frac{\pi\alpha\left(1 - e^{-\alpha}\right)}{2\gamma T_p\left(\alpha + e^{-\alpha} - 1\right)}$

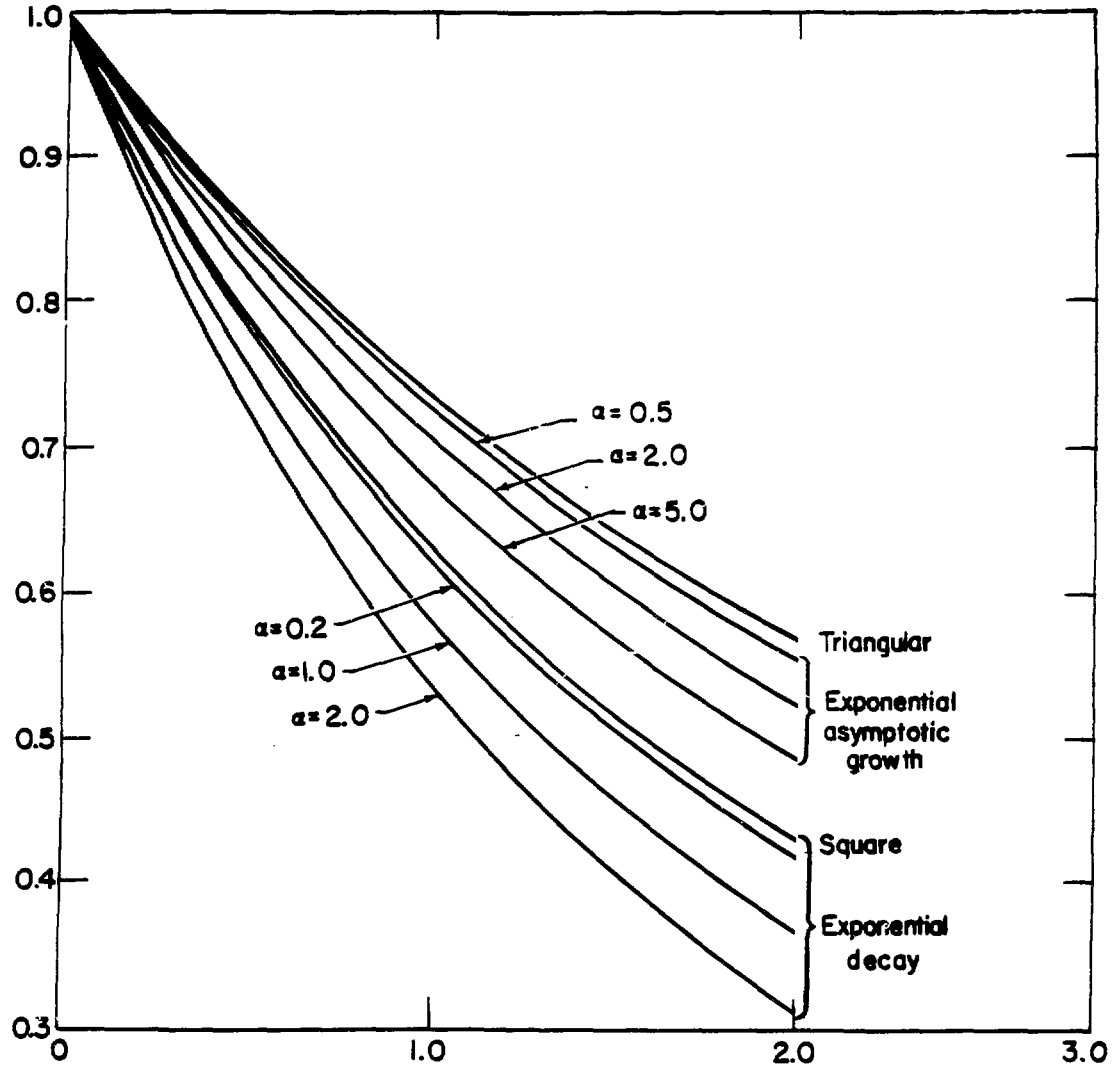

Figure H-1. Signal Loss for Finite Excitation Pulse Length

#789-004